電 子 427

Fabrication of Nitride-Based Quantum Dots and Their Application to Optical Devices

（窒化物半導体量子ドットの形成と光デバイスへの応用）

A Thesis Presented to
the Graduate School of the University of Tokyo
in Partial Fulfillment of the Requirements
for the Degree of Doctor of Philosophy
in Electronic Engineering

by
Koichi Tachibana

December 14, 2001

To My Family

&

To the Memory of Roppongi Campus

Preface

This thesis presents an essential part of the research carried out at the Institute of Industrial Science, the Research Center for Advanced Science and Technology, and the Center for Collaborative Research in the University of Tokyo under the supervision of Professor Yasuhiko Arakawa, while the author was a graduate student at the Department of Electronic Engineering in the University of Tokyo from 1997 to 2002.

In this thesis, the author describes the growth and optical properties of nitride-based quantum dots for the application to optical devices.

December 14, 2001

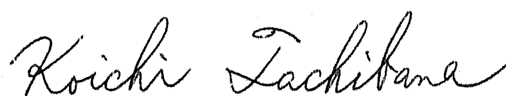

Koichi Tachibana

Acknowledgements

The author would like to express his sincere gratitude to his dissertation supervisor, Professor Yasuhiko Arakawa, Research Center for Advanced Science and Technology, the University of Tokyo, for his constant guidance, encouragement, and enthusiasm. His excellent insight led the author to the proper direction in this work. Without them, this work could not be accomplished.

The author also expresses his sincere thanks to Dr. Takao Someya, Research Center for Advanced Science and Technology, the University of Tokyo, for his guidance, continuous encouragement, and fruitful discussions, which were invaluable for this work.

The author would like to acknowledge Professor H. Sakaki, Institute of Industrial Science, the University of Tokyo, Professor K. Hirakawa, Institute of Industrial Science, the University of Tokyo, Professor Y. Nakano, Department of Electronic Engineering, the University of Tokyo, Professor M. Tanaka, Department of Electronic Engineering, the University of Tokyo, and Professor T. Takahashi, Institute of Industrial Science, the University of Tokyo, the committee of this thesis, for fruitful discussions and their encouragement.

The author acknowledges Professor A. Forchel, Dr. R. Werner, Mr. J. Moosburger, and Mr. M. Kamp, Technische Physik, Julius-Maximilians-Universität Würzburg, for their collaboration of a reactive ion etching of the samples.

The author acknowledges Professor J. H. Christen and Mr. T. Riemann, Institut für Experimentelle Physik, Otto-von-Guericke-Universität Magdeburg, for their collaboration of cathodoluminescence study of the selectively-grown quantum dots.

The author is indebted to Advanced Discrete Semiconductor Technology Laboratory, Corporate Research & Development Center, Toshiba Corporation, for the collaboration of the fabrication and characterization of $In_xGa_{1-x}N$ self-assembled quantum dot lasers by current injection.

The author wishes to express his appreciation to Professor H. Sakaki, Professor H. Fujita, Institute of Industrial Science, the University of Tokyo, Professor K. Hirakawa, and Professor T. Hiramoto, Institute of Industrial Science, the University of Tokyo, for their kindness of his using of their facilities.

The author is grateful to many colleagues for the collaborations; the author acknowledges Mr. M. Nishioka for his excellent technical support with the metalorganic chemical vapor deposition system and other experimental aspects. The author acknowledges Mr. S. Ishida for his collaboration of device processing such as the electron-beam lithography, super high-quality scanning electron microscope images, and other experimental aspects. The author acknowledges Mr. O. Moriwaki for his collaboration of microscopic photoluminescence study of $In_xGa_{1-x}N$ self-assembled quantum dots. The author acknowledges Mr. M. Miyamura for his collaboration of the growth and optical properties of GaN self-assembled quantum dots. The author acknowledges Dr. J. C. Harris for her careful reading of the manuscripts and fruitful discussions. The author acknowledges Dr. K. Hoshino for his technical support with the metalorganic chemical vapor deposition system. The author acknowledges Mr. S. Kako for his technical support with the optical measurement system. The author acknowledges Mr. M. Arita for his support of characterizing p-type GaN.

The author acknowledges many other colleagues for their support, discussions, and enjoyable collaborations: Dr. M. Ozaki, Dr. T. Saito, Professor Y. Toda (at present, Hokkaido University), Dr. F. Sogawa, Dr. K. Suzuki, Dr. M. Kitamura, Dr. T. Nakaoka, Dr. K. Watanabe, Dr. H. Watabe, Dr. S. Shinomori, Mr. Y. Matsuda, Mr. K. Yamanaka, Mr. H. Kakuma, Mr. J. Tatebayashi, Mr. C. O. Tang, Mr. T. Sugimoto, Mr. Q. C. Tran, Mr. T. Imada, Mr. T. Yukutake, Professor B. Shen (Nanjing University), Dr. R. A. Hogg, Dr. X. Q. Li, Mr. L. Finger, Ms. K. Matsuoka, Ms. N. Kaya, Ms. S. Yamazaki, Ms. T.

Sorin, Ms. R. Takano, Ms. M. Miyauchi, Ms. M. Hino, and Ms. A. Nakagawa.

The author was in Nishinaga and Tanaka Laboratory when an undergraduate student at Department of Electronic Engineering, the University of Tokyo. The author acknowledges Professor T. Nishinaga (at present, Meijo University), Professor M. Tanaka, and Professor S. Naritsuka (at present, Meijo University) for their education of electronic engineering, crystal growth, and experimental aspects.

This work was partly supported by the Grant in-aid for COE Research from Ministry of Education, Culture, Sports, Science and Technology (#12CE2004), Research for the Future Program of the Japan Society for the Promotion of Science (JSPS) (Project No. JSPS–RFTF96P00201), and University–Industry Joint Project on Quantum Nanoelectronics. The author acknowledges JSPS Research Fellowships for Young Scientists for partial financial support.

Finally, the author would like to express his sincere gratitude to his parents, Takehiro and Yoshiko, his brother, Junji, and his sister, Yumiko, for their constant encouragement and support. Last but not least, the author wishes to acknowledge Manami for her continuous and hearty support. Without their support, this work could not be compiled.

Abstract

The author describes GaN-based quantum dots (QDs) from the viewpoints of both the fabrication process and application to optical devices in this thesis.

First, $In_xGa_{1-x}N$ self-assembled QDs are grown using atmospheric-pressure metalorganic chemical vapor deposition. The lateral size of the QDs is as small as 10-nm-scale and the intense photoluminescence is observed at room temperature. The very sharp luminescence lines are measured with the linewidth of 170 μeV, by the microscopic photoluminescence to investigate single dot spectroscopy. Second, selective growth of $In_xGa_{1-x}N$ QDs on uniform array of hexagonal pyramids of GaN is demonstrated to improve the uniformity of QDs. The microphotoluminescence intensity images with a spatial resolution of a few hundred nanometers show that the InGaN emission is only from the tops of hexagonal pyramids and the QDs are formed on the tops of pyramids. Third, selective growth of GaN QDs is discussed for the application to ultraviolet optical devices.

Finally, the lasers are fabricated with $In_xGa_{1-x}N$ self-assembled QDs embedded in the active layer. A clear threshold is observed in the dependence on the emission intensity on the excitation intensity at room temperature under optical excitation. The growth conditions are also investigated for $In_xGa_{1-x}N$ self-assembled QD lasers by current injection.

Contents

Preface i

Acknowledgements ii

Abstract v

1 Introduction 1

1.1 Background of this study . . . 1

1.1.1 Nitride semiconductors for short-wavelength optical devices . . . 1

1.1.2 Low-dimensional quantum nanostructures for laser applications . 2

1.2 Motivation and objectives of this study . . . 3

1.3 Synopses of this thesis . . . 6

2 InGaN Quantum Dots by Self-Assembled Growth 10

2.1 Introduction . . . 10

2.2 Epitaxial growth of GaN on Al_2O_3 substrate by metalorganic chemical vapor deposition . . . 11

2.3 Epitaxial growth of InGaN self-assembled quantum dots under various growth conditions . . . 12

2.3.1 Dependence on InGaN coverage . . . 12

2.3.2 Dependence on growth temperature . . . 14

2.4 Optical properties of InGaN quantum dots . . . 15

2.4.1 Photoluminescence from InGaN quantum dots . . . 15

2.4.2 Microscopic photoluminescence study of InGaN quantum dots . . 16

2.5 Multiple-layer stacked InGaN quantum dots . . . 18

2.6 Concluding remarks . . . 19

3 InGaN Quantum Dots by Selective Growth **30**
3.1 Introduction 30
3.2 Metalorganic chemical vapor selective deposition in GaN-based system . 31
3.2.1 Dependence on growth rate 32
3.2.2 Dependence on NH_3 flow rate 33
3.2.3 Dependence on growth temperature 33
3.2.4 Dependence on growth time 34
3.2.5 Summary 34
3.3 Selective growth of InGaN quantum dots 35
3.4 Optical characterization of selectively-grown InGaN quantum dots 36
3.4.1 Microphotoluminescence intensity images of InGaN quantum dots 36
3.4.2 Photoluminescence dependence on excitation power 37
3.5 Higher-density InGaN quantum dots on a substrate prepared by electron-beam lithography 38
3.5.1 Fabrication of higher-density selectively-grown InGaN quantum dots 39
3.5.2 Cathodoluminescence study of InGaN quantum dots 40
3.6 Concluding remarks 41

4 GaN Quantum Dots by Selective Growth **55**
4.1 Introduction 55
4.2 Fabrication of GaN quantum dots by selective growth 56
4.3 Photoluminescence from GaN quantum dots 57
4.4 Higher-density GaN quantum dots using a substrate prepared by electron-beam lithography 59
4.5 Concluding remarks 60

5 Application of GaN-Based Quantum Dots to Optical Devices **65**
5.1 Introduction 65
5.2 InGaN quantum dot lasers under optical excitation 66
5.3 InGaN quantum dot lasers by current injection 69
5.3.1 Growth conditions of *p*-type GaN 69
5.3.2 Cladding layer of GaN/AlGaN superlattices 72
5.3.3 Fabrication of laser structures 74
5.4 Concluding remarks 75

6 Conclusions **88**

6.1 Summary 88

6.2 Future prospect 89

A Carrier Density at Transparent Condition **92**

Bibliography **94**

Publication List **109**

Chapter 1

Introduction

1.1 Background of this study

1.1.1 Nitride semiconductors for short-wavelength optical devices

GaN and related materials have been studied intensively, because of their having wide bandgap energy (2.0–6.2 eV at room temperature in InAlGaN alloy) and their usefulness for optical devices emitting light at wavelengths from the ultraviolet (UV) to the visible.[1–3] For example, the short-wavelength light emitting diodes (LEDs) are applied to full-color flat display panels and illumination systems. The short-wavelength laser diodes (LDs) are expected to be used as the light sources for higher-density optical storages, such as next-generation DVDs, and laser printing with higher resolution.

In 1980s or earlier, the research of GaN-based semiconductors faced on many difficulties; i) there were no lattice-matched substrates, or ii) the epitaxial layer had many donor impurities and it was difficult to realize *p*-type GaN. Al_2O_3 (sapphire) has been usually used as the substrate in the growth of GaN-based semiconductors. However, there exists lattice mismatch of as large as 16% between GaN and *c*-face Al_2O_3 in *a*-axis direction. Amano and Akasaki *et al.* have demonstrated high-quality GaN film using AlN buffer grown at low temperature on Al_2O_3 substrate.[4] Moreover, they have demonstrated *p*-type GaN by Mg-doped GaN treated with low-energy electron beam irradiation.[5] In addition,

Nakamura has demonstrated high-quality GaN by also using GaN buffer layer grown at low temperature on Al_2O_3 substrate.[6] After that, Nakamura *et al.* have demonstrated high-quality InGaN films, which have the strong band edge emission.[7]

InGaN quantum well (QW) structures are now used as the active layer of optical devices such as UV or visible LEDs,[8] violet LDs,[9–20] and blue LDs.[21] More efforts are being paid for the further improvement of the device characteristics.

1.1.2 Low-dimensional quantum nanostructures for laser applications

To realize devices with superior characteristics, quantum dot (QD) structures are desirable; a laser with QDs embedded in the active layer is expected to have lower threshold current and other superior characteristics, compared to QW lasers. The concept of QD lasers was first proposed in 1982 by Arakawa and Sakaki.[22] It has been demonstrated that the three-dimensional (3-D) quantum confinement, provided by QD structures, should lead to the suppression of temperature dependence of the threshold current density. After that, reduced threshold current density, reduced total threshold current,[23,24] enhanced differential gain, and high spectral purity/no-chirping[25,26] were theoretically discussed.

The remarkable progress of self-assembled growth of the QDs such as In(Ga)As/GaAs QDs[27] brought the QD lasers[28] into a real world. At present stage, however, inhomogeneous broadening due to size fluctuations in the self-assembled QDs tremendously reduces the advantage expected from the use of 0-D systems. Nevertheless, the success of low threshold current due to volume effect and 1.3-μm light emission on GaAs substrates[29,30] convinces ones that the QD lasers will appear in optical communication systems.

1.2 Motivation and objectives of this study

The use of QDs is also expected to be effective in GaN-based lasers. The 0-D electronic states in the QDs play an essential role for improving threshold current characteristics particularly in wide bandgap semiconductors.[31)]

The improvement in lasing characteristics of QD lasers can be categorized according to two different types of effect: *quantum effects* and *non-quantum effects*. The *quantum effect* here is the effect resulting from the 3-D quantum confinement of electrons (i.e., δ-function density of states).

The threshold current I_{th} is given by

$$I_{th} = eVn_{th}/\tau, \tag{1.1}$$

where e, V, n_{th}, and τ are the electron charge, the volume of active layer, the carrier density at the threshold, and carrier lifetime, respectively. From Eq. (1.1), even if there is no quantum effect, low threshold current can be achieved by making V small. However, when V is too small, the necessary gain for lasing action cannot be obtained. Therefore, by careful optimization of V, a very low threshold current can be achieved even without the quantum effect. It should be noted that the main contribution to the low threshold current in the recently reported InAs self-assembled QD lasers is this volume effect, if one takes account of the very large inhomogeneous broadening in the gain spectrum of the QD lasers.

Another important non-quantum effect is the localization of carriers. The localization of carriers restrains them from being trapped into the defects, which leads to suppression of the effect of non-radiative recombination on the total carrier recombination time τ. It is believed that QD-like effects can be already seen through nanometer-scale fluctuations of indium composition[32,33)] due to phase separation in InGaN QWs, which may be useful for suppressing non-radiative recombination process.

On the other hand, the quantum effect should also play an essential role in enhanced improvements of threshold current due to the following reason. Threshold current de-

pends on various material parameters; a threshold current of the QW lasers increases if the effective mass of electrons m_c or the ratio of the effective mass of holes m_v to that of electrons m_v/m_c is larger. Unfortunately, in GaN-based system (and most of wide bandgap semiconductors), these values are larger compared to those in GaAs-based system.

To see this phenomenon, the carrier density n_{tr} under the condition that the material becomes transparent is discussed. Equation (1.1) can be re-written using n_{tr} as follows:

$$I_{th} = \gamma e V n_{tr}/\tau, \quad (1.2)$$

where γ is a constant of which the value is in the range of 1.2–1.5.

Figure 1.1 shows calculated sheet carrier density at transparent condition n_{str} ($= n_{tr} \cdot l_z$, where l_z is the thickness of QWs.) as a function of m_v/m_c for two effective masses of electrons ($m_c = 0.18m_0$ in GaN[34] and $0.066m_0$ in GaAs[35]). Here, m_0 is the free-electron mass and $T = 300$ K is used in the calculation. The calculation method is described in Appendix A. As shown in Fig. 1.1, n_{str} increases monotonically with the increase of m_v/m_c. Moreover, n_{str} is also larger when m_c becomes larger. The difference in n_{tr} leads to a difference in the minimal threshold current density J_{th}; J_{th} of GaN-based QW lasers is $\sim 10^3$ A/cm^2, while that of GaAs-based QW lasers is $\sim 10^2$ A/cm^2.

On the other hand, if QDs are used in the active region and the size of the QDs is small enough that the population of carriers in higher subband can be ignored (i.e., the energy separation between the ground states and excited states in the QDs is larger than $2k_BT$, where k_B is the Boltzmann constant.), the achievable threshold current I_{th} in both GaAs-based lasers and GaN-based lasers is almost the same, ~0.1–1 μA. Therefore, with the use of QDs, the achievable threshold current is enhanced by a factor of 10 in GaN-based lasers compared to GaAs-based lasers. Thus, the impact of the use of QDs is bigger in GaN-based lasers than that in GaAs-based ones. Owing to the large effective mass, however, QDs with smaller lateral size (~8–10 nm) are required in GaN-based semiconductors so that the effects of higher subbands are negligible.[36]

Some studies into the growth of QDs have already begun in GaN-based system. Two growth methods have been so far demonstrated: i) self-assembled growth and ii) selective

growth. Generally speaking, the self-assembled QDs are formed by choosing different growth conditions from those of bulk or QWs under the *in situ* procedure. It is easy to realize small QD structures and high density of the QDs, however it is a problem how to get uniformity or control the positions of the QDs. In contrast, the QDs by selective growth have the advantage of the uniformity and the control of positions, compared to the QDs by self-assembled growth, because the selective growth is performed on a patterned substrate. But, it remains how to get high density, since the density of selectively-grown QDs is almost determined by pattern size on the substrate. Therefore, the research of formation of QDs has been conducted by these methods of both self-assembled growth and selective growth.

In the self-assembled growth of nitride-based dots, "anti-surfactants" were sometimes introduced at the initial stage of research to form GaN[37,38)] or InGaN[39)] dots on an AlGaN layer. Before dots are grown, Si is supplied on the AlGaN surface as anti-surfactants. It is believed that Si acts like a self-assembling mask and the dots are formed on the Si-uncovered area. The macroscopic photoluminescence (PL),[37,39,40)] cathodoluminescence (CL),[41)] or resonant Raman scattering[42)] was investigated with respect to the self-assembling dots by anti-surfactant method. For laser application, stimulated emission from GaN self-assembling dots was observed at 20 K.[43)] As another method of self-assembling dots, GaN dots have been formed using Ga droplets.[44)] This growth method is known as the droplet epitaxy.[45)]

The Stranski–Krastanow (S–K) growth mode,[46)] which has been reported in systems of various materials such as InAs/GaAs, has been successful for growing GaN dots by molecular beam epitaxy (MBE).[47–49)] The GaN dots grown by MBE were characterized using macroscopic PL,[48,50,49)] time-resolved PL,[51)] or Raman scattering.[52,53)] InGaN dots by S–K mode have been also reported by MBE.[54,55)] The InGaN dots grown by MBE were characterized by macroscopic PL[54,55)] or time-resolved PL.[56)] Moreover, the S–K growth of GaN QDs on an AlN layer has been demonstrated using a 6H-SiC substrate by low-pressure metalorganic chemical vapor deposition (MOCVD).[57)]

On the other hand, a few tens of InGaN dots fabricated by selective growth technique have been investigated by CL.[58]

In addition, the electronic states of $In_{0.2}Ga_{0.8}N$/GaN QDs[36] or GaN/AlN QDs[59] have been investigated by the numerical calculation.

However, the research with respect to GaN-based QDs has just begun. The detail of growth mechanism or single dot spectroscopy had not been investigated closely.

1.3 Synopses of this thesis

In this thesis, the growth and optical properties of GaN-based QDs are investigated to establish the growth mechanism of the QDs and understand the physical properties of the QDs deeply for the realization of GaN-based QD devices. The relationship between the chapters in this thesis and previous works is shown in Fig. 1.2.

In Chapter 2, the growth and optical properties of nanometer-scale $In_xGa_{1-x}N$ self-assembled QDs are described. $In_xGa_{1-x}N$ self-assembled QDs have been successfully grown on a GaN layer without any anti-surfactants using atmospheric-pressure MOCVD. The dependence of the QDs on the growth conditions is investigated systematically. The intense PL is observed from the QDs at room temperature. The very sharp peaks are measured with the linewidth of 170 μeV, by the microscopic PL (μ-PL) using the QD sample with 400-nm square apertures on metal-masked surface. The narrow PL peak is a support of the 3-D quantum confinement of carriers in the QDs. To increase total QD density, the multi-layer stacked QDs are investigated. As the number of stacked layers increases, the higher total QD density and PL intensity are realized.

In Chapter 3, selective growth of $In_xGa_{1-x}N$ QDs and their optical properties are discussed to realize high uniformity of the QDs. By selective growth, the $In_xGa_{1-x}N$ QDs have been formed on the uniform array of hexagonal pyramids of GaN. The intense PL from InGaN is observed at room temperature. To identify the emitting region, the micro-PL intensity images are taken with a high spatial resolution as high as a few hundred

nanometers. It is found that the InGaN PL is only from the tops of hexagonal pyramids. Therefore, it is confirmed that $In_xGa_{1-x}N$ QDs are formed on the tops of hexagonal pyramids of GaN. To realize the higher-density selectively-grown $In_xGa_{1-x}N$ QDs, the substrate is used with a fine pattern prepared by electron-beam (EB) lithography. The uniform array of hexagonal pyramids including $In_xGa_{1-x}N$ QDs is obtained even such a fine pattern is formed.

In Chapter 4, selective growth of GaN QDs and their optical properties are discussed. As GaN has wider bandgap than $In_xGa_{1-x}N$, GaN QDs are expected to be used in the shorter-wavelength (UV) optical devices. Also, as GaN is binary, the physical properties of GaN QDs are simpler to discuss, compared to $In_xGa_{1-x}N$ QDs. GaN QDs embedded in $Al_xGa_{1-x}N$ matrix have been formed on the array of hexagonal pyramids of GaN. The clear PL peak of 3.61 eV is observed from GaN QDs at room temperature.

In Chapter 5, the application of GaN-based QDs to optical devices is described. The laser structure is fabricated with 10-layer stacked $In_xGa_{1-x}N$ self-assembled QDs embedded in the active layer. First, the $In_xGa_{1-x}N$ self-assembled QD lasers are characterized at room temperature under optical excitation. A clear threshold can be observed in the relation between the emission intensity in transverse-electric (TE) mode and excitation energy. The linewidth is reduced to below 0.1 nm (resolution limit) and the emission is strongly TE-polarized above the threshold. These results indicate lasing action is achieved at room temperature. Next, the growth conditions are investigated with respect to *p*-type GaN and GaN/$Al_xGa_{1-x}N$ superlattices for cladding layer of laser structures. The *p-i-n* laser structure is fabricated and characterized with $In_xGa_{1-x}N$ self-assembled QDs embedded in the active layer.

In Chapter 6, the conclusions of this thesis are described.

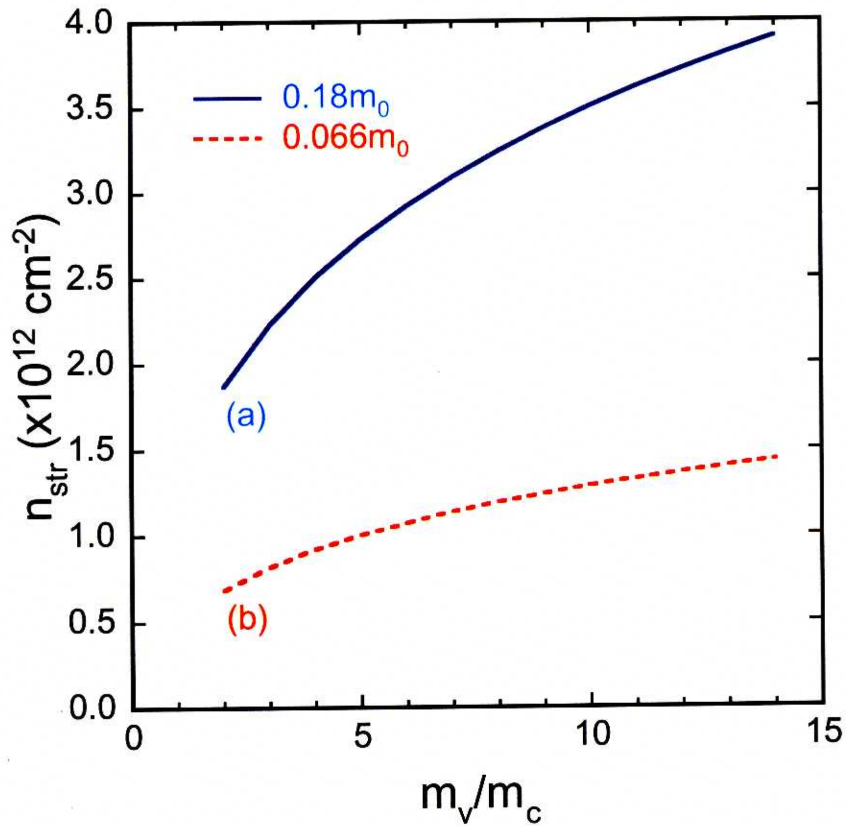

Figure 1.1: The sheet carrier density at transparent condition n_{str} at room temperature as a function of the ratio of the effective mass of holes to that of electrons m_v/m_c under different m_c: (a) $m_c = 0.18m_0$ in GaN and (b) $m_c = 0.066m_0$ in GaAs.

Self-assembled growth
- S. Tanaka *et al.*, APL **69**, 4096 (1996). (anti-surfactant)

- B. Daudin *et al.*, PRB **56**, R7069 (1997). (MBE)
- B. Damilano *et al.*, APL **75**, 962 (1999). (MBE)
- M. Miyamura *et al.*, JCG (in print). (MOCVD)
- J. Brown *et al.*, PSS(b) **228**, 199 (2001). (MBE)

Selective growth
- **Chapter 4**

- *Small size, high density*
- Uniformity?

GaN QDs

InGaN QDs

- *Uniformity, control of position*
- High density?

Self-assembled growth
- H. Hirayama *et al.*, APL **72**, 1736 (1998). (anti-surfactant)

- **Chapter 2**
- B. Damilano *et al.*, APL **75**, 3751 (1999).
- C. Adelmann *et al.*, APL **76**, 1570 (2000).

Selective growth
- J. Wang *et al.*, APL **75**, 950 (1999).

- **Chapter 3**

Figure 1.2: The relationship between the chapters in this thesis and previous works in GaN-based QDs.

Chapter 2

InGaN Quantum Dots by Self-Assembled Growth

2.1 Introduction

Some studies into the QDs have begun in GaN-based system, to realize the superior characteristics of the devices such as LDs.[22] Nanometer-scale fluctuations of indium composition occur in InGaN QWs,[32,33] so it has been said that this fluctuation leads to "QD like" states. However, to realize QD lasers with the predicted characteristics, an intentionally-controlled QD structure is needed.

Some growth methods have been demonstrated for self-assembled QDs in GaN-based system. In one method, "anti-surfactants" are introduced; before QDs are grown, Si is supplied on the surface. It has been believed that the growth mode is changed from 2-D to 3-D island growth by this anti-surfactant, Si. By this method, GaN dots on an AlGaN layer were first reported, using low-pressure MOCVD.[37] In addition, InGaN dots on an AlGaN layer have been reported, using low-pressure MOCVD.[39] The S–K growth mode is also reported in GaN-based QDs, which has been reported in systems of various materials such as In(Ga)As/GaAs.[27] Using the S–K mode, GaN dots on an AlN layer were reported, in MBE.[47–49] InGaN QDs on a GaN layer were demonstrated, without

any surfactants, using atmospheric-pressure MOCVD and the intense PL was observed at room temperature.[60] After that, InGaN dots on a GaN layer were also reported using the S–K mode in MBE.[54,55]

There is research not only into self-assembled QDs, but also into dots by selective growth. The selectively-grown QDs are discussed in Chapters 3 and 4.

In Chapter 2, the growth and optical properties of $In_xGa_{1-x}N$ self-assembled QDs on a GaN layer are discussed. The average diameter of the QDs is as small as 8.4 nm and the dependence of the QDs on growth conditions is investigated systematically. The intense PL is observed from the QDs at room temperature. The single QD spectroscopy is investigated by μ-PL, so that the very sharp luminescence is clearly observed with the linewidth of 170 μeV. To increase the total density of $In_xGa_{1-x}N$ QDs, a vertically-stacked QD structure has been studied. The PL intensity increases drastically as the number of stacked layers increases.

2.2 Epitaxial growth of GaN on Al_2O_3 substrate by metalorganic chemical vapor deposition

All the samples were grown, using two-flow MOCVD system (by NIPPON SANSO). The growth was performed at the atmospheric-pressure of 1.0×10^5 Pa. $Ga(CH_3)_3$ (trimethylgallium, TMG), $Al(CH_3)_3$ (trimethylaluminum, TMA), and $In(CH_3)_3$ (trimethylindium, TMI) were used as the group III sources. NH_3 was used as the group V source. SiH_4 (10 ppm in H_2) and $(C_5H_5)_2Mg$ (bis-cyclopentadienylmagnesium, Cp_2Mg) were used as n-type and p-type dopants, respectively. H_2 and N_2 were used as the carrier gases. As the additional lines, the sub-flow lines of H_2 and N_2 were equipped. The schematic of the reactor is shown in Fig. 2.1. The substrate is put on the carbon-susceptor coated with SiC. The substrate is heated using rf-coils. The (0001)-oriented Al_2O_3 substrates have the misorientation angle of within 0.25°.

After a 25-nm-thick GaN nucleation layer was deposited at 480 °C on a (0001)-

oriented Al_2O_3 substrate, a 2-μm-thick GaN layer was grown at 1071 °C at a growth rate of 2.2 μm/h. During the growth of the GaN layer, the flow rate of TMG was 88 μmol/min with carrier gases of H_2 and N_2 at 4.0 and 11.5 standard liters per minute (slm), respectively. NH_3 was used with a flow rate of 4.0 slm, which corresponded to a V/III ratio of about 2000.

Figure 2.2 shows an atomic force microscope (AFM)* image of the surface morphology of the GaN layer. The some dark spots and steps can be seen in Fig. 2.2. These dark spots are due to threading dislocations between the GaN layer and Al_2O_3 substrate.[61] Hence, the dislocation density in this sample can be estimated roughly to be 6×10^8 cm^{-2}, which is as good as a previous report.[61] The height of the steps is about 0.3 nm, which corresponds to half the value of the c-axis length of GaN, therefore, these steps are mono-layer steps. The root-mean-square roughness is 0.17 nm, so the GaN surface is quite flat. This growth condition of GaN layer is used in all the samples described below.

2.3 Epitaxial growth of InGaN self-assembled quantum dots under various growth conditions

2.3.1 Dependence on InGaN coverage

After a 1.5-μm-thick GaN layer was grown under the condition described in Section 2.2, the growth temperature was set to 750 °C. The flow rates of TMG and TMI during the growth of InGaN were 10 and 35 μmol/min, respectively. The gas flow rates of NH_3, H_2, and N_2 were 10.0, 0.20, and 12.3 slm, respectively. The growth rate was estimated to be 0.21 mono-layer (ML)/s. The nominal indium composition in the $In_xGa_{1-x}N$ QDs is between 0.2 and 0.4. This growth rate is derived from the thickness of InGaN QWs, which were measured using cross-sectional transmission electron microscopy (TEM). The indium composition is estimated using x-ray diffraction (XRD) and the PL peak value. Note

---

*NanoScope E or Nanoscope IIIa (by Digital Instruments) was used for AFM observation.

that it is impossible to know the exact composition in such small structures. The samples were grown, which differ in the growth time of the InGaN. The InGaN coverage was varied from 0.53 to 11 ML. The dependence on the InGaN coverage was closely investigated, especially in the range between 0.53 and 2.1 ML. After InGaN was deposited, the samples were put for 30 s at the same growth temperature of 750 °C under the atmosphere of NH_3 and N_2.

Figure 2.3 shows AFM images of $In_xGa_{1-x}N$ QDs under the various coverages: (a) 0.53, (b) 1.1, (c) 1.6, (d) 2.1, and (e) 6.3 ML. In Fig. 2.3(a), the average diameter and height of the QDs are 23 and 8.7 nm, respectively. The QD density is 4.8×10^8 cm^{-2}. In Fig. 2.3(b), the QD density increases up to 1.0×10^9 cm^{-2} by the coverage of 1.1 ML. Here, the average diameter and height of the QDs are 18 and 7.4 nm, respectively. In Fig. 2.3(c), the $In_xGa_{1-x}N$ QDs and locally-formed islands can be seen. As the InGaN coverage increases, locally-formed islands get collided in Figs. 2.3(d) and 2.3(e) and the QDs are formed on the collided islands. In Fig. 2.3(e), the average diameter and height of the QDs are 16 and 2.9 nm, respectively. The QD density is 1.3×10^{10} cm^{-2}.

Figure 2.4 shows the dependence of the QD density on the InGaN coverage. The QD density increases drastically as the InGaN coverage increases up to 2.1 ML. After that, the QD density is saturated at the value of around 10^{10} cm^{-2}. Note that the density of the QDs is varied from 5×10^8 to 1×10^{10} cm^{-2} by choosing the InGaN coverage in the range between 0.53 and 11 ML.

From the curve in Fig. 2.4, the critical thickness from 2-D growth to 3-D growth is estimated to be around 1 ML. The lattice mismatch in the $In_xGa_{1-x}N$/GaN in a-axis direction is as small as ~2–4% when x is ~0.2–0.4, so that it might be considered that the larger critical thickness is needed to form $In_xGa_{1-x}N$ QDs by strain effect, considering the fact that the critical thickness is around 1.5 ML[62)] in the InAs/GaAs QDs at the lattice mismatch in the InAs/GaAs of 7%. However, the critical thickness depends on the many parameters such as the exact value of x in the $In_xGa_{1-x}N$ QDs, lattice mismatch in the $In_xGa_{1-x}N$/GaN, and surface energy. The precious determination of the critical thickness

in the $In_xGa_{1-x}N/GaN$ QDs will be the next step.

The dependence of the $In_xGa_{1-x}N$ QD density on the coverage in Fig. 2.4 is partially similar to that of InAs/GaAs QDs by S–K growth mode.[62] InAs QDs are formed when the InAs coverage is between 1.5 and 2.0 ML,[62] so the QDs grown by the S–K mode are sensitive to the coverage. Here, $In_xGa_{1-x}N$ QDs are found to be formed with a wide range of coverages from 0.53 to 11 ML, although the rapid increase of the QD density can be observed in the range between 0.53 and 2.1 ML. The formation of $In_xGa_{1-x}N/GaN$ QDs may be due to phase separation as well as strain effect dominantly. More investigation is needed of the effect of the growth conditions to better understand the growth mechanism of $In_xGa_{1-x}N/GaN$ self-assembled QDs.

2.3.2 Dependence on growth temperature

Here, investigated was the dependence of $In_xGa_{1-x}N$ QD properties on the growth temperature. The growth temperature was varied from 720 to 820 °C under the same growth conditions as described in Section 2.3.1. The InGaN coverage was fixed at 1.1 ML.

Figure 2.5 shows the surface morphology of the samples grown at (a) 720, (b) 750, and (c) 820 °C. In Fig. 2.5(a), the average diameter and height of the QDs are 16 and 4.2 nm, respectively. The QD density is 1.6×10^{10} cm^{-2}. In Fig. 2.5(b), the average diameter and height of the QDs are 18 and 7.4 nm, respectively. The QD density is 1.0×10^{9} cm^{-2}. From Fig. 2.5, the each QD is bigger and the QD density decreases as the growth temperature is raised. As shown in Fig. 2.5(c), the step-flow surface can be observed and no QDs are formed at 820 °C, because of too high growth temperature. The dark spots in Fig. 2.5(c) are the same as those in Fig. 2.2, due to the dislocations between the GaN layer and Al_2O_3 substrate.

Note that the average diameter is reduced from 18 to 16 nm by changing the growth temperature from 750 to 720 °C. This is because the lower growth temperature suppresses the migration of In and Ga atoms, so that the QDs with the smaller diameter are realized. Indeed, the smallest QDs can be realized with the average diameter of 8.4 nm and the

height of 2.1 nm at the growth temperature of 700 °C after choosing the proper InGaN coverage and flow rates of TMG/TMI. This dependence of the $In_xGa_{1-x}N$ QDs on the growth temperature is similar to that of InAs/GaAs QDs.[63)]

2.4 Optical properties of InGaN quantum dots

2.4.1 Photoluminescence from InGaN quantum dots

To investigate optical properties of the QDs, a single layer of $In_xGa_{1-x}N$ self-assembled QDs was capped with a 14-nm-thick $In_{0.02}Ga_{0.98}N$ at the same growth temperature as the QDs. To ensure intense PL, the growth temperature of the QDs was set to 770 °C. The flow rates of TMG and TMI during the growth of $In_xGa_{1-x}N$ QDs were 10 and 71 μmol/min,[†] respectively. The gas flow rates of NH_3, H_2, and N_2 were 10.0, 0.20, and 12.3 slm, respectively. The growth rate was around 0.21 ML/s. The InGaN coverage for the QDs was 11 ML. The average diameter and height of the QDs are 23 and 4.6 nm, respectively, in the uncapped sample as shown in Fig. 2.6(a). The QD density is 1.0×10^{10} cm^{-2}.

PL measurements were performed using a He–Cd laser (IK3351R–G by KIMMON Electric) as the excitation source. The peak energy and power density at sample were 3.82 eV and 5 W/cm^2, respectively. The collected light was dispersed by a 0.3 m monochromator (SpectraPro 300i by ACTON Research)[‡] and detected by a liquid nitrogen-cooled charge-coupled device (CCD) camera (LN/CCD-1340/1 by Princeton Instruments) with 1340×100 pixels.[§]

Figure 2.6(b) shows the PL spectrum of the $In_xGa_{1-x}N$ QDs at room temperature. The

[†]The high TMI flow rate is due to compensating for the indium evaporation at high growth temperature. It is also favorable for the stronger quantum confinement in $In_xGa_{1-x}N$ QDs.

[‡]This monochromator has three gratings: (a) 300 grooves/mm with 500 nm blaze, (b) 1200 grooves/mm with 500 nm blaze, and (c) 2400 grooves/mm with 240 nm blaze.

[§]The spectral resolution is (a) 0.8 nm when using the monochromator grating of 300 grooves/mm, (b) 0.2 nm when using the monochromator grating of 1200 grooves/mm, or (c) 0.1 nm when using the monochromator grating of 2400 grooves/mm. Here, the monochromator grating of 300 grooves/mm was used, so the spectral resolution was 0.8 nm.

peak energy is 2.86 eV and the full width at half maximum (FWHM) is 390 meV, which is more than that for InGaN QWs (~ 100 meV). It is considered that this broad spectrum is attributed to the fluctuations in size and indium composition.

2.4.2 Microscopic photoluminescence study of InGaN quantum dots

In macroscopic PL, so many (10^6–10^8) QDs have been excited by a He–Cd laser. At present stage, the QDs have the size variation and indium composition fluctuation. Therefore, if so many QDs are excited, it is almost impossible to investigate the single dot spectroscopy. Here, μ-PL is investigated using the QD sample with 400-nm square apertures on metal-masked surface, which enables ones to investigate the single dot spectroscopy.

The sample was same as discussed in Section 2.4.1. A 100-nm-thick Al layer was evaporated on the sample surface and a mask pattern was fabricated by EB lithography. By wet chemical etching, square apertures of side length 400 nm were formed on the Al mask. It is estimated that about 20 QDs are contained in each aperture.

As the excitation source, 351 nm line of an Ar^+ laser was used. The laser beam was focused on the sample surface by an objective lens of which the nominal magnification factor was 50. The diameter of laser spot was about 2 μm. The sample was mounted in a He flow cryostat and could be cooled down to about 3.5 K. The PL signal was collected by the same objective lens, and detected by a liquid nitrogen-cooled CCD camera (LN/CCD-1340/100-EB/1 by Princeton Instruments) with 1340×100 pixels through a 0.5 m monochromator (SpectraPro 500i by ACTON Research). The highest spectral resolution of this measurement system was about 0.03 nm (170 μeV) when using the monochromator grating of 2400 grooves/mm. The laser spot and its position on the sample surface were monitored by another CCD camera. The detail of the single dot spectroscopy has been discussed elsewhere.[64)]

A typical μ-PL spectrum of $In_xGa_{1-x}N$ QDs is shown in Fig. 2.7. The μ-PL spectrum is measured at 3.5 K. The narrowest line has FWHM of about 170 μeV, which is limited by the spectral resolution of this measurement system. This narrow line can be regarded as

luminescence from a localized electronic state.[65] It should be noted that such sharp peaks are measured by reducing the number of QDs in the observation area to 20 because of 400-nm square apertures on Al-covered QD sample and using μ-PL. Indeed, in Fig. 2.7, about 20 discrete lines can be observed, showing good agreement the number of excited QDs.

Figure 2.8 shows the temperature dependence from 4 to 60 K of the narrow luminescence line. Figure 2.8(a) shows spectra of a narrow line at different temperatures. Figure 2.8(b) shows the temperature dependence of the FWHM, which is derived from Lorentzian fitting of the spectra. In Fig. 2.8(b), the thermal energy $k_B T$ and spectral resolution are also shown. The FWHM is limited by spectral resolution below 30 K and broadens above 30 K. The large linewidth broadening above 40 K is also seen in InAs QD structures and the rate of broadening in $In_xGa_{1-x}N$ QDs is almost the same as that in InAs QDs.[66,67] This behavior in InAs QDs can be explained by the contribution of acoustic phonons to the dephasing process as temperature increases. In $In_xGa_{1-x}N$ QDs, this behavior could be also explained by the same reason, however, the further investigation is needed. Note that this rate of broadening is much smaller than the thermal energy dispersion. This supports the idea that the narrow luminescence lines are considered to be originating from the 3-D quantum confinement states in the QD structures.

For comparison, μ-PL was investigated using the 400-nm square apertures on the Al-covered surface of $In_xGa_{1-x}N$ single QW sample. However, the discrete narrow luminescence lines could not be observed. This fact also indicates that the narrow luminescence lines in Fig. 2.7 are considered to be due to the 3-D quantum confinement states in the QD structures. It is expected that the sharp peaks from InGaN QWs could be observed using high spatial resolution measurements, since it has been said that nanometer-scale fluctuations of the indium composition in $In_xGa_{1-x}N$ QWs create "QD-like" states.[32,33] The reason why such sharp peaks could not be observed from $In_xGa_{1-x}N$ QWs using μ-PL is considered to be the same as the reason why no direct evidence of electron confinement from indium composition fluctuations in $In_xGa_{1-x}N$ QWs using other measurements with

high spatial resolution such as CL[68] or near-field optical microscopy (NSOM);[69,70] if the period of compositional fluctuations is 20 nm, about 400 potential minima will exist in one 400-nm square aperture and luminescence signals of individual potential minima cannot be distinguished. If much higher spatial resolution could be achieved, discrete emissions from nanometer-scale fluctuations of indium composition might be investigated.

2.5 Multiple-layer stacked InGaN quantum dots

To increase the total QD density, vertical stacking of the QDs is an interesting method. Stacked QDs have been investigated in various material systems such as InAs/GaAs.[71–74] In GaN-based system, stacked QDs have been demonstrated in the GaN/AlN system, which were investigated by cross-sectional TEM,[47,50,75,76] PL,[77] or XRD.[78] In this section, the growth and optical properties of stacked $In_xGa_{1-x}N$ QDs are discussed.

After a 2-μm-thick GaN layer was grown by the same method as described in Section 2.2, the growth temperature was set to 750 °C. The flow rates of TMG and TMI during the growth of InGaN QDs were 10 and 35 μmol/min, respectively, which were same as those in Section 2.3.1. The gas flow rates of NH_3, H_2, and N_2 were 10.0, 0.20, and 12.3 slm, respectively. The growth rate was 0.21 ML/s. Here, the InGaN coverage was 11 ML. Then, 5.0 nm of $In_{0.02}Ga_{0.98}N$ was grown as a spacing layer and $In_xGa_{1-x}N$ QDs were grown again under the same growth conditions as above.

Figure 2.9 shows AFM images of (a) single-layer, (b) 3-layer, (c) 10-layer $In_xGa_{1-x}N$ QD structures. From Fig. 2.9, it is seen that $In_xGa_{1-x}N$ QDs are formed even when the number of stacked layers is 10. In Fig. 2.9(a), the average diameter and height of the QDs are 18 and 3.1 nm, respectively. The QD density is 1.2×10^{10} cm^{-2}. In Figs. 2.9(b) and 2.9(c), the QD densities are 1.2×10^{10} and 2.5×10^{10} cm^{-2}, respectively. As the number of the stacked layers increases, the QD density per layer increases.

To investigate optical properties of stacked $In_xGa_{1-x}N$ QDs, each sample was capped with 14 nm of $In_{0.02}Ga_{0.98}N$. Figure 2.10 shows PL spectra at room temperature of (a)

single-layer, (b) 3-layer, and (c) 10-layer $In_xGa_{1-x}N$ QD structures. The PL intensity of the 3-layer $In_xGa_{1-x}N$ QD structure is about 40 times as much as that of the single-layer structure. The PL intensity of the 10-layer stacked structure is about 180 times as much as that of the single-layer structure. It is considered that this is because the quality of the QD epitaxial layer improves as the QDs are stacked. The stacking of $In_xGa_{1-x}N$ QDs lead to high total QD density and intense PL.

2.6 Concluding remarks

In Chapter 2, the growth and optical properties of $In_xGa_{1-x}N$ self-assembled QDs were reviewed. $In_xGa_{1-x}N$ self-assembled QDs have been successfully grown on a GaN layer without any surfactants using atmospheric-pressure MOCVD. The smallest diameter and height of the QDs were 8.4 and 2.1 nm, respectively. The QD density was 1.0×10^{10} cm^{-2}. The size and density of the QDs could be controlled by changing the growth conditions such as the InGaN coverage and growth temperature.

The intense PL was observed from the QDs even at room temperature. To investigate single dot spectroscopy, μ-PL was performed using the QD sample with 400-nm square apertures on the Al-covered surface. The very sharp luminescence was observed with the typical linewidth of 170 μeV. This narrow linewidth is a support of 3-D quantum confinement of carriers in $In_xGa_{1-x}N$ QDs.

The stacked $In_xGa_{1-x}N$ QDs were investigated to increase total QD density. $In_xGa_{1-x}N$ QDs were formed even when the number of stacked layers was 10. The higher PL intensity was observed as the number of stacked layers increased. These results that the higher QD density and PL intensity are realized by stacking the QDs are favorable to be applied to the active layer of the optical devices.

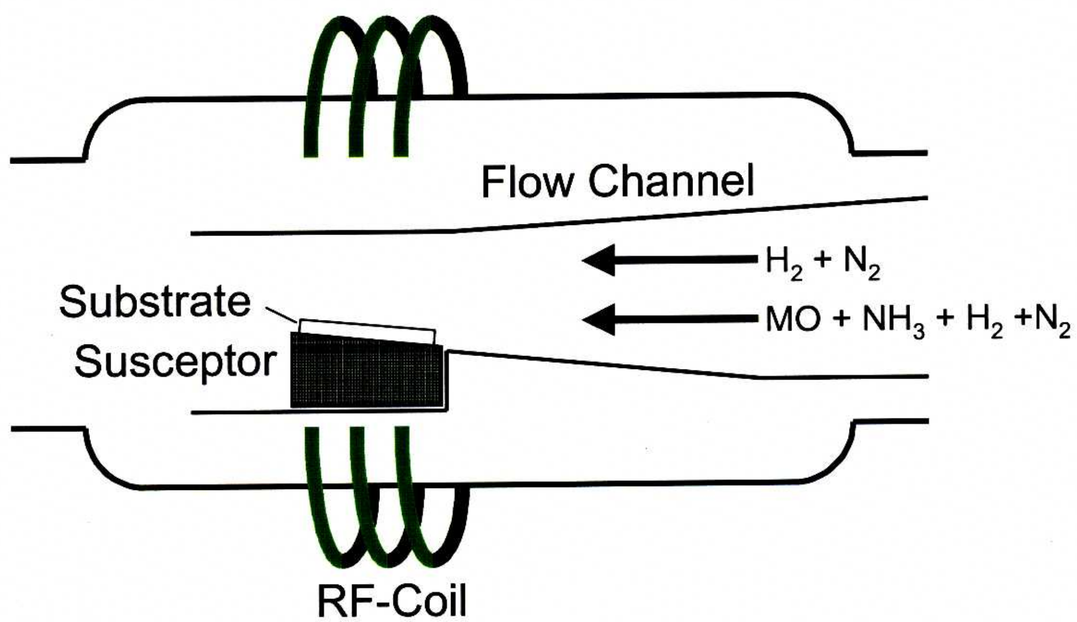

Figure 2.1: An illustration of the reactor in the two-flow MOCVD under the reactor pressure of 1.0×10^5 Pa. The Al_2O_3 substrate is put on the carbon-susceptor coated with SiC. The substrate is heated using rf-coils.

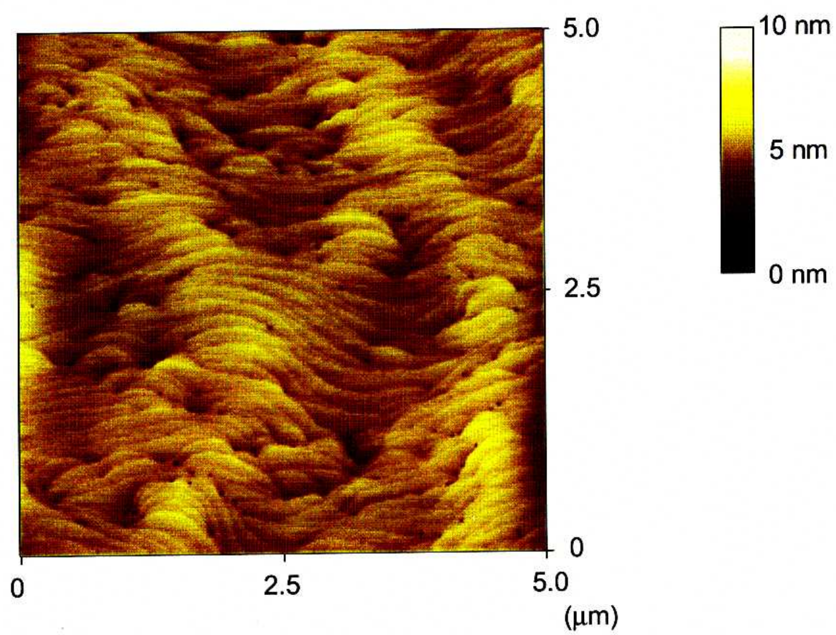

Figure 2.2: An AFM image showing the surface morphology of the GaN layer. The mono-layer steps and dark spots due to dislocations between GaN and Al_2O_3 are observed. The root-mean-square roughness is 0.17 nm.

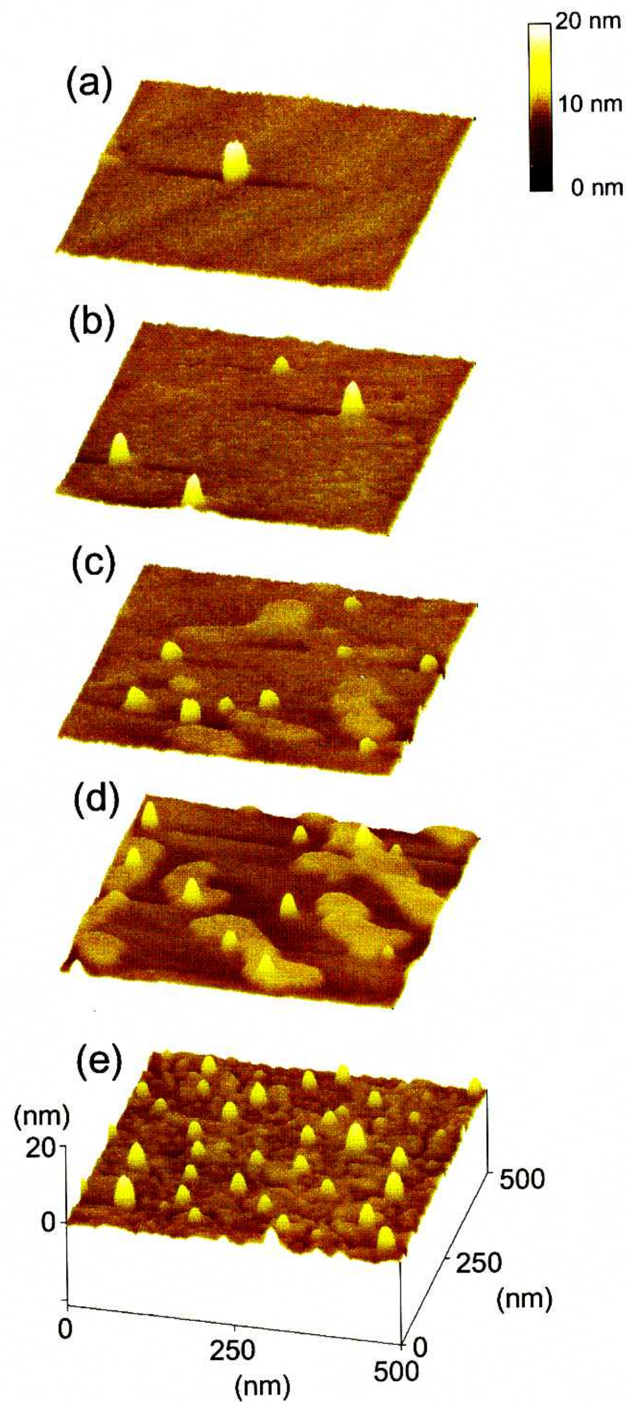

Figure 2.3: Formation process of $In_xGa_{1-x}N$ self-assembled QDs at the coverage of (a) 0.53, (b) 1.1, (c) 1.6, (d) 2.1, and (e) 6.3 ML, measured by AFM. The growth rate was 0.21 ML/s and growth temperature was 750 °C.

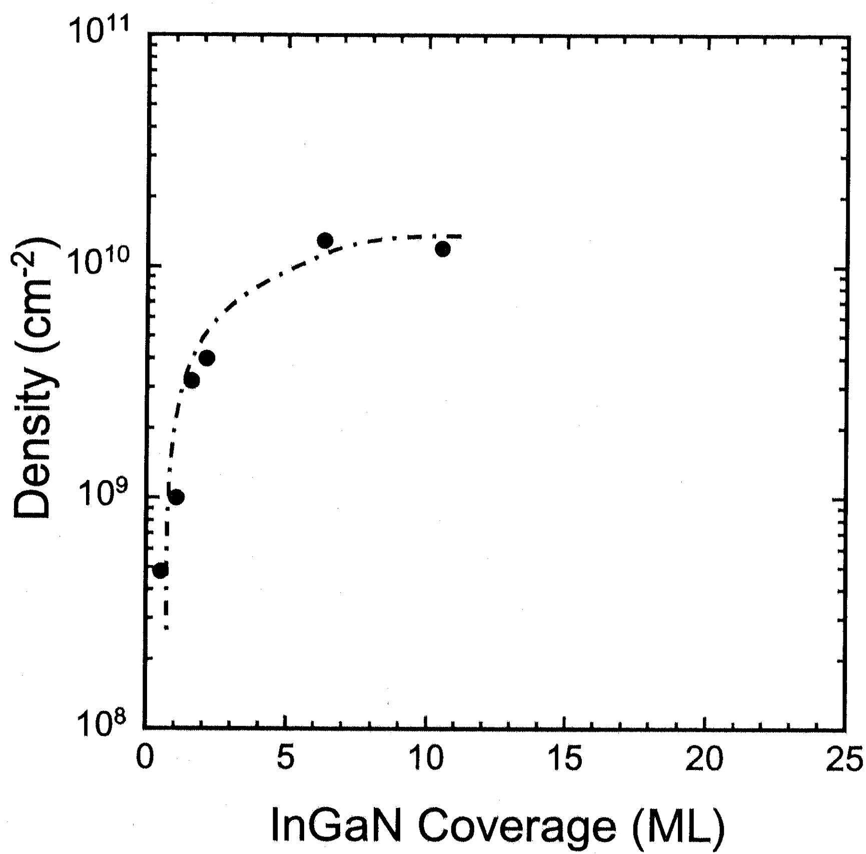

Figure 2.4: Dependence of $In_xGa_{1-x}N$ QD density on the coverage. A part of the surface morphology is shown in Fig. 2.3. The growth rate was 0.21 ML/s and growth temperature was 750 °C.

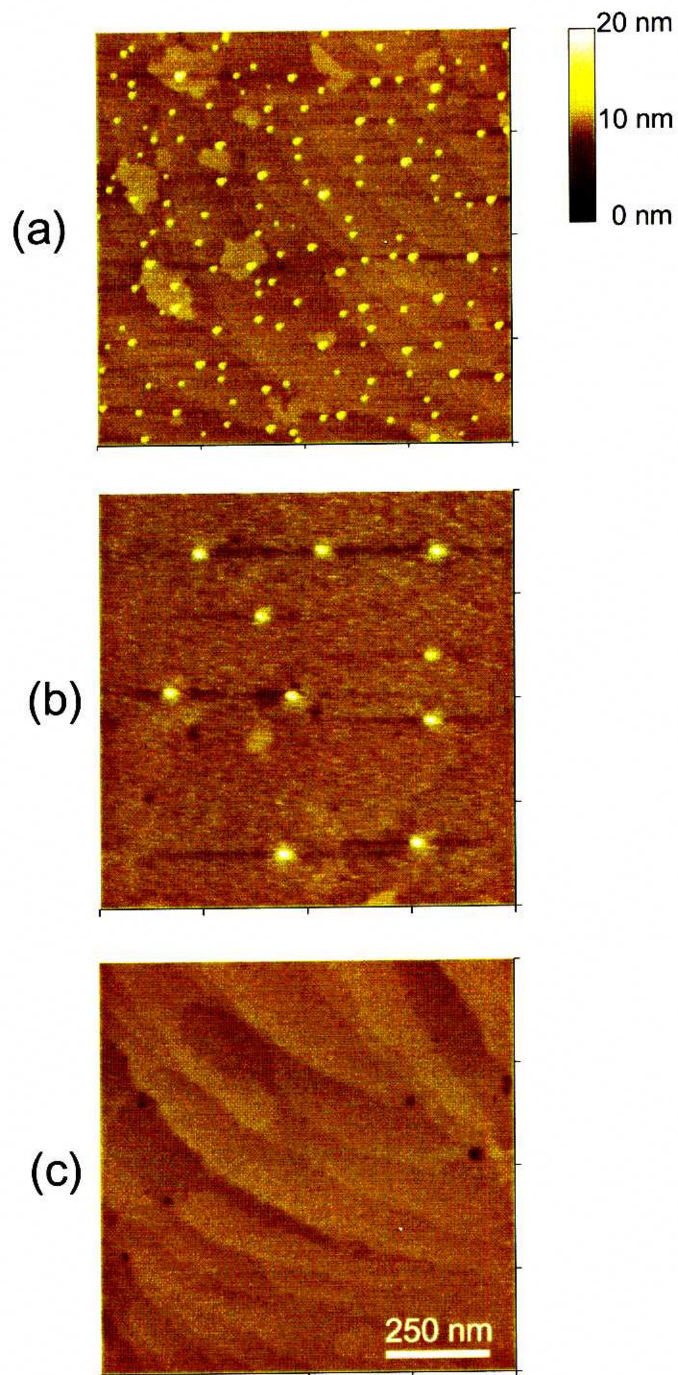

Figure 2.5: AFM images of $In_xGa_{1-x}N$ self-assembled QDs, at the growth temperature of (a) 720, (b) 750, and (c) 820 °C, in the initial stage of the formation. The InGaN coverage was 1.1 ML.

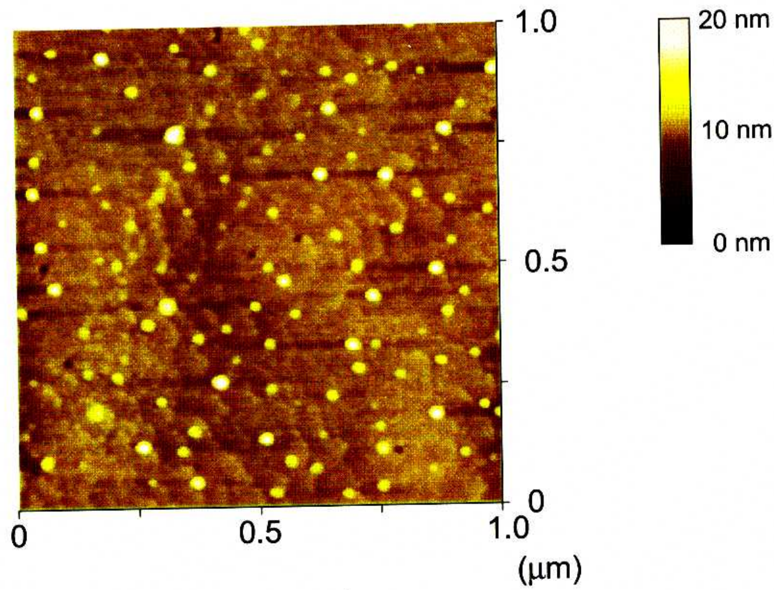

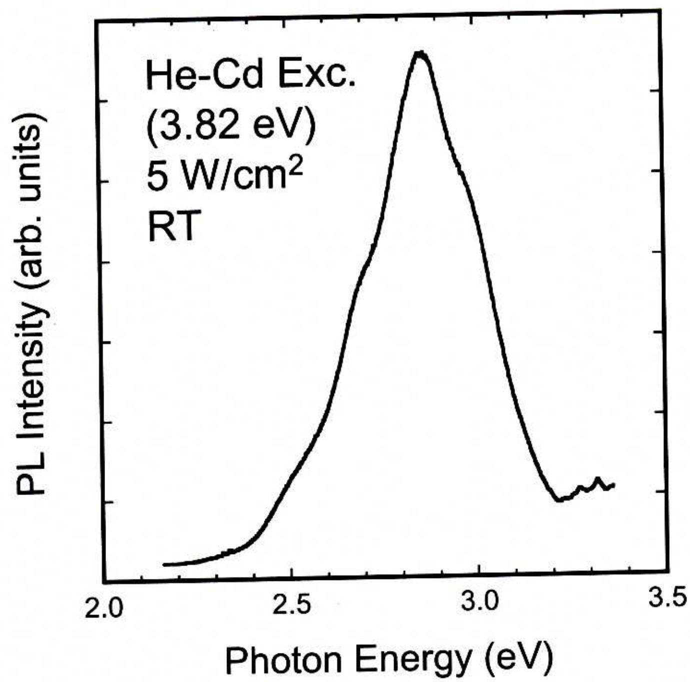

Figure 2.6: (a) An AFM image of uncapped $In_xGa_{1-x}N$ QD sample. The average diameter and height of the QDs are 23 and 4.6 nm, respectively. The QD density is 1.0×10^{10} cm^{-2}. (b) PL spectrum of $In_xGa_{1-x}N$ self-assembled QDs at room temperature.

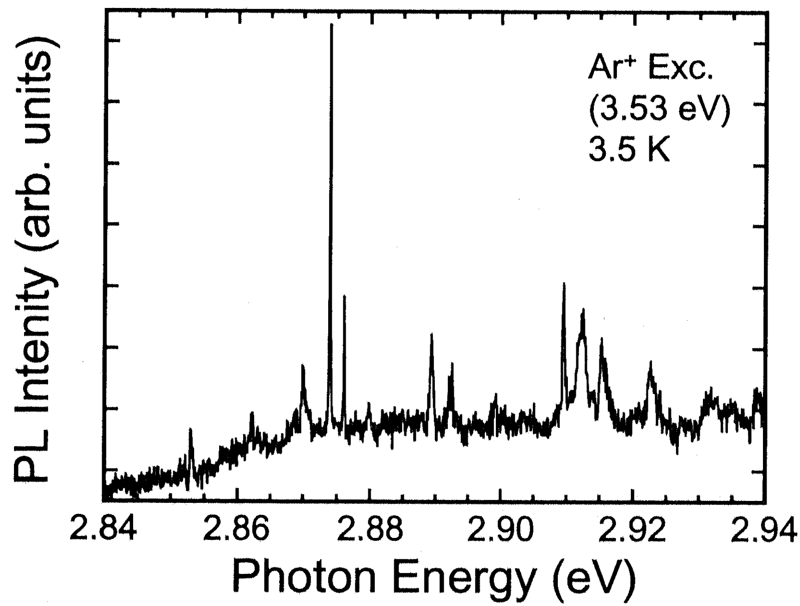

Figure 2.7: Typical μ-PL spectrum of $In_xGa_{1-x}N$ self-assembled QDs. The narrowest FWHM is 170 μeV. This spectrum is measured at 3.5 K.

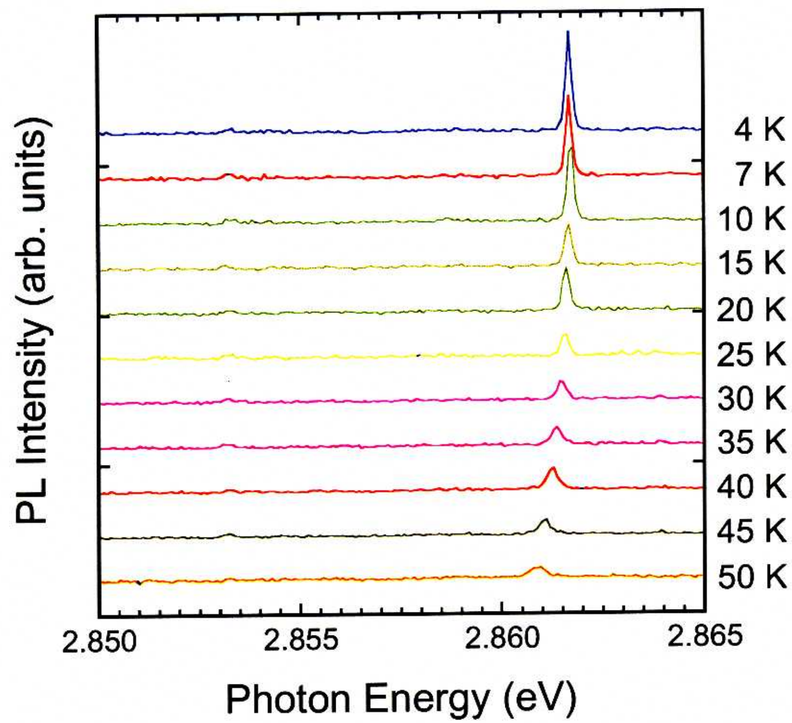

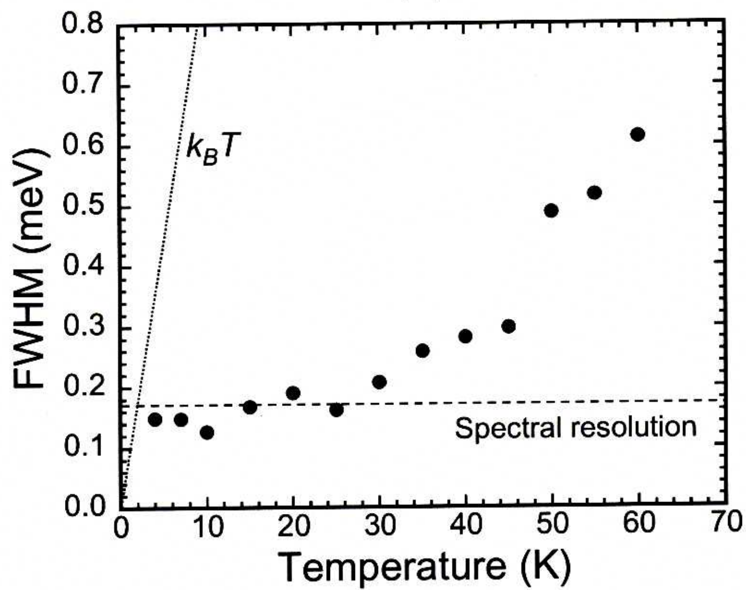

Figure 2.8: (a) μ-PL spectra of a narrow line from $In_xGa_{1-x}N$ self-assembled QDs at various temperatures and (b) temperature dependence of the FWHM. The thermal energy k_BT and spectral resolution are also shown.

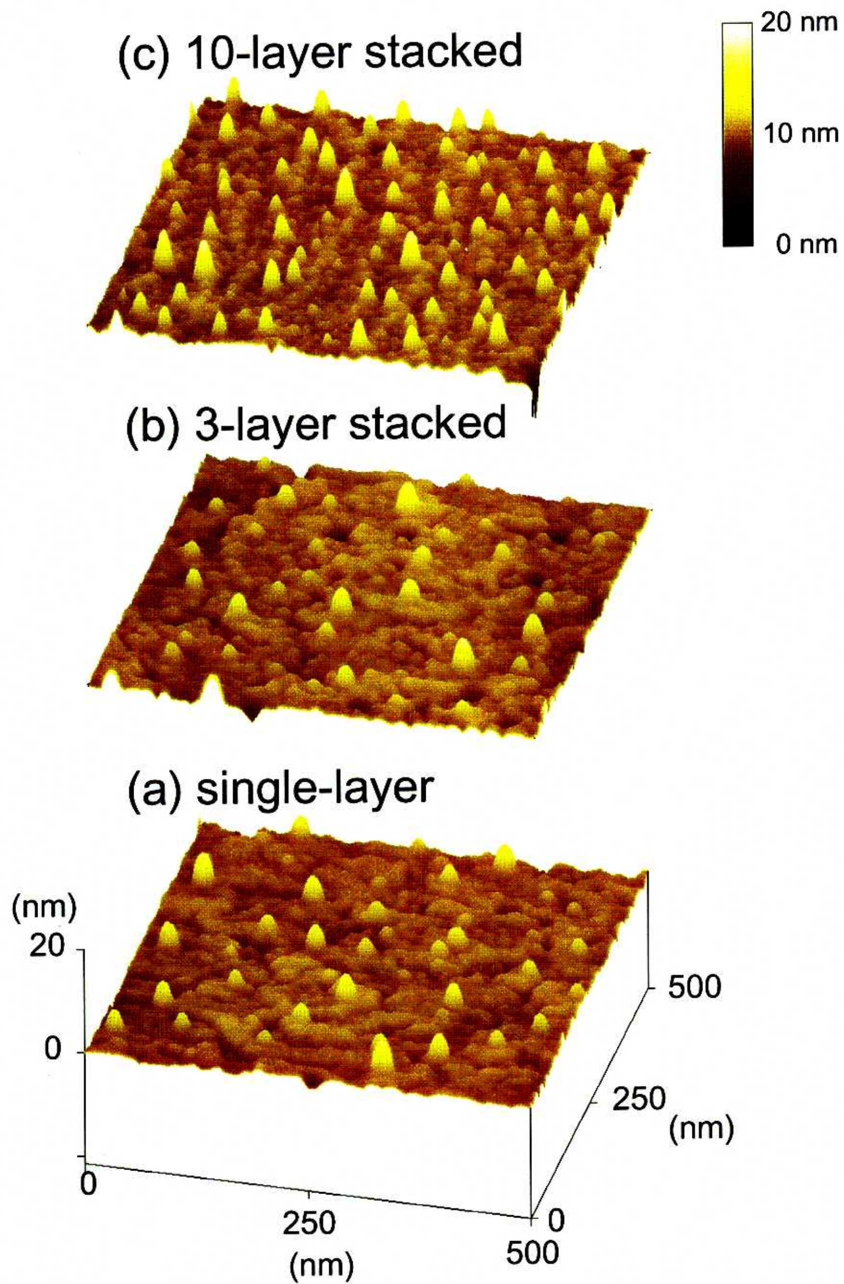

Figure 2.9: AFM images of (a) single-layer $In_xGa_{1-x}N$ QDs, (b) 3-layer stacked QDs, and (c) 10-layer stacked QDs.

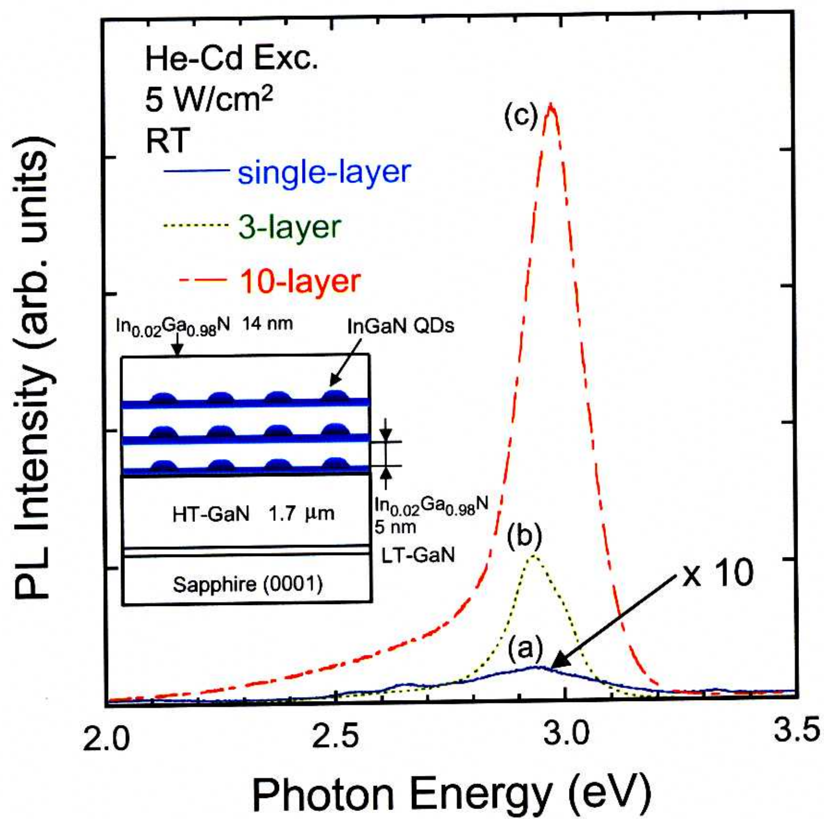

Figure 2.10: PL spectra of (a) single-layer $In_xGa_{1-x}N$ QDs, (b) 3-layer stacked QDs, and (c) 10-layer stacked QDs at room temperature. Inset: schematic of stacked $In_xGa_{1-x}N$ QDs.

Chapter 3

InGaN Quantum Dots by Selective Growth

3.1 Introduction

In Chapter 2, the growth and optical properties of $In_xGa_{1-x}N$ self-assembled QDs were described. The self-assembled QDs are easy to get small structures in nanometer-scale and high density. However, they have the problems how to realize uniformity and control of the positions of structures. To realize the QD lasers with the predicted characteristics,[22] high uniformity of the QD structures is needed. On the other hand, selectively-grown QDs have the advantage of uniformity and control of the position of structures because the selective growth is performed using a patterned substrate, although it remains how to get high QD density.

In GaN-based system, the selective growth was first performed using line and space patterns.[79] After that, the selectively-grown hexagonal pyramids, with (0001) facet on the top and $\{1\bar{1}01\}$ facets on the sides, were realized on a $SiO_2/GaN/Al_2O_3$ substrate with dot patterns.[80] The stimulated emission was observed from selectively-grown GaN by optical pumping[81,83,82] and the electroluminescence was observed from selectively-grown InGaN laser structures by *p-n* junction.[84] Many efforts about selective growth in GaN-

based system have been focused on reducing the dislocation density in GaN/Al_2O_3[85] or $GaN/AlN/6H\text{-}SiC$[86] by the method of epitaxial lateral overgrowth.[87] However, only a few studies have been conducted on the selective growth of InGaN.[58,84,88,89] The growth of pyramids of bulk InGaN on a GaN layer was demonstrated on a $SiO_2/GaN/Al_2O_3$ substrate patterned by photolithography.[89] Also InGaN dots were formed on a $Si/GaN/Al_2O_3$ substrate patterned by focused ion beam etching, and CL was investigated at 80 K for a few tens of dots.[58] Investigated were the micro-PL intensity images of selectively-grown $In_xGa_{1-x}N$ QDs formed on hexagonal pyramids of GaN on a $SiO_2/GaN/Al_2O_3$ substrate.[90]

In Chapter 3, selective growth of $In_xGa_{1-x}N$ QDs is discussed. $In_xGa_{1-x}N$ QD structures have been realized, with good uniformity across the sample, after choosing the growth conditions carefully. The PL spectrum shows a clear peak of InGaN at room temperature. To observe the emitting regions directly, micro-PL intensity images are measured with a spatial resolution of a few hundred nanometers. It is found that the PL originates only from the tops of the hexagonal pyramid structures. The FWHM of the spatial distribution of the intensity is 330 nm, which is comparable to the spatial resolution of the micro-PL intensity images. Such a narrow width of emission areas is support that $In_xGa_{1-x}N$ QDs are formed on the tops of pyramids.

3.2 Metalorganic chemical vapor selective deposition in GaN-based system

To fabricate selectively-grown $In_xGa_{1-x}N$ QDs, it is quite important to realize uniform array of hexagonal pyramids with their radius of curvature at the tops nanometer-scale. In this section, the selectively-grown hexagonal pyramids of GaN under the various growth conditions are discussed.

After a 2.6-μm-thick GaN layer was grown by the same method as described in Sec-

tion 2.2, a 40-nm-thick SiO_2 was deposited using rf sputtering.* The pattern was grid-like, with the period 4 μm and square openings of side length 2 μm, prepared by a conventional photolithography† and a buffered HF solution.‡ Selective growth of GaN was then performed using MOCVD again.

3.2.1 Dependence on growth rate

The set of TMG flow rate and growth time was varied: i) 32 μmol/min and 10 min, ii) 16 μmol/min and 20 min, and iii) 8.0 μmol/min and 40 min. The flow rate of NH_3 was fixed at 4.0 slm and the growth temperature was 1045 °C. When the flow rate of TMG was 32 μmol/min, a V/III mole fraction was 5600. The flow rates of the H_2 and N_2 carrier gases were 4.0 and 11.5 slm, respectively. In planar growth, the growth rate of GaN was 0.80 μm/h under the TMG flow rate of 32 μmol/min with NH_3, H_2, and N_2 at 4.0, 4.0, and 11.5 slm, respectively.

Figure 3.1 shows scanning electron microscope (SEM) (S–5000 by HITACHI) images of selectively-grown GaN under the TMG flow rate and growth time: (a) 32 μmol/min and 10 min, (b) 16 μmol/min and 20 min, and (c) 8.0 μmol/min and 40 min. Although the amounts of GaN deposited are same, the structures are different. In Fig. 3.1(a), the structures have $\{1\bar{1}01\}$ facets on the sides.[80,91,92] Some structures have a large (0001) facet on the top. In Fig. 3.1(b), the formed structures are almost same, but there are no pyramidal structures formed and a few materials deposited in some points. In Fig. 3.1(c), there are no pyramidal structures formed and a few materials deposited in more points than those in Fig. 3.1(b). It is hard to form the pyramidal shapes under too low growth

*SPF–430HS (by ANELVA) was used as rf sputtering. The background pressure was below 6.7×10^{-4} Pa. The rf power was 0.60 kW with the target material of SiO_2. The flow rates of Ar and O_2 were 7.0 and 20.9 sccm, respectively, under the chamber pressure of 4.5×10^{-1} Pa. The deposition rate of SiO_2 was 0.078 nm/s under this condition.

†AZ P1350 (by Clariant) was used as the photo-resist. The sample coated with the photo-resist was spun at 500 rpm for 5 s in the first stage and at 4000 rpm for 40 s in the second stage. It was heated to 90 °C for 30 min as pre-baking. MJB 3UV 300/400 (by Karl Suss) was used as mask aligner. The exposure time was set to 8 s and the developing time was 30 s. The dilute Microposit Developer 351 (by SHIPLEY) was used as the developing solution. It was heated to 90 °C for 15 min as post-baking.

‡The buffered HF solution is cooled to 0 °C. The etching rate of SiO_2 was 3 nm/s.

rate.

It is found that the higher flow rate of TMG is favorable to fabricate the pyramidal structures from Fig. 3.1.

3.2.2 Dependence on NH_3 flow rate

Three samples of selectively-grown GaN have been investigated, which differ in the flow rate of NH_3: i) 0.50, ii) 4.0, and iii) 10.0 slm. The flow rate of TMG was 32 μmol/min with H_2 at 4.0 slm. The flow rate of N_2 was controlled to keep the total gas flow rates 19.5 slm. The growth temperature was 1045 °C and the growth time was 10 min.

Figure 3.2 shows SEM images of samples in which the flow rates of NH_3 were (a) 4.0 and (b) 10.0 slm. When the flow rate of NH_3 was 4.0 slm in Fig. 3.2(a), the structures had the (0001) facet on the top and $\{1\bar{1}01\}$ facets on the sides. In contrast, when the flow rate of NH_3 was 10.0 slm in Fig. 3.2(b), the structures have the larger (0001) facet on top. The side facets cannot be clearly observed. When the flow rate of NH_3 was 0.50 slm, the structures are not uniform. From these results, it is considered that the optimal flow rate of NH_3 is 4.0 slm.

3.2.3 Dependence on growth temperature

Three samples of selectively-grown GaN have been investigated, which differ in the growth temperature: i) 945, ii) 1045, and iii) 1145 °C. The flow rate of TMG was 32 μmol/min with NH_3, H_2, and N_2 at 4.0, 4.0, and 11.5 slm, respectively. The growth time was 10 min.

Figure 3.3 shows SEM images of samples in which the growth temperatures were (a) 945 and (b) 1045 °C. The uniform array of hexagonal pyramids is realized in Fig. 3.3(a). When the growth temperature is higher in Fig. 3.3(b), the structures have the (0001) facet on the top. When the growth temperature is much higher, 1145 °C, the structures are not uniform and some GaN materials under SiO_2 are evaporated.

The $\{1\bar{1}01\}$ facets on the sides are stable at lower growth temperature, which is consistent with the previous study.[92] It is found that the growth temperature of 945 °C is suitable to realize hexagonal pyramids of GaN.

3.2.4 Dependence on growth time

Two samples of selectively-grown GaN have been investigated, which differ in the growth time: i) 6.0 and ii) 12 min. The flow rate of TMG was 32 μmol/min with NH_3, H_2, and N_2 at 4.0, 4.0, and 11.5 slm, respectively. The growth temperature was 945 °C.

Figure 3.4 shows SEM images of samples in which the growth times of GaN were (a) 6.0 and (b) 12 min. In the case of the smaller amount of GaN deposited (Fig. 3.4(a)), the islands have a (0001) facet on the top and some pits can be observed. These pits are due to the dislocations occurring between the GaN layer in planar growth and Al_2O_3 substrate. The side facets cannot be clearly observed. In contrast, uniform hexagonal pyramids are realized in the 12 min growth time sample (Fig. 3.4(b)). The hexagonal pyramids of GaN have $\{1\bar{1}01\}$ side facets. No pits can be observed, because it is considered that the dislocations bend to the side facets as the epitaxial growth proceeds.[93]

3.2.5 Summary

In this section, the selectively-grown GaN has been investigated under the various conditions such as growth rate, NH_3 flow rate, growth temperature, and growth time. The growth rate along the c-axis was enhanced and the $\{1\bar{1}01\}$ facets on the sides were stable as the growth temperature or NH_3 flow rate decreases. The higher growth rate was needed to form pyramidal shapes of GaN. The pyramidal shapes could be realized as the growth time was longer. These phenomena are favorable to the formation of hexagonal pyramids of GaN with their radius of curvature at the tops nanometer-scale.

3.3 Selective growth of InGaN quantum dots

When hexagonal pyramids of GaN were grown, the flow rates of TMG and NH_3 were 32 μmol/min and 4.0 slm, respectively. The flow rates of the H_2 and N_2 carrier gases were 4.0 and 11.5 slm, respectively. The growth temperature was 945 °C and growth time was 12 min.

Selective growth of three periods of $In_{0.2}Ga_{0.8}N/In_{0.02}Ga_{0.98}N$ multiple QWs (MQWs) followed at 720 °C. The growth times for the $In_{0.2}Ga_{0.8}N$ QW and $In_{0.02}Ga_{0.98}N$ barrier materials were such as to give 2.4 and 4.1 nm thicknesses, respectively, in planar growth. The flow rates of TMG and TMI during the growth of the QWs were 2.5 and 7.6 μmol/min, respectively. The flow rates of TMG and TMI during the growth of the barriers were 2.5 and 1.2 μmol/min, respectively. The gas flow rates of NH_3, H_2, and N_2 during the growth of the QWs and barriers were 10.0, 0.20, and 12.3 slm, respectively. Then, a 14-nm-thick $In_{0.02}Ga_{0.98}N$ layer was capped. It is considered that $In_xGa_{1-x}N$ QD structures are formed at the tops of the hexagonal pyramids, as illustrated schematically in Fig. 3.5(a), as demonstrated in a GaAs system.[94)]

Figure 3.5(b) shows an SEM bird's-eye-view of the final structures. As can be seen in Fig. 3.5(b), selective growth of InGaN occurred: no material was deposited on the SiO_2 mask. Figure 3.5(c) shows a cross-sectional image after the sample was cleaved. In Fig. 3.5(c), there is a pattern of horizontal streaks and the top of a hexagonal pyramid looks as if it was damaged in cleaving the sample. It is difficult to estimate the exact radius of curvature, however, the radius of curvature is no more than 30 nm. This indicates that very sharp tops were realized. The lateral size of $In_xGa_{1-x}N$ QDs is considered to be comparable to the radius of curvature, no more than 30 nm, from the value obtained by cross-sectional SEM images. To discuss the lateral size of $In_xGa_{1-x}N$ QDs more precisely, cross-sectional TEM would be help.

3.4 Optical characterization of selectively-grown InGaN quantum dots

3.4.1 Microphotoluminescence intensity images of InGaN quantum dots

PL spectra were measured at room temperature, excited by a He–Cd laser. The diameter of the laser spot on the sample was 0.7 mm, so about 10^5 QD structures were excited. As the monochromator grating of 300 grooves/mm was used, the spectral resolution was 0.8 nm. Figure 3.6 shows the PL spectrum of the sample. The PL peak energy of the $In_xGa_{1-x}N$ structures is 2.88 eV (430 nm), and the FWHM is 290 meV. The spectrum is broad because so many QD structures were excited. The intensity of the $In_xGa_{1-x}N$ PL peak is smaller than that of the GaN PL peak at 3.42 eV, because the volume of $In_xGa_{1-x}N$ QDs is much smaller than that of GaN bulk.

To identify the regions giving the PL at 430 nm, micro-PL intensity images were recorded at room temperature, using a conventional optical microscope (ECLIPSE E400 by Nikon) equipped with an objective lens of which the nominal magnification factor was 100 and the numerical aperture (NA) was 1.3 when immersion oil was used, giving a typical spatial resolution as high as 150 nm.[95)§] The experimental setup is shown in Fig. 3.7. The excitation source was a mercury lamp and the excitation wavelength could be selected using an excitation filter. The sample was uniformly excited and the collected light could be filtered by a high-pass barrier filter and a band-pass filter with a bandwidth of 5 nm, before being detected by an electrically cooled CCD camera (RTE/CCD-1317-K/1 by Princeton Instruments) with 1317 × 1035 pixels.

Figure 3.8(a) shows an image obtained only through a barrier filter of which the cut-off wavelength was 400 nm, without the excitation filter or band-pass filter, so consists mainly of reflected light. In Fig. 3.8(a), hexagonal shapes can be seen very clearly. This

§Here, the spatial resolution Δ is determined from the calculation: $\Delta = 0.52\lambda/\mathrm{NA}$, where λ is the wavelength.

demonstrates that high spatial resolution is achieved. This is because used are an excitation source of short wavelength and an objective lens of NA as high as 1.3 with the immersion oil.

Figure 3.8(b) shows a micro-PL intensity image of PL of wavelength around 430 nm, accumulated over 10 s. The same area was observed in Fig. 3.8(b) as in Fig. 3.8(a). A 365 nm filter was used in excitation and excitation power density at the sample was 1 W/cm^2. In collection, wavelengths shorter than 390 nm were cut off by a barrier filter and a 430 nm band-pass filter of bandwidth 5 nm was used, so the detected light was from the $In_xGa_{1-x}N$ structures only, not from the GaN bulk or from the excitation source. PL in Fig. 3.8(b) is only from the tops of the pyramids. In the cross-sectional profile of PL intensity in Fig. 3.8(c), the FWHM of 330 nm is comparable to the spatial resolution. Such a narrow width of emission areas indicates that the PL originates from $In_xGa_{1-x}N$ QD structures embedded in $In_{0.02}Ga_{0.98}N$ matrix.

The FWHM with respect to the micro-PL intensity image is discussed. As the PL was accumulated for 10 s, drift of the sample is not negligible. As the FWHM is comparable to the spatial resolution of the micro-PL intensity images, the emission width from the micro-PL intensity images cannot be accurately compared with the radius of curvature (no more than 30 nm) from the SEM images. Further investigation is needed to verify the 3-D quantum confinement effect in detail, using magneto-PL or a measurement method with high spatial and spectral resolution, such as NSOM or CL. However, from the micro-PL intensity images, it is demonstrated that the PL is only from the tops of the hexagonal pyramids, not from the edges.

3.4.2 Photoluminescence dependence on excitation power

The single layer of selectively-grown $In_xGa_{1-x}N$ QDs were formed on the uniform array of hexagonal pyramids of GaN. The growth conditions were same as in Section 3.3, except for the following conditions. Selective growth of $In_xGa_{1-x}N/In_{0.02}Ga_{0.98}N$ single QWs was performed on hexagonal pyramids of GaN at 770 °C. The higher growth temperature, than

that in Section 3.3, is chosen to ensure intense PL. The growth times for the $In_xGa_{1-x}N$ QW and $In_{0.02}Ga_{0.98}N$ barrier materials were such as to give 2.0 and 4.1 nm thicknesses, respectively, in planar growth. The flow rates of TMG and TMI during the growth of the QW were 2.5 and 6.4 μmol/min, respectively. The In content x was ~0.10–0.15.

PL measurement was carried out at 5 K. The sample was mounted in a closed-cycle He cryostat. As the monochromator grating of 1200 grooves/mm was used, the spectral resolution was 0.2 nm. Figure 3.9 shows PL dependence on the excitation power density of the He–Cd laser in the range between 5 W/cm^2 and 50 μW/cm^2. In the high excitation intensity of 5 W/cm^2 of Fig. 3.9(a), three peaks are observed at 3.17, 3.22, and 3.27 eV. As lower excitation power density, the peak energy of 3.22 eV disappears and only two peaks remains in such as Figs. 3.9(b) and 3.9(c). From this result, it is considered that the peak energy of 3.17 eV is due to the ground states in the QDs and that of 3.22 eV is due to the excited states in the QDs. The peak of 3.27 eV is considered to be from InGaN QWs on the side facets. The energy separation between the ground states and excited states in the QDs is 50 meV. The energy separation of 50 meV is comparable to the value of $2k_BT$ at room temperature, which is favorable to the application of QDs to the lasers.

3.5 Higher-density InGaN quantum dots on a substrate prepared by electron-beam lithography

The density of selectively-grown QDs is almost determined by the pattern size on the substrate. For the realization of the higher-density selectively-grown QDs, the finer pattern is needed. There were a few researches about selective growth in GaN-based system on a patterned substrate in sub-micrometer scale by laser holography with a He–Cd laser[96] or focused ion beam etching.[58] The EB lithography is useful for the uniform pattern and control of position in nanometer-scale. In this section, higher-density $In_xGa_{1-x}N$ QDs is discussed, using the SiO_2/n-GaN/Al_2O_3 substrate patterned by EB lithography.

3.5.1 Fabrication of higher-density selectively-grown InGaN quantum dots

After a 25-nm-thick GaN nucleation layer was deposited on a (0001)-oriented Al_2O_3 substrate, a 1.1-μm-thick undoped GaN layer was grown under the same growth condition as described in Section 2.2. Next, a 1.5-μm-thick Si-doped GaN layer was grown, to prevent the charge-up due to using a dielectric substrate of Al_2O_3 when the EB lithography was performed. During the growth of the Si-doped GaN, the flow rates of TMG and SiH_4 were 88 μmol/min and 0.89–1.8 nmol/min, respectively. The gas flow rates of NH_3, H_2, and N_2 were 4.0, 4.0, and 11.5 slm, respectively. The electron concentration was 2–4 $\times$ 10^{18} cm^{-3}, confirmed by Van der Pauw (VdP) measurement (HL5500 by Bio-Rad).

A 40-nm-thick SiO_2 was deposited on the surface by rf sputtering. The three grid-like patterns were fabricated: (a) with period 4 μm and square openings of side length 2 μm by conventional photolithography, (b) with period 1 μm and square openings of side length 0.5 μm, and (c) with period 0.6 μm and square openings of side length 0.3 μm by EB lithography.[¶]

Selective growth of GaN was performed under the same growth condition as in Section 3.3. The growth time for the realization of hexagonal pyramids of GaN was different in these patterned substrates, but other growth conditions were same. The growth times for GaN pyramids were 12, 3.0, 1.8 min in the substrates patterned with square openings of side length (a) 2, (b) 0.5, and (c) 0.3 μm, respectively. Selective growth of three periods of $In_{0.2}Ga_{0.8}N/In_{0.02}Ga_{0.98}N$ MQWs followed at 720 °C. The growth times for the $In_{0.2}Ga_{0.8}N$ QW and $In_{0.02}Ga_{0.98}N$ barrier materials were such as to give 2.4 and 4.1 nm thicknesses, respectively, in planar growth. The flow rates of TMG and TMI during the growth of the QWs were 2.5 and 6.4 μmol/min, respectively. The flow rates of TMG and TMI during

[¶]OEBR1000 (by TOKYO OHKA) was used as the polymethylmethacrylate (PMMA) resist. The sample coated with the PMMA resist was spun at 500 rpm for 10 s in the first stage and at 5000 rpm for 60 s in the second stage. It was heated to 190 °C for 90 min as pre-baking. JBX–6000 (by JEOL) was used as EB lithography. After the exposure, developing, and transferring patterns to SiO_2 layer using wet chemical etching with the buffered HF, UV–1 (by SAMCO) was used as UV and ozone stripper at the heating temperature of 300 °C for 30 min, to remove the PMMA resist.

the growth of the barriers were 2.5 and 1.2 μmol/min, respectively. The gas flow rates of NH_3, H_2, and N_2 during the growth of the QWs and barriers were 10.0, 0.20, and 12.3 slm, respectively. Then, a 14-nm-thick $In_{0.02}Ga_{0.98}N$ layer was capped.

Figure 3.10(a) shows SEM bird's-eye-view of the final structures on a substrate patterned with period 0.6 μm and square openings of side length as small as 0.3 μm. As can be seen in Fig. 3.10(a), uniform hexagonal pyramids including the $In_xGa_{1-x}N$ QDs at the tops are realized even when such a fine pattern was formed. Figure 3.10(b) shows a magnified photograph of a hexagonal pyramid. The hexagonal pyramids have $\{1\bar{1}01\}$ side facets. The radius of curvature at the tops of pyramids is no more than 30 nm, as confirmed by cross-sectional SEM images. This indicates that very sharp tops were realized. The lateral size of $In_xGa_{1-x}N$ QDs is considered to be comparable to the radius of curvature at the tops of hexagonal pyramids.

To investigate PL dependence on the pattern size, PL spectra of these samples were measured at room temperature, excited by a He–Cd laser. The excitation power density at the sample was 5 W/cm^2. The diameter of the laser spot on the sample was 0.7 mm. The monochromator grating of 300 grooves/mm was used, so the spectral resolution was 0.8 nm.

Figure 3.11 shows the PL spectra of these samples, in which the spectra are normalized at the value of GaN PL peak around 3.42 eV. $In_xGa_{1-x}N$ PL peak is observed around 2.9 eV in these spectra. The PL intensity increases drastically as the pattern size is finer. Considering that the diameter of laser spot is constant, the number of excited QDs increases as the pattern size is finer. The increase of PL intensity can be explained by the fact that the number of excited QDs increases as the pattern size is finer.

3.5.2 Cathodoluminescence study of InGaN quantum dots

CL is useful for characterizing optical properties with a high spatial resolution. Here, the higher-density $In_xGa_{1-x}N$ QDs were investigated by CL study, on a substrate prepared by EB lithography with the period 1 μm and square openings of side length 0.5 μm.

CL measurement was carried out at 5 K,[97] with the typical acceleration voltage of 5 kV and the beam current of 720 pA. At this condition, the excitation power corresponded to 3.6 μW with the diameter of 250 nm. The spectral resolution was around 2 nm.

Figure 3.12 shows CL intensity mapping of higher-density $In_xGa_{1-x}N$ QDs at the various wavelengths of (a) 350–365, (b) 406–412, and (c) 433–444 nm. In Fig. 3.12(a), the luminescence only from GaN is recorded. The GaN luminescence can be observed mainly from GaN layer under SiO_2, because InGaN is intensively excited due to the high absorption coefficient and GaN is hardly excited in pyramidal structures. In Fig. 3.12(b), the luminescence around InGaN peak is recorded. The luminescence is strongly detected from the tops of hexagonal pyramids, therefore it is confirmed that $In_xGa_{1-x}N$ QDs embedded in $In_{0.02}Ga_{0.98}N$ matrix are formed on the tops of hexagonal pyramids of GaN. In Fig. 3.12(c) at the wavelengths of 433–444 nm, the tail of InGaN CL is recorded. The high CL intensity can be seen on the bases of pyramidal structures, while the small CL intensity can be seen on the top of pyramids.

From CL study, it was confirmed that the InGaN luminescence was intensively observed from the tops of hexagonal pyramids. This result indicates that $In_xGa_{1-x}N$ QDs were formed on the tops of hexagonal pyramids of GaN even when the substrate was used with such a fine pattern.

3.6 Concluding remarks

In Chapter 3, the selectively-grown $In_xGa_{1-x}N$ QDs were described. The uniform array of hexagonal pyramids of GaN were formed at the growth temperature of 945 °C under the flow rates of TMG and NH_3 at 32 μmol/min and 4.0 slm, respectively. The $In_xGa_{1-x}N$ QDs were formed by performing the selective growth of $In_xGa_{1-x}N/In_{0.02}Ga_{0.8}N$ QWs on hexagonal pyramids of GaN.

The intense PL was observed at the wavelength of 430 nm at room temperature. To identify the emitting area of InGaN, micro-PL intensity images were recorded at room

temperature. The uniform array of hexagonal pyramids could be seen in the reflective image, while the PL was observed only from the tops of hexagonal pyramids in the micro-PL intensity image at the wavelength of 430 nm. This result indicates that the selectively-grown $In_xGa_{1-x}N$ QDs were formed on the tops of hexagonal pyramids of GaN.

To get higher-density $In_xGa_{1-x}N$ QDs, the selective growth was performed using a substrate prepared by EB lithography. Even when such a fine pattern was formed, the uniform array of hexagonal pyramids including the QDs at the tops was realized. It was confirmed that the luminescence from InGaN was strongly detected on the tops of hexagonal pyramids by CL study.

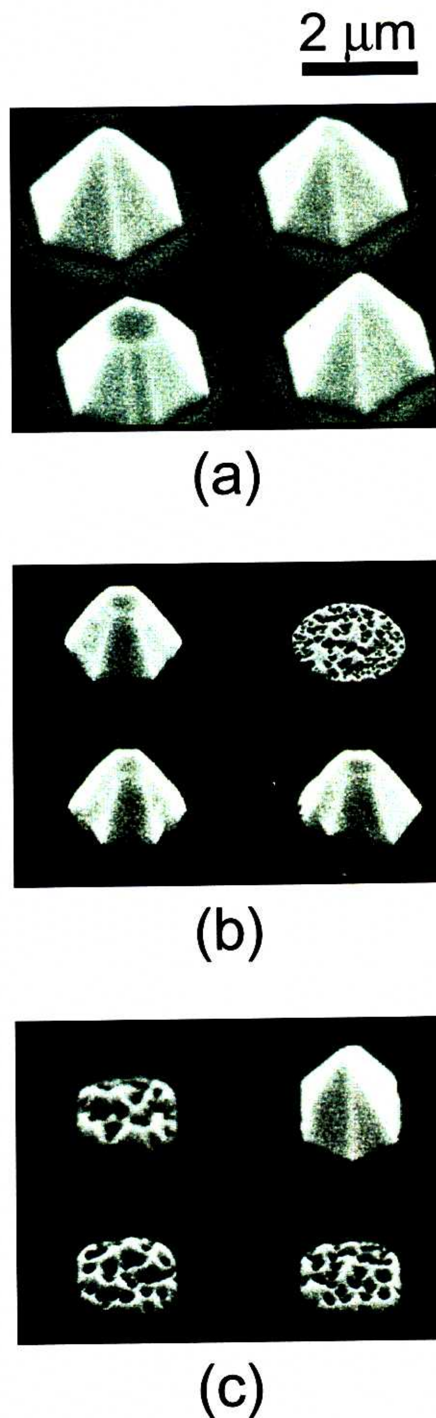

Figure 3.1: SEM bird's-eye-views of GaN formed by selective growth under the set of TMG flow rate and growth time: (a) 32 μmol/min and 10 min, (b) 16 μmol/min and 20 min, and (c) 8.0 μmol/min and 40 min.

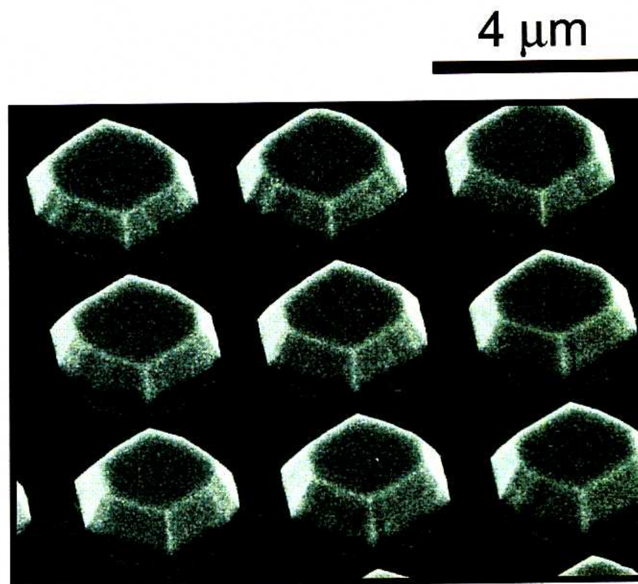

(a)

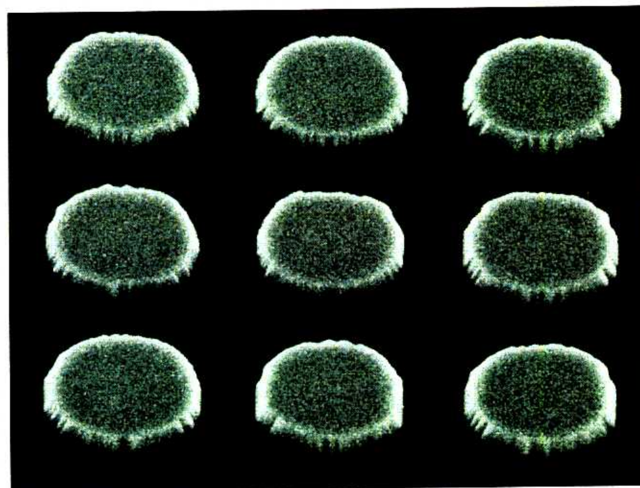

(b)

Figure 3.2: SEM bird's-eye-views of GaN formed by selective growth under the NH_3 flow rates of (a) 4.0 and (b) 10.0 slm.

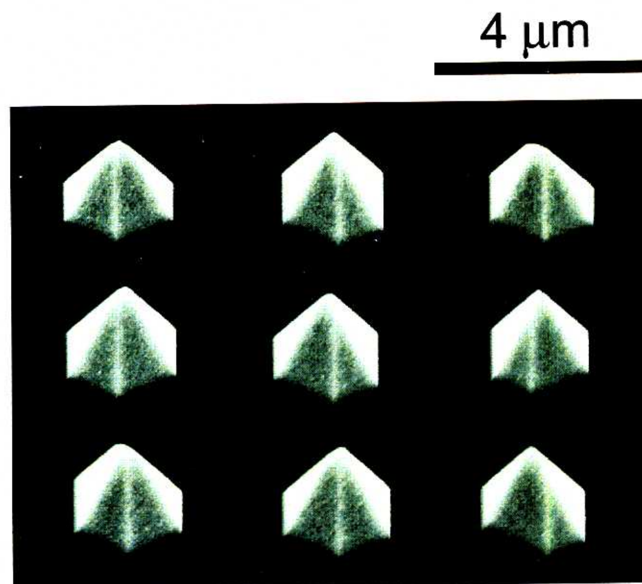

(a)

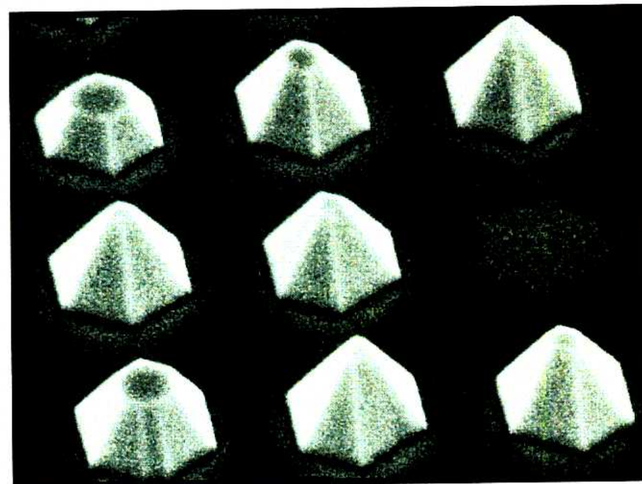

(b)

Figure 3.3: SEM bird's-eye-views of GaN formed by selective growth at the growth temperatures of (a) 945 and (b) 1045 °C.

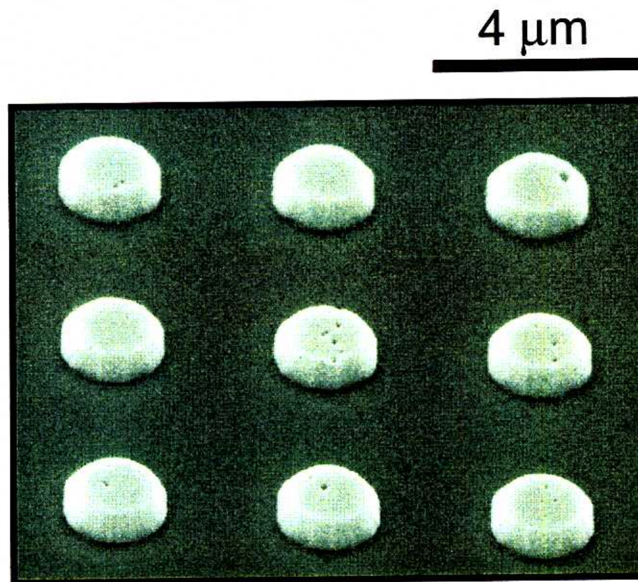

(a)

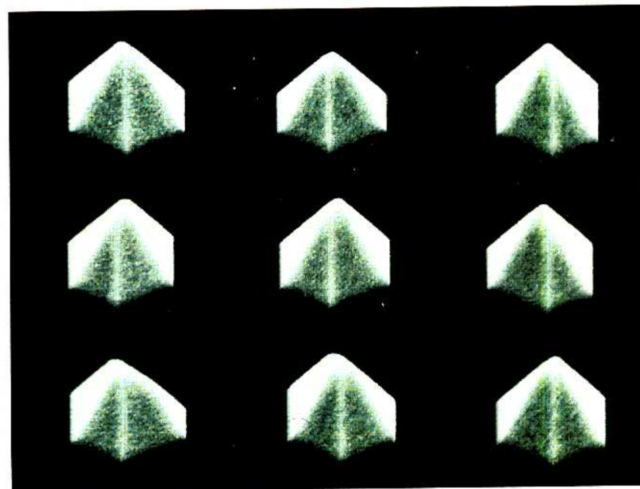

(b)

Figure 3.4: SEM bird's-eye-views of GaN formed by selective growth for growth times of (a) 6.0 and (b) 12 min.

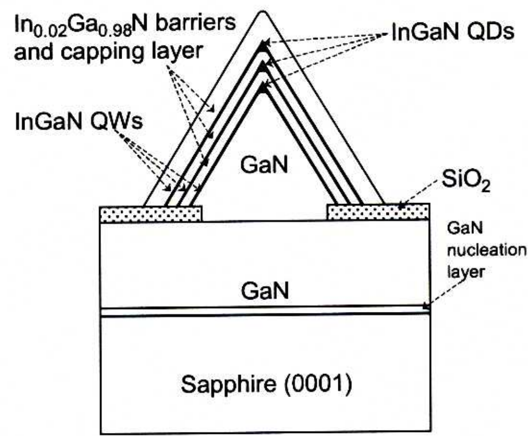

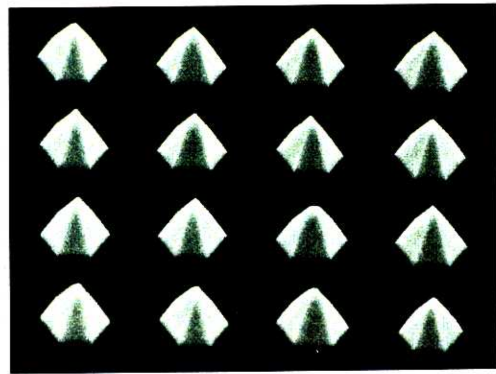

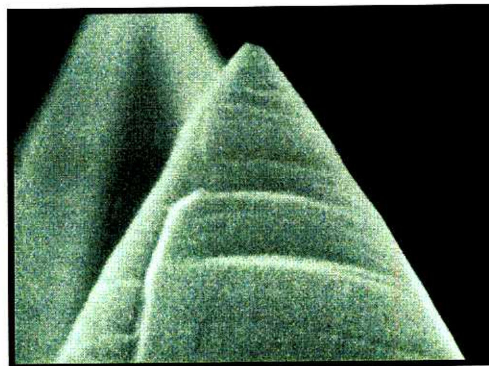

Figure 3.5: (a) A schematic of $In_xGa_{1-x}N$ QDs formed on the tops of hexagonal pyramids of GaN. SEM pictures of the sample: (b) bird's-eye-view and (c) cross section.

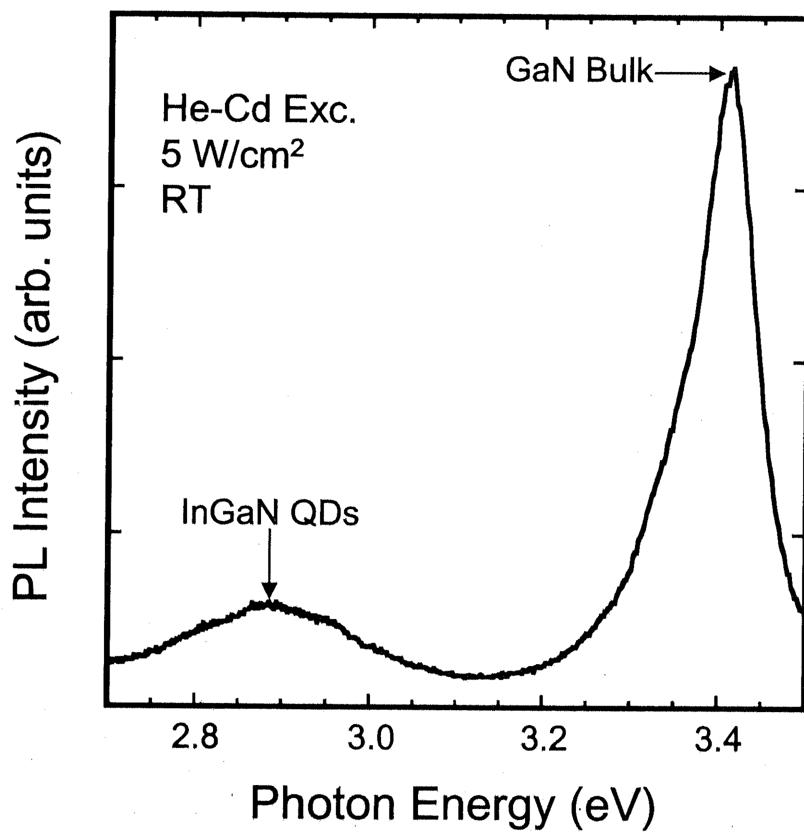

Figure 3.6: PL spectrum of selectively-grown $In_xGa_{1-x}N$ QDs at room temperature.

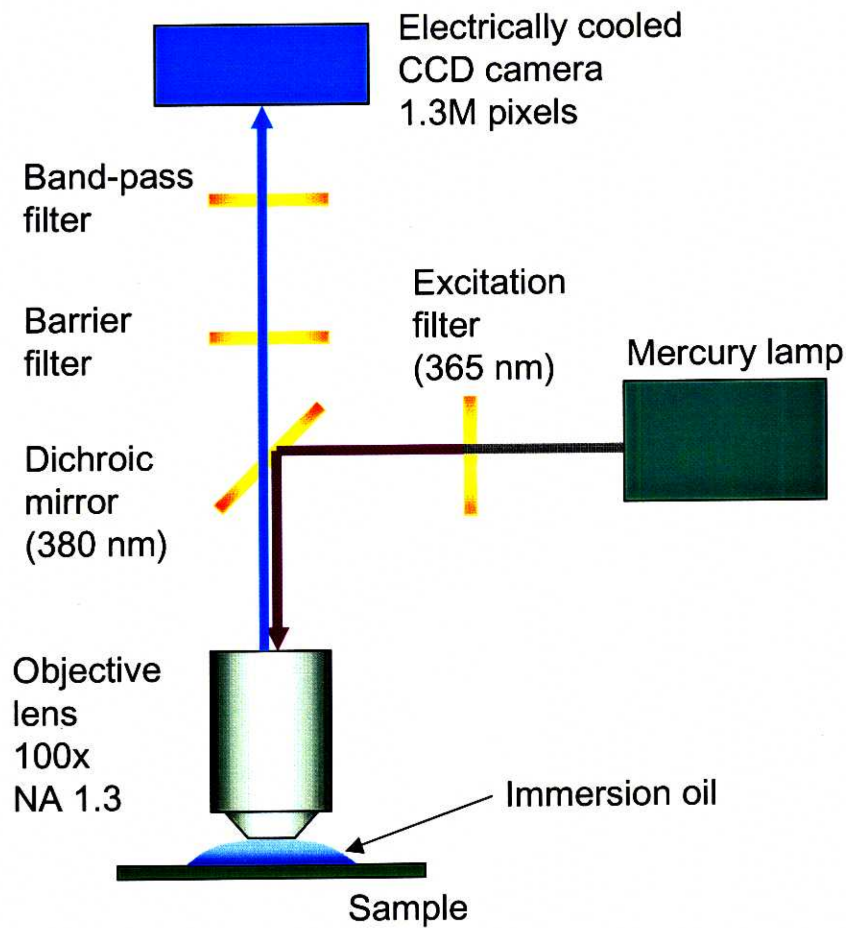

Figure 3.7: Schematic of the experimental setup of micro-PL.

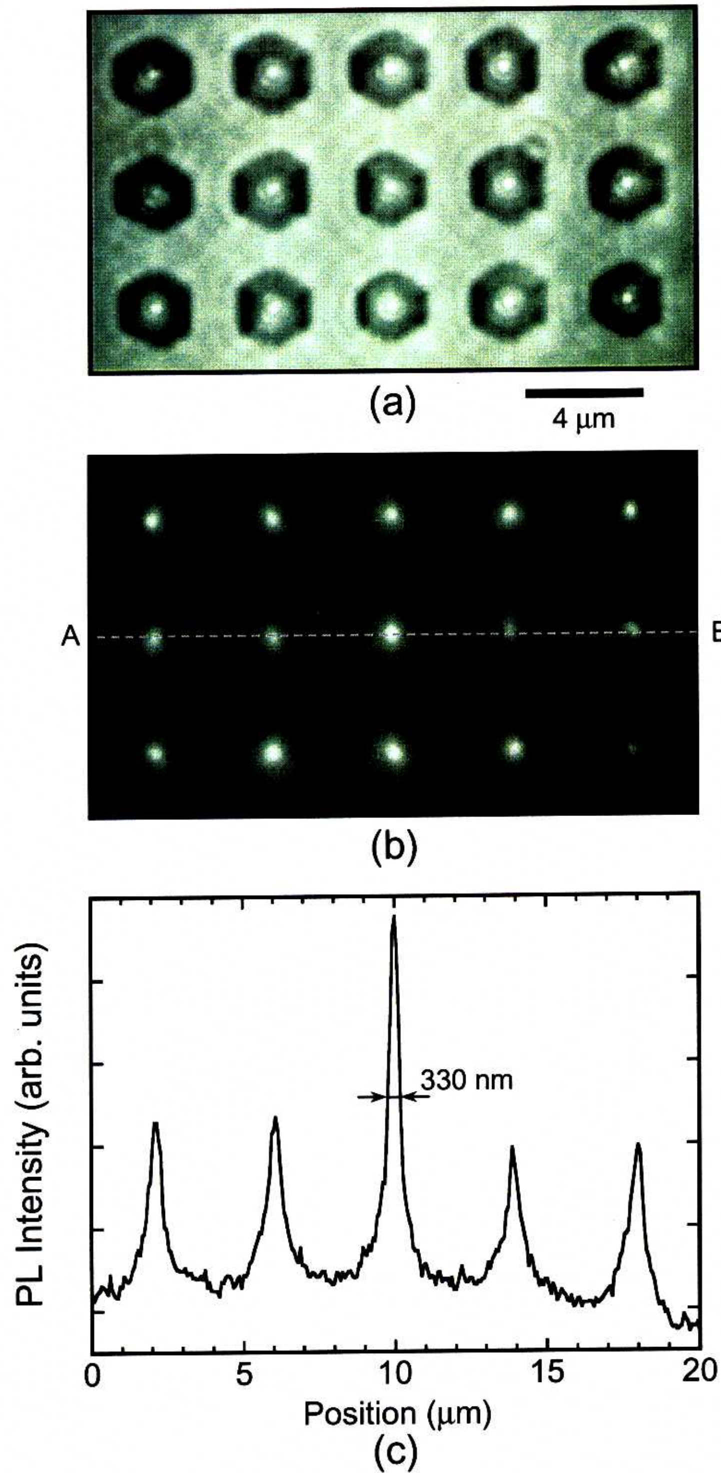

Figure 3.8: (a) Reflective image, (b) micro-PL intensity image at a wavelength of 430 nm, and (c) cross-sectional profile of PL intensity along the line AB in (b).

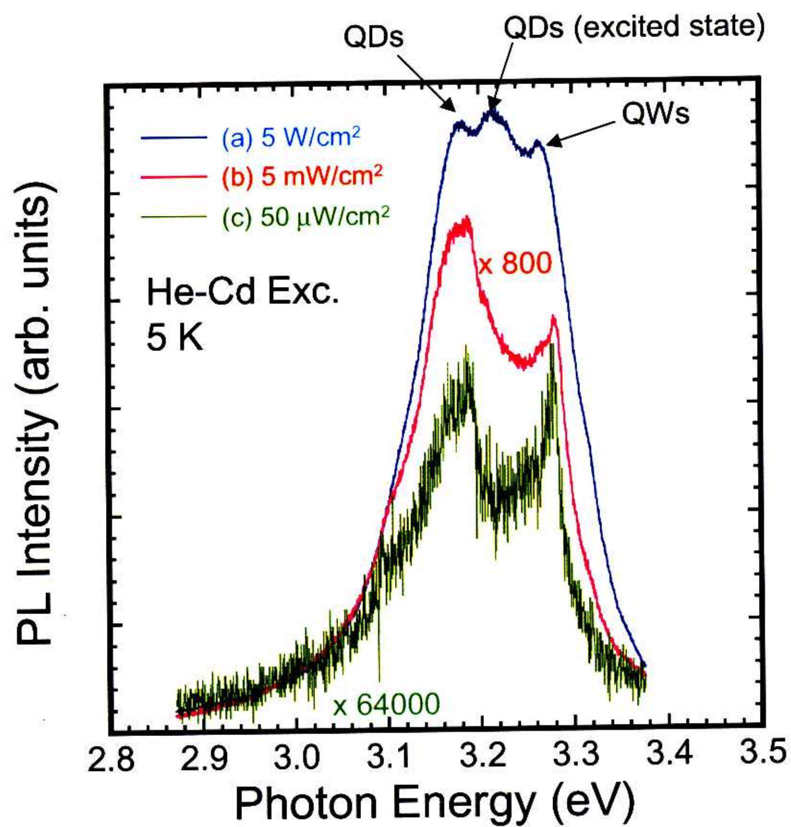

Figure 3.9: PL spectra at 5 K under various excitation intensities: (a) 5 W/cm^2, (b) 5 mW/cm^2, and (c) 50 $\mu W/cm^2$.

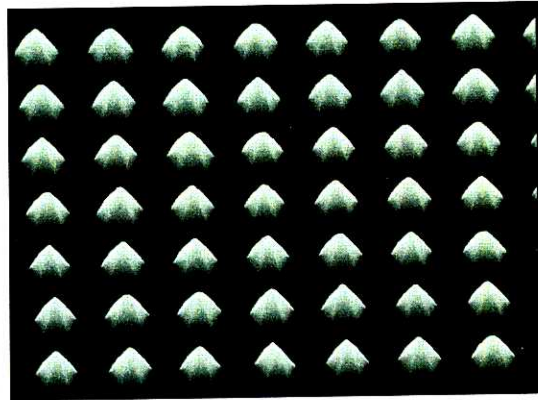

(a) 1 μm

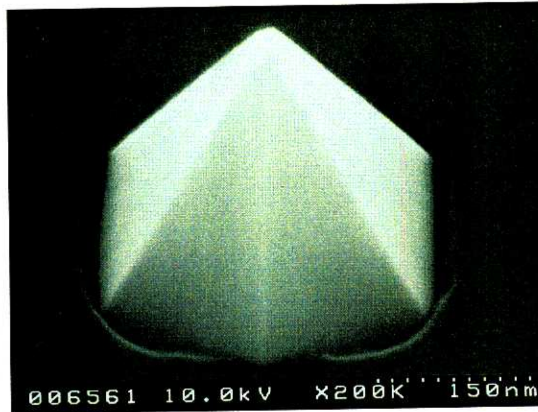

(b)

Figure 3.10: (a) SEM bird's-eye-view of $In_xGa_{1-x}N$ QDs using a substrate patterned with square openings of side length as small as 0.3 μm and (b) magnified image of a structure.

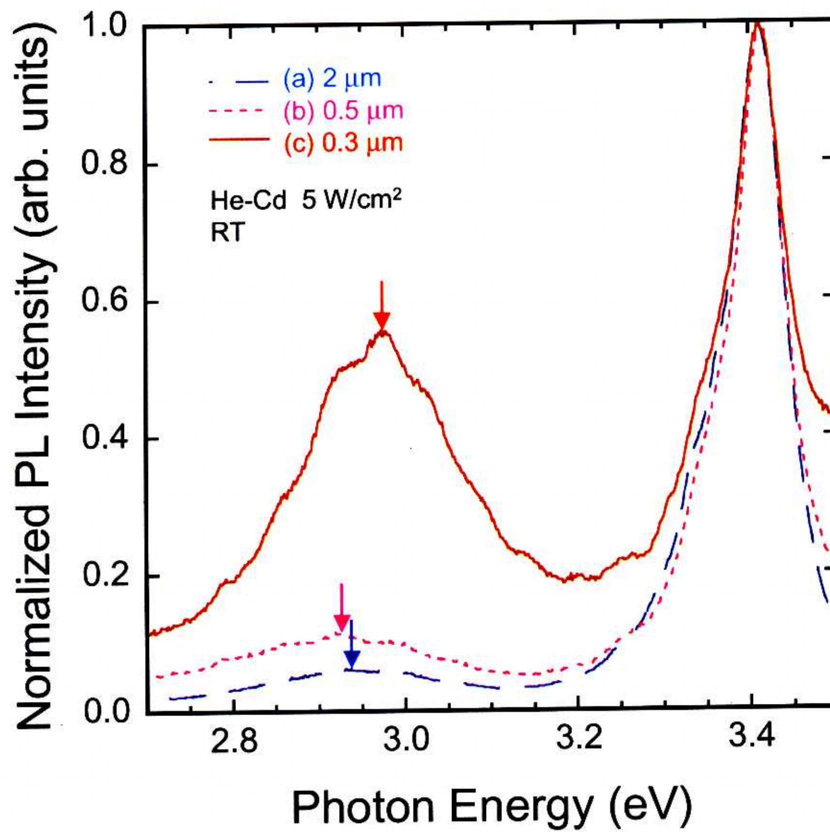

Figure 3.11: PL spectra of $In_xGa_{1-x}N$ QDs using a substrate patterned with square openings of side length: (a) 2, (b) 0.5, and (c) 0.3 μm. The arrows show $In_xGa_{1-x}N$ PL peak and the spectra are normalized at the value of GaN PL peak.

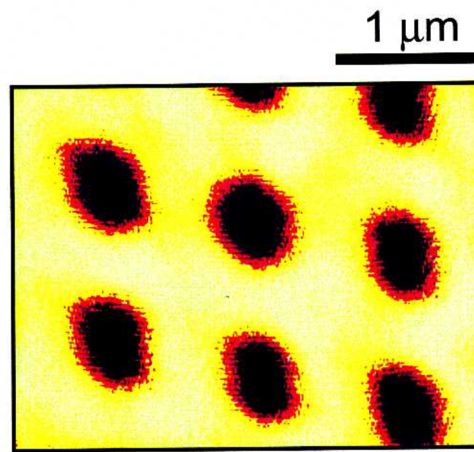

(a)

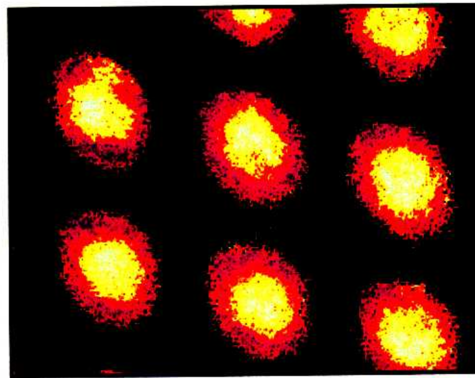

(b)

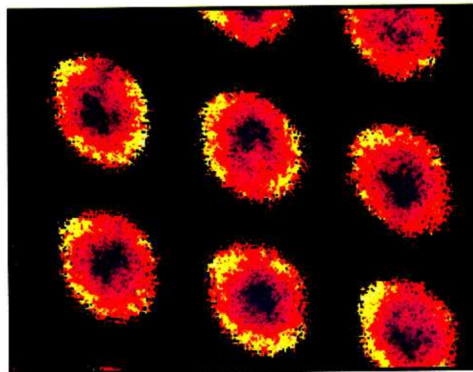

(c)

Figure 3.12: CL intensity mapping of higher-density selectively-grown $In_xGa_{1-x}N$ QDs at the wavelengths of (a) 350–365, (b) 406–412, and (c) 433–444 nm.

Chapter 4

GaN Quantum Dots by Selective Growth

4.1 Introduction

GaN or AlGaN has the wider bandgap than InGaN; therefore (Al)GaN/AlGaN MQW structures are useful for the realization of optical devices such as LEDs[98] and LDs[99] in the UV region. However, the number of dislocations strongly affects the emission efficiency of GaN/AlGaN MQWs.[100] One promising approach for higher emission efficiency is to replace QW structures with QD structures. The QD structures do not contain any dislocations, as demonstrated in InGaAs/GaAs system,[27,101] therefore it is expected to get higher emission efficiency. Moreover, the 3-D quantum confinement provided by QD structures should lead to lower threshold current density and other superior characteristics when the QDs are applied to an active layer of the laser structures.[22]

In previous works, some researches have been conducted about GaN self-assembled QDs. GaN self-assembling dots have been demonstrated on an $Al_{0.2}Ga_{0.8}N$ surface using anti-surfactants.[37] GaN self-assembling dots were formed using the Ga droplets.[44] In addition, GaN dots on an AlN layer by S–K growth mode were demonstrated using MBE.[47–49] The S–K growth of GaN/AlN QDs has been successfully demonstrated using

a SiC substrate by low-pressure MOCVD.[57] However, the selective growth of GaN QDs has never been reported yet. The selectively-grown QDs on a pattered substrate by lithography have the advantage of the control of the position and uniformity of the structures.

In Chapter 4, fabrication and optical properties of selectively-grown GaN QDs are discussed. GaN QDs embedded in AlGaN matrix have been formed on uniform array of hexagonal pyramids of GaN. The extremely sharp tops of hexagonal pyramids are realized because their radius of curvature at the tops is not larger than 10 nm. The PL peak of GaN QDs is clearly observed even at room temperature.

4.2 Fabrication of GaN quantum dots by selective growth

The selectively-grown hexagonal pyramids of GaN were formed by the same method as described in Chapter 3; after a 2.6-μm-thick GaN layer was grown under the condition described in Section 2.2, a 40-nm-thick SiO_2 was deposited using rf sputtering. The pattern was grid-like, with the period 4 μm and square openings of side length 2 μm, prepared by a conventional photolithography. Selective growth of GaN was performed using MOCVD again at the growth temperature of 945 °C. The flow rates of TMG was 32 μmol/min with the flow rates of NH_3, H_2, and N_2 at 4.0, 4.0, and 11.5 slm, respectively.

Then, selective growth of 20 periods of GaN/$Al_{0.2}Ga_{0.8}N$ MQWs was performed. Three samples were grown, in which the growth temperatures of GaN/$Al_{0.2}Ga_{0.8}N$ MQWs were different: i) 980, ii) 1030, and iii) 1060 °C. The growth times for the GaN QW and $Al_{0.2}Ga_{0.8}N$ barrier materials were such as to give 1.4 and 3.2 nm thicknesses, respectively, in planar growth. The flow rate of TMG during the growth of the GaN QWs was 4.0 μmol/min. The flow rates of TMG and TMA during the growth of the $Al_{0.2}Ga_{0.8}N$ barriers were 4.0 and 1.8 μmol/min, respectively.* The gas flow rates of NH_3, H_2, and N_2 during the growth of the QWs and barriers were 4.0, 4.0, and 28.0 slm, respectively. It

*This aluminum content is nominal value. The selectivity of AlN is low in the selective growth of $Al_xGa_{1-x}N$,[79,82] so that some AlN materials are deposited on SiO_2 mask and the aluminum content of $Al_xGa_{1-x}N$ in selective growth is lower than that in planar growth under same flow rates.

is considered that GaN QDs embedded in $Al_{0.2}Ga_{0.8}N$ matrix were formed on the tops of hexagonal pyramids of GaN, as schematically shown in Fig. 4.1(a), as demonstrated in InGaN[90)] or GaAs[94)] system.

Figure 4.1(b) shows SEM bird's-eye-view of hexagonal pyramids including GaN QDs embedded in $Al_{0.2}Ga_{0.8}N$ matrix at the tops, when selective growth of GaN/$Al_{0.2}Ga_{0.8}N$ was performed at 1030 °C. The uniform array of hexagonal pyramids can be seen in Fig. 4.1(b). The hexagonal pyramids have clear $\{1\bar{1}01\}$ side facets. The surface morphology of the samples was almost same when the growth temperature of GaN/$Al_{0.2}Ga_{0.8}N$ was 980 or 1060 °C, because the surface morphology observed by SEM was almost determined by hexagonal pyramids of GaN.

Figure 4.1(c) shows SEM cross-sectional view of one pyramid structure after the sample was cleaved. The radius of curvature at the tops is not larger than 10 nm, which indicates that extremely sharp tops are realized. The lateral size of GaN QDs is estimated to be comparable to the radius of curvature at the tops.

4.3 Photoluminescence from GaN quantum dots

The PL measurement was carried out, using an excimer laser (ArF) (OPTex by LAMBDA PHYSIK) as an excitation source with the peak energy of 6.42 eV and the repetition rate of 100 Hz. The monochromator grating of 300 grooves/mm was used, so the spectral resolution was 0.8 nm.

First, investigated was PL dependence on the growth temperature of GaN/$Al_{0.2}Ga_{0.8}N$. PL spectra were measured at 77 K. Figure 4.2 shows PL dependence on growth temperature of GaN/$Al_{0.2}Ga_{0.8}N$: (a) 980, (b) 1030, and (c) 1060 °C. The PL spectra are normalized at the PL intensity of GaN bulk around 3.48 eV. In Fig. 4.2(a), the small peak of GaN QD PL can be observed at 3.73 eV. The clear PL peak of GaN QDs can be observed at 3.65 eV in Fig. 4.2(b) at the growth temperature of 1030 °C. In Fig. 4.2(c), the PL peak of GaN QDs cannot be observed because of too high growth temperature. From these

results, it is found that PL from GaN QDs is very sensitive to the growth temperature and the optimal growth temperature is 1030 °C.

Next, PL dependence on measurement temperature was investigated with respect to the sample in which the growth temperature of GaN/$Al_{0.2}Ga_{0.8}N$ was 1030 °C. The sample was mounted in a closed-cycle He cryostat, providing temperatures 5–300 K. Figure 4.3 shows the PL spectra of selectively-grown GaN QDs. All the spectra were shown in the same scale. The two peaks of GaN bulk were observed: 3.34 and 3.42 eV at 300 K. The lower peak energy of 3.34 eV at 300 K (or 3.44 eV at 5 K) is due to hexagonal pyramids of GaN and the higher peak energy of 3.42 eV at 300 K (or 3.48 eV at 5 K) is due to the GaN layer under SiO_2, from the CL study of selectively-grown hexagonal pyramids of GaN.[102] The lower peak energy of PL can be explained by the strain relaxation in hexagonal pyramids of GaN.

There were no clear PL peaks observed above 3.42 eV at 300 K (or 3.48 eV at 5 K) in the PL spectra of bulk $Al_{0.2}Ga_{0.8}N$ without GaN QDs, on hexagonal pyramids of GaN. Moreover, as the bandgap energy of $Al_{0.2}Ga_{0.8}N$ is 3.9 eV at room temperature,† the PL peak of 3.61 eV at 300 K in Fig. 4.3 is considered to be due to GaN QDs.

The PL intensity of GaN QDs is smaller than that of GaN bulk, because the volume of GaN QDs is much smaller than that of GaN bulk. The PL peak intensity of GaN QDs decreases above 180 K, although it decreases more slowly than that of GaN bulks. This indicates that there exists stronger confinement of carriers in the QDs, however, the effect of the suppression of non-radiative recombination in the QDs becomes relatively small at higher temperature because the carriers are captured into the non-radiative centers such as the defects around the QDs.

---

†The bandgap energy of $Al_xGa_{1-x}N$ at room temperature is calculated using the following equation, when the Al content x is between 0 and 0.25: $E_g(Al_xGa_{1-x}N) = xE_g(AlN) + (1-x)E_g(GaN) - bx(1-x)$. Here, these values are used: $b = 0.25$ eV,[103] $E_g(GaN) = 3.42$ eV, and $E_g(AlN) = 6.20$ eV.

4.4 Higher-density GaN quantum dots using a substrate prepared by electron-beam lithography

To get higher-density GaN QDs, the selective growth was performed using a substrate prepared by EB lithography as described in Section 3.5.

After a 25-nm-thick GaN nucleation layer was deposited on a (0001)-oriented Al_2O_3 substrate, a 1.1-μm-thick undoped GaN layer was grown under the same growth condition as described in Section 2.2. Next, a 1.5-μm-thick Si-doped GaN layer was grown, where the electron concentration was 2–4 $\times$ 10^{18} cm^{-3}. After that, a 40-nm-thick SiO_2 was deposited on the surface by rf sputtering. The pattern was grid-like, with the period 0.6 μm and square openings of side length as small as 0.3 μm, prepared by EB lithography.

The hexagonal pyramids of GaN were realized at 945 °C with the flow rates of TMG at 32 μmol/min. The gas flow rates of NH_3, H_2, and N_2 were 4.0, 4.0, and 11.5 slm, respectively. The growth time was 2.0 min. Then, the selective growth of 20 periods of GaN/$Al_{0.2}Ga_{0.8}N$ MQWs was performed at 1030 °C. The growth times for the GaN QW and $Al_{0.2}Ga_{0.8}N$ barrier materials were such as to give 1.4 and 3.2 nm thicknesses, respectively, in planar growth. The flow rate of TMG during the growth of the GaN QWs was 4.0 μmol/min. The flow rates of TMG and TMA during the growth of the $Al_{0.2}Ga_{0.8}N$ barriers were 4.0 and 1.8 μmol/min, respectively. The gas flow rates of NH_3, H_2, and N_2 during the growth of the QWs and barriers were 4.0, 4.0, and 28.0 slm, respectively.

Figure 4.4 shows SEM bird's-eye-views of higher-density hexagonal pyramids including GaN QDs embedded in $Al_{0.2}Ga_{0.8}N$ matrix at the tops. The uniform array of higher-density hexagonal pyramids can be seen in Fig. 4.4(a) even when such a fine pattern was formed, although some AlN materials are deposited on SiO_2 mask. From Fig. 4.4(b), the hexagonal pyramids have clear $\{1\bar{1}01\}$ facets on the sides.

It was found that the uniform array of higher-density hexagonal pyramids including GaN QDs at the tops when the substrate was used with such a fine pattern prepared by EB lithography.

4.5 Concluding remarks

In Chapter 4, the selectively-grown GaN QDs embedded in AlGaN matrix were demonstrated, which were formed on uniform array of hexagonal pyramids of GaN. The radius of curvature of hexagonal pyramids at the tops was not larger than 10 nm, which indicates that the extremely sharp tops were realized. The clear PL peak was observed from GaN QDs even at room temperature.

To realize the higher-density GaN QDs, the selective growth was performed, using the substrates with a fine pattern prepared by EB lithography. The uniform array of hexagonal pyramids were realized even when such a fine pattern was used.

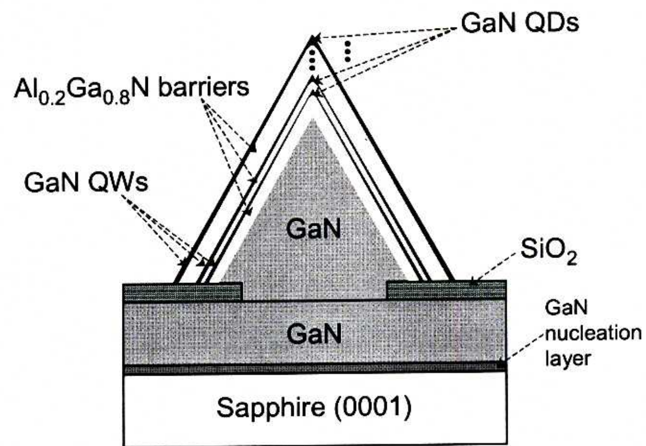

(a)

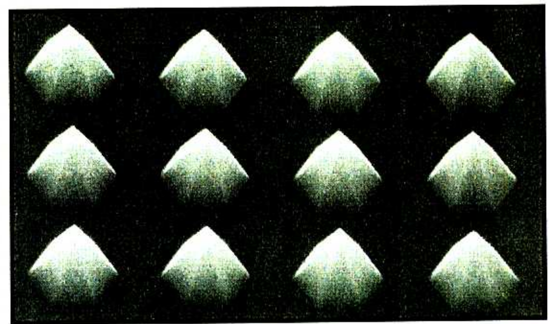

(b)

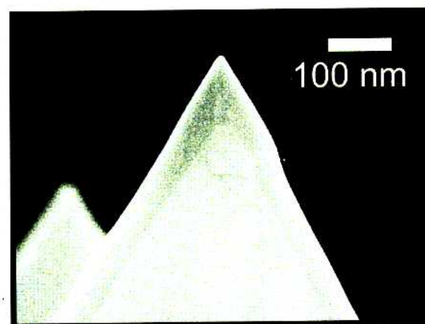

(c)

Figure 4.1: (a) Illustration of GaN QDs embedded in $Al_{0.2}Ga_{0.8}N$ matrix on hexagonal pyramids of GaN. (b) SEM bird's-eye-view of uniform array of hexagonal pyramids including GaN QDs embedded in $Al_{0.2}Ga_{0.8}N$ matrix at the tops and (c) cross-sectional image after the sample was cleaved.

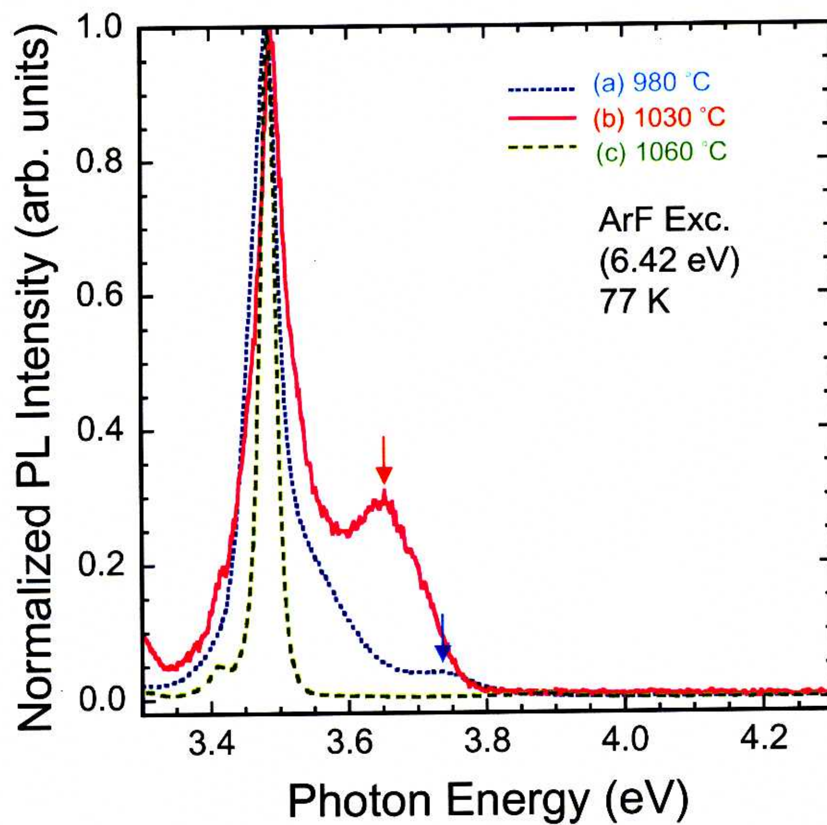

Figure 4.2: PL spectra of selectively-grown GaN QDs when the growth temperatures of $GaN/Al_{0.2}Ga_{0.8}N$ were (a) 980, (b) 1030, and (c) 1060 °C.

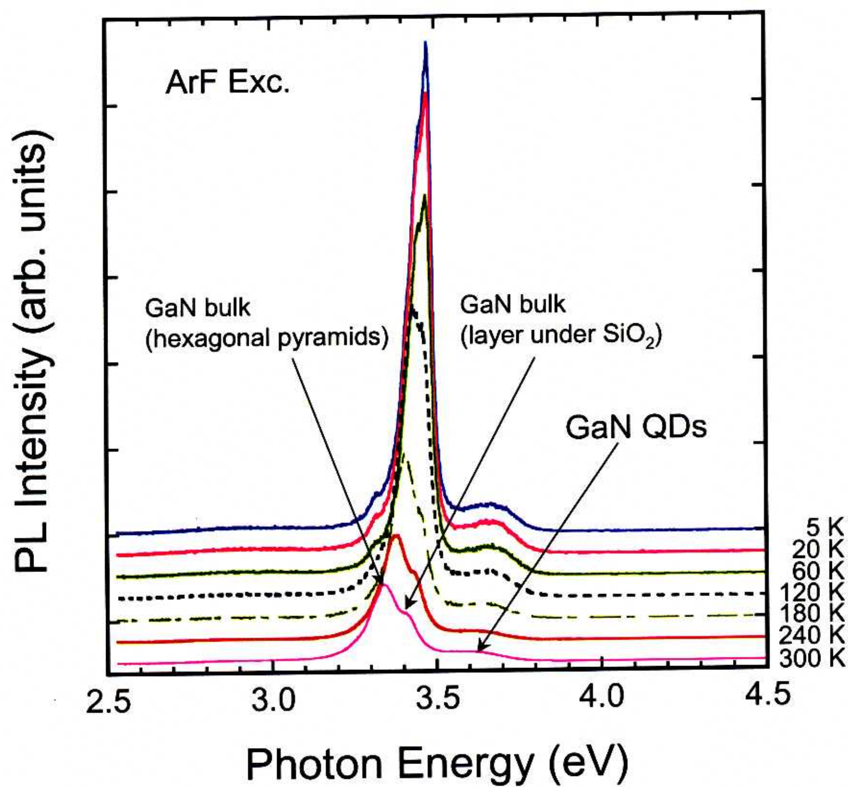

Figure 4.3: PL spectra of selectively-grown GaN QDs, excited by an excimer laser (ArF) with the excitation energy of 6.42 eV. The spectra were measured from 5 to 300 K. All the spectra were shown in the same scale.

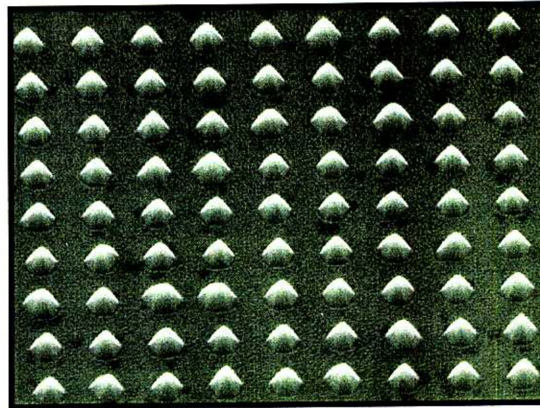

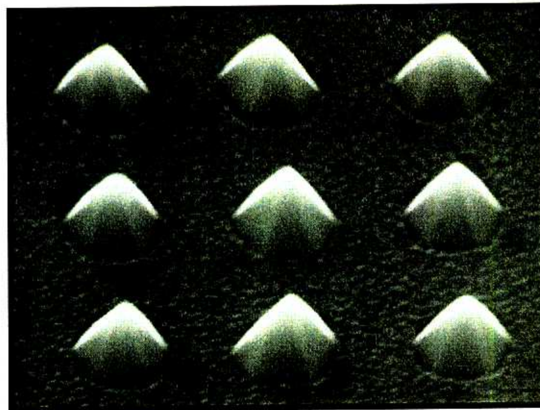

Figure 4.4: (a) SEM bird's-eye-view of higher-density GaN QDs on a substrate with the period 0.6 μm and square openings of side length as small as 0.3 μm. (b) The magnified image of the structures.

Chapter 5

Application of GaN-Based Quantum Dots to Optical Devices

5.1 Introduction

As discussed in Chapter 1, the QD lasers have the superior characteristics such as lower threshold currents and suppression of the temperature dependence of threshold current, compared to conventional QW lasers.[22] For the realization of the QD lasers in GaN-based system, stimulated emission from GaN dots was observed at 20 K,[43] however lasing oscillation was not reported. This is because it was still difficult to fabricate a uniform QD structure with the high density required for lasing oscillation. In Chapter 2, demonstrated were the growth of $In_xGa_{1-x}N$ self-assembled QDs on a GaN layer without any surfactants and their optical properties.

In Chapter 5, laser action of an InGaN self-assembled QD laser at room temperature is discussed.[104] The laser structure is fabricated with the stacked $In_xGa_{1-x}N$ self-assembled QDs embedded in the active layer. A clear threshold is observed in the relation between the excitation energy and emission intensity at room temperature by the optically pumped excitation. The width of the emission spectra is as narrow as 0.1 nm (resolution limit), and the emission is strongly polarized in the TE mode above the threshold. These results

demonstrate that lasing has been achieved. Moreover, the growth conditions are investigated with respect to *p*-type GaN and GaN/$Al_xGa_{1-x}N$ superlattices for cladding layer of laser structures. The *p-i-n* laser structure is fabricated and characterized with $In_xGa_{1-x}N$ self-assembled QDs embedded in the active layer.

5.2 InGaN quantum dot lasers under optical excitation

A laser structure was grown with 10 layers of $In_xGa_{1-x}N$ self-assembled QDs embedded in the active layer. For the QDs the InGaN coverage was 12 ML. The spacing layer was 5-nm-thick $In_{0.02}Ga_{0.98}N$. Figure 5.1(a) shows an AFM image of the reference sample of 3-layer stacked $In_xGa_{1-x}N$ self-assembled QDs grown under the same growth conditions as the active layer. Here, the indium content x in the QDs is about 0.2. From Fig. 5.1(a), the average diameter and height of the QDs are 20 and 4.5 nm, respectively. The QD density is 6.0×10^9 cm^{-2} per layer.

As shown in Fig. 5.1(b), a 25-nm-thick GaN nucleation layer was deposited on a (0001)-oriented Al_2O_3 substrate, followed by 1500-nm-thick GaN layer. Then, 250-nm-thick $Al_{0.1}Ga_{0.9}N$ for cladding layer and 150-nm-thick GaN for guide layer were grown at 1092 °C. The 10 periods of $In_xGa_{1-x}N$ self-assembled QDs and 5-nm-thick $In_{0.02}Ga_{0.98}N$ spacers were grown at 770 °C as the active layer. The active layer was capped with 40-nm-thick $In_{0.02}Ga_{0.98}N$ at 770 °C, 80-nm-thick GaN at 1075 °C for guide layer, 160-nm-thick $Al_{0.1}Ga_{0.9}N$ for cladding layer, and 20-nm-thick GaN at 1092 °C. The cavity was fabricated by low-damage electron-cyclotron-resonance reactive-ion-etching (ECR-RIE) with Ar and Cl_2 gases. By SEM, the cavity facet was observed to be smooth. The length and width of the cavity were 540 and 10 μm, respectively. The mirror facets in the cavity were not coated.

PL measurements were carried out at room temperature, as schematically shown in Fig. 5.2. The excitation source was a dye laser (BPBD365) with a peak wavelength of 367 nm, excited by a nitrogen laser (YKN–900 by USHO) with a repetition rate of 3

Hz and a typical pulse width of 10 ns. Note that only the active layer was excited and the $Al_{0.1}Ga_{0.9}N$ cladding layer or GaN layer was not excited by the dye laser. The laser beam was of rectangular cross-section and focused on the top of the cavity using two cylindrical lenses. The emission from the edge of the cavity was dispersed by the 0.3 m monochromator and detected by the liquid nitrogen-cooled CCD camera.

Figure 5.3 shows the emission intensity polarized in the TE or transverse magnetic (TM) mode, accumulated over 15 pulses, as a function of the excitation energy per pulse. In Fig. 5.3, the excitation energy measurement has an error of about 2%. A clear threshold is observed in the dependence of the TE polarized emission intensity on the excitation energy. The threshold energy I_{th} is 6.0 mJ/cm^2. The ratio of the TE-polarized intensity to the TM-polarized intensity is as much as 160 at the highest excitation energy, while it is 60 below the threshold.

Figure 5.4(a) shows the conventional PL spectrum of the laser structure, excited by a He–Cd laser. As the monochromator grating of 300 grooves/mm was used, the spectral resolution was 0.8 nm. The peak wavelength is 404 nm and the FWHM is 200 meV. The FWHM depends on the growth conditions of the QDs, so it is in the range between 200 and 400 meV. Therefore, this FWHM is consistent with the results described in Chapter 2.

Figures 5.4(b) and 5.4(c) show the emission spectra above the threshold at excitation energy of $1.4I_{th}$ and $1.8I_{th}$, respectively. The monochromator grating of 2400 grooves/mm was used, therefore, the spectral resolution was 0.1 nm. In Fig. 5.4(b), the linewidth is reduced to below 0.1 nm. Such a narrow spectrum indicates laser action at room temperature. In Fig. 5.4(c), multi-mode oscillation is seen because the emission is observed from states which have different energies due to the variations in size and indium content in the QDs. The noise level is high in Figs. 5.4(b) and 5.4(c) because the spectral resolution was as high as 0.1 nm and the emission was accumulated only for one pulse. The peak wavelength in Fig. 5.4(b) is 404.9 nm, while that in Fig. 5.4(c) is 405.5 nm. The longer peak wavelength at the higher excitation energy is attributed to mode hopping because of

heat produced by the higher excitation.

The carrier concentration at the threshold is discussed briefly. From the threshold energy in Fig. 5.3 of 6.0 mJ/cm^2 and the excitation wavelength of 367 nm, the threshold carrier concentration is estimated to be about 1×10^{12} cm^{-2}.* From this carrier concentration at the threshold of 1×10^{12} cm^{-2}, about 10 energy states are occupied in each $In_xGa_{1-x}N$ QD, because the QD density is 6×10^9 cm^{-2} per layer, the number of stacked layers is 10, and there are two carriers in each energy state due to the spin. This number of electrons in each QD is shown as just one example for understanding the laser action more deeply. It is considered that this number of electrons in each QD is valid because the lateral confinement of carriers at room temperature has not been sufficiently achieved yet, taking account of the lateral size of the QDs of 20 nm and the large effective masses in the QDs. To realize the predicted performances of QD laser, the size of the QDs must be small enough that the population of carriers in higher subband can be ignored. Owing to the large effective mass, the QDs with the lateral size of ~8–10 nm will be required.[36] Further investigation is needed to reduce the lateral size of the QDs, with high uniform.

The merit of the stacked QD structure is mentioned briefly. Feasibility of stacking QDs has been already demonstrated in In(Ga)As, QD density reaching as high as 10^{11} cm^{-2}.[107] Established was the condition for growth of $In_xGa_{1-x}N$ QDs without any surfactants as well as for that of the $In_xGa_{1-x}N$ self-assembled QDs and $In_{0.02}Ga_{0.98}N$ spacer at the same growth temperature. This establishment led to successful growth of the stacked $In_xGa_{1-x}N$ QD structure. The spacer thickness of 5 nm is almost same as the average QD height of 4.5 nm. It is considered that the coupling between vertically aligned QDs is not so strong due to the large effective mass of electrons and pyramid-shaped QD structures. However more investigation is needed to confirm this characteristic.

*The following parameters are assumed: the reflectivity on the top of the cavity of 20%, the effective absorption in the active region of 20%, the quantum efficiency in the active layer of 1%, the carrier lifetime at the QDs of 1 ns, and the pulse width of the dye laser of 10 ns. In this assumption, the absorption coefficient in the InGaN of 1×10^5 cm^{-1} [105] is used and the quantum efficiency of 1% is derived as a consequence of assumptions that the internal quantum efficiency of 20%[106] and the capture efficiency of 5% from 2-D layer into the QDs.

In summary, a laser structure was fabricated, in which $In_xGa_{1-x}N$ self-assembled QDs were grown as the active layer. A clear threshold was seen in the relation between excitation energy and emission intensity at room temperature under the optical pumping. The emission linewidth was reduced to below 0.1 nm (resolution limit) as the excitation energy increases. The emission was strongly TE polarized above the threshold. These results demonstrate that lasing oscillation has been achieved in an $In_xGa_{1-x}N$ self-assembled QD laser at room temperature.

5.3 InGaN quantum dot lasers by current injection

In Section 5.2, the $In_xGa_{1-x}N$ QD lasers were demonstrated at room temperature by optical pumping. To utilize the real lasers, the whole design is needed, including *n*-type or *p*-type semiconductors for current injection. In Section 5.3, fabrication of $In_xGa_{1-x}N$ QD lasers by current injection is described, including the growth conditions of *p*-type GaN and modulation-doped superlattices for *n*-type or *p*-type cladding layer.

5.3.1 Growth conditions of *p*-type GaN

5.3.1.1 Introduction

In 1980s or earlier, the epitaxial layer of GaN had many donor impurities and it was difficult to realize *p*-type GaN. Amano *et al.* have demonstrated *p*-type GaN by Mg-doped GaN treated with low-energy electron beam irradiation.[5] Moreover, Nakamura *et al.* have demonstrated *p*-type GaN by Mg-doped GaN treated with thermal annealing under N_2 atmosphere,[108] which is suitable for mass production of devices. They have also proposed that Mg–H neutral complexes created in the epitaxial growth by MOCVD cause the high resistivity and thermal annealing after the growth can remove H atoms from the complexes, to realize *p*-type GaN.[109] However, the acceptor level of Mg in GaN is very deep (~170 meV[110]), so that only ~1% of Mg is activated at room temperature. It is necessary to choose growth conditions of *p*-type GaN carefully to get the hole concentration

of ~ 10^{18} cm^{-3}, because very high Mg doping of ~ 10^{20} cm^{-3} is needed.

In this section, the growth conditions are investigated with respect to *p*-type GaN using Nomarski microscopy, PL, and VdP measurement.

5.3.1.2 Surface morphology under various growth conditions

First, investigated was the dependence of the surface morphology of Mg-doped GaN on growth temperature. After a 1.1-μm-thick undoped GaN was grown on Al_2O_3 substrate by two-step growth as described in Section 2.2, the growth of Mg-doped GaN was performed. The flow rates of TMG and Cp_2Mg were 44 and 0.053 μmol/min, respectively, during the growth of Mg-doped GaN. The gas flow rates of NH_3, H_2, and N_2 were 3.0, 4.0, and 35.0 slm, respectively. Under this growth condition, the growth rate was 0.51 μm/h. The layer thickness of Mg-doped GaN was 0.51 μm. Figure 5.5 shows the surface morphology of Mg-doped GaN grown at (a) 1045 and (b) 1071°C. The surface morphology of two samples in Fig. 5.5 is so different although the difference in the growth temperatures is only 26 °C. The surface is smooth and flat in Fig. 5.5(a), which is favorable for the application to laser structures.

Next, investigated was the dependence on flow rate of Cp_2Mg. After a 1.1-μm-thick undoped GaN was grown on Al_2O_3 substrate by two-step growth as described in Section 2.2, a 0.51-μm-thick Mg-doped GaN was grown at 1045 °C. During the growth of Mg-doped GaN, the flow rate of TMG was 44 μmol/min. The flow rate of Cp_2Mg was varied from 0.044 to 0.074 μmol/min. The gas flow rates of NH_3, H_2, and N_2 were same as described above. Under this growth condition, the growth rate was 0.51 μm/h. Figure 5.6 shows the surface morphology of the grown samples. The surface is flat in Figs. 5.6(a) and 5.6(b). In contrast, the surface morphology gets worse in Figs. 5.6(c) and 5.6(d) as the flow rate of Cp_2Mg gets higher.

5.3.1.3 Optical characterization by photoluminescence

PL measurement of these grown samples was carried out at room temperature. The He–Cd laser was used as the excitation source with the excitation power density of 5 W/cm^2. As the monochromator grating of 300 grooves/mm was used, the spectral resolution was 0.8 nm.

Figure 5.7 shows the PL spectra of the as-grown samples of which the surface morphology is shown in Fig. 5.6. The fringes in PL spectra in Fig 5.7 are Fabry–Pérot type ones, which indicate that the smooth interfaces can be realized. The peak energy of around 3.27 eV in Figs. 5.7(a) and 5.7(b) is due to donor–acceptor pair recombination.[111,112) In contrast, the peak energy of around 2.9 eV in Figs. 5.7(c) and 5.7(d) is considered to be due to conduction band–to–impurity transition involving doping related deep-level impurities.[113) In Figs. 5.7(c) and 5.7(d), the PL peak of 2.9 eV is dominant and that of 3.27 eV can be hardly observed. This result indicates too high Mg-doping in the samples under the flow rate of Cp_2Mg at 0.062 or 0.074 μmol/min with the flow rate of TMG at 44 μmol/min.

5.3.1.4 Comparison of carrier concentration

The VdP measurement was carried out to characterize the hole concentration. The detail will be discussed elsewhere with respect to thermal annealing of Mg-doped GaN, contact metals of Au/Ni, or VdP measurement.[114)

Figure 5.8 shows the hole concentrations at various flow rates of Cp_2Mg grown at 1045 or 1071 °C. The growth conditions were same as described in Section 5.3.1.2. The thickness of *p*-type GaN was 0.51 μm. The surface morphology of the samples grown at 1045 °C is shown in Fig. 5.6. As can be seen in Fig. 5.8, the hole concentration is very sensitive to the flow rate of Cp_2Mg. The hole concentration does not always increase as the flow rate of Cp_2Mg increases. The maximum hole concentration is 7.5×10^{17} cm^{-3} when the flow rates of TMG and Cp_2Mg are 44 and 0.053 μmol/min, grown at 1045 °C.

5.3.1.5 Summary

The growth conditions were investigated with respect to p-type GaN. It was found that the high hole concentration of 7.5×10^{17} cm^{-3} was realized when the growth temperature was slightly low (1045 °C) with the flow rates of TMG and Cp_2Mg at 44 and 0.053 μmol/min, respectively.

5.3.2 Cladding layer of GaN/AlGaN superlattices

The use of GaN/$Al_xGa_{1-x}N$ superlattices as the cladding layer of laser structures was first reported by Nakamura *et al.*[115] $Al_xGa_{1-x}N$ cladding layers with high Al content or large thickness are essential to improve the laser characteristics. However, there exists lattice mismatch of 2.5% between GaN and AlN in a-axis direction. It is very difficult to grow $Al_xGa_{1-x}N$ cladding layers with high Al content or large thickness without cracking. Therefore it is desirable to grow the GaN/$Al_xGa_{1-x}N$ superlattices as cladding layers with the individual layer thickness below critical thickness. In addition, it is found that the hole generation is enhanced using the modulation-doped superlattices of Mg-doped GaN/undoped $Al_xGa_{1-x}N$, due to piezoelectric and spontaneous electric fields.[116–119]

In this section, the growth conditions are investigated with respect to GaN/$Al_xGa_{1-x}N$ superlattices for cladding layers.

First, 200 pairs of 2.6-nm-thick Si-doped GaN and 2.6-nm-thick undoped $Al_xGa_{1-x}N$ were grown for n-type cladding layer of the laser structures. Here, the Al content x was 0.14. After a 1.5-μm-thick undoped GaN was grown on Al_2O_3 substrate by two-step growth as described in Section 2.2, the superlattices were grown at 1080 °C. During the growth of Si-doped GaN, the flow rates of TMG and SiH_4 were 32 μmol/min and 0.22 nmol/min, respectively. During the growth of undoped $Al_{0.14}Ga_{0.86}N$, the flow rates of TMG and TMA were 32 and 8.1 μmol/min, respectively. The gas flow rates of NH_3, H_2, and N_2 during the growth of superlattices were 4.0, 4.0, and 28.0 slm, respectively. Figure 5.9(a) shows Nomarski microscope image of the surface morphology of the superlattices. In Fig. 5.9(a), the cracking can be observed, because of higher Al content or larger total

layer thickness.

To prevent cracking, 180 pairs of 2.6-nm-thick Si-doped GaN and 2.6-nm-thick undoped $Al_{0.12}Ga_{0.88}N$ were grown. During the growth of Si-doped GaN, the flow rates of TMG and SiH_4 were 44 μmol/min and 0.22 nmol/min, respectively. During the growth of undoped $Al_{0.12}Ga_{0.88}N$, the flow rates of TMG and TMA were 44 and 9.2 μmol/min, respectively. The gas flow rates of NH_3, H_2, and N_2 during the growth of superlattices were 4.0, 4.0, and 28.0 slm, respectively. Figure 5.9(b) shows Nomarski microscope image of the surface morphology of the superlattices. In Fig. 5.9(b), the cracking cannot be observed. This structure of n-GaN/i-$Al_{0.12}Ga_{0.88}N$ will be used as n-type cladding layer of the laser structures.

Next, investigated were modulation-doped superlattices of 120 pairs of 2.6-nm-thick Mg-doped GaN and 2.6-nm-thick undoped $Al_{0.12}Ga_{0.88}N$ for p-type cladding layer of the laser structures. The growth temperature was set to 1045 °C. During the growth of Mg-doped GaN, the flow rates of TMG and Cp_2Mg were 44 and 0.029 μmol/min, respectively. During the growth of undoped $Al_{0.12}Ga_{0.88}N$, the flow rates of TMG and TMA were 44 and 9.2 μmol/min, respectively. The gas flow rates of NH_3, H_2, and N_2 during the growth of superlattices were 3.0, 4.0, and 35.0 slm, respectively. Under this growth condition, the growth rates of GaN and $Al_{0.12}Ga_{0.88}N$ were 0.15 and 0.17 nm/s, respectively.

Figure 5.10 shows $\omega/2\theta$ scan of (0002)-reflection XRD in 120 pairs of the superlattices.† The smooth and abrupt interfaces with good periodicity can be obtained even when modulation-doping was performed, because the higher satellite peaks can be observed in Fig. 5.10(a). The simulation results are also shown in Fig. 5.10(a) with respect to the dependence of XRD curve on the layer thickness in GaN/$Al_{0.12}Ga_{0.88}N$. Note that the individual layer thickness has the accuracy in the order of 0.1 nm. Figure 5.10(b) shows the XRD curve of the sample and the simulation results of dependence on the Al content x of $Al_xGa_{1-x}N$ layer in pairs of 2.6-nm-thick GaN and 2.6-nm-thick $Al_xGa_{1-x}N$. From Fig. 5.10(b), it is confirmed that the Al content is 12% in the superlattices of

†X'Pert–MRD (by Philips) was used as XRD measurement system with Cu$K\alpha_1$ radiation (λ = 0.154056 nm).

$GaN/Al_xGa_{1-x}N$. This growth condition will be used as *p*-type cladding layer of the laser structures.

5.3.3 Fabrication of laser structures

The *p-i-n* laser structure was grown as schematically shown in Fig. 5.11. After a 25-nm-thick GaN nucleation layer was deposited on a (0001)-oriented Al_2O_3 substrate, a 360-nm-thick undoped GaN layer was grown under the same growth conditions as described in Section 2.2. Next, a 2.2-μm-thick Si-doped GaN layer was grown, followed by modulation-doped superlattices of 180 pairs of 2.6-nm-thick Si-doped GaN and 2.6-nm-thick undoped $Al_{0.12}Ga_{0.88}N$ for *n*-type cladding layer at 1040 °C as described in Section 5.3.2. The electron concentration was estimated to be 2.0×10^{18} cm^{-3}, from VdP measurement. Then, a 100-nm-thick Si-doped GaN was grown for guide layer, in which the electron concentration was 4.0×10^{17} cm^{-3}.

As the active layer, 10 periods of $In_{0.2}Ga_{0.8}N$ QDs and 5-nm-thick $In_{0.02}Ga_{0.98}N$ spacers were grown at 740 °C. The growth condition of the QDs was same as described in Section 5.2, except for the growth temperature. The average diameter and height of the QDs were 20 and 4.5 nm, respectively. The QD density was 6.0×10^9 cm^{-2} per layer.

A 40-nm-thick $In_{0.02}Ga_{0.98}N$ spacer was grown at 740 °C and 20-nm-thick Mg-doped $Al_{0.16}Ga_{0.84}N$ was grown at 1045 °C. A 100-nm-thick Mg-doped GaN was grown for guide layer, in which the hole concentration was 4.0×10^{17} cm^{-3}. Grown were modulation-doped superlattices of 120 pairs of 2.6-nm-thick Mg-doped GaN and 2.6-nm-thick undoped $Al_{0.12}Ga_{0.88}N$ for *p*-type cladding layer. Finally, a 100-nm-thick Mg-doped GaN was grown for contact layer.

The cavity and ridge geometry were fabricated by RIE. The ridge width was 2 μm. The sides of the ridge were covered with SiO_2. The cavity length was 1000 μm. The *n*-type and *p*-type electrodes consisted of Ti/Pt/Au and Pt/Ti/Pt/Au, respectively. The mirror facets in the cavity were not coated.

Figure 5.12 shows the relationship between the current I and voltage V in the QD

lasers under dc operation at room temperature. A clear rectification characteristic can be observed in Fig. 5.12, however, the lasing action was not achieved. The optimization of growth conditions of cladding layers as well as active layers will be needed.

5.4 Concluding remarks

In Chapter 5, the application of GaN-based QDs to the optical devices such as lasers was described.

The laser structure was fabricated with 10-layer stacked $In_xGa_{1-x}N$ self-assembled QDs embedded in the active layer. The laser structure was characterized at room temperature under optical excitation. A clear threshold could be seen in the relationship between the emission intensity and excitation energy. The linewidth was reduced to below 0.1 nm (resolution limit). These results support lasing action at room temperature.

To realize $In_xGa_{1-x}N$ self-assembled QD lasers by *p-n* junction, the growth conditions were investigated with respect to *p*-type GaN and cladding layer of $GaN/Al_{0.12}Ga_{0.88}N$ superlattices. The *p-i-n* laser structure was fabricated and characterized with $In_xGa_{1-x}N$ self-assembled QDs embedded in the active layer.

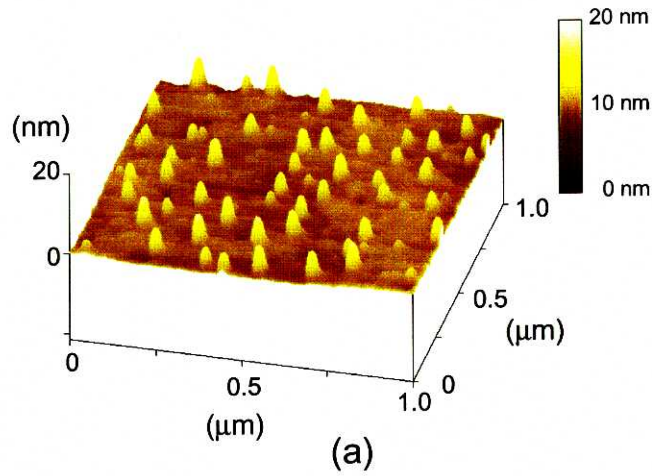

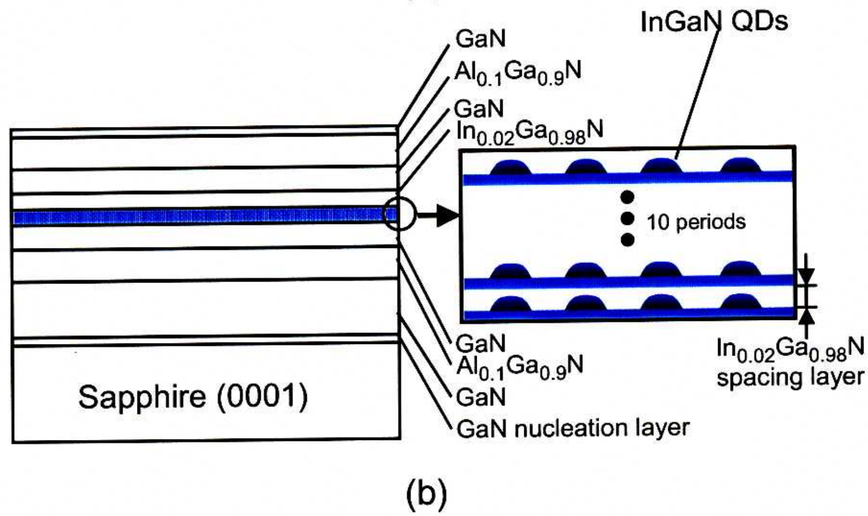

Figure 5.1: (a) AFM image of a 3-layer stacked $In_xGa_{1-x}N$ self-assembled QD sample grown under the same growth conditions as the active layer of the laser structure. (b) Schematic of the laser structure with active layer of stacked $In_xGa_{1-x}N$ self-assembled QDs.

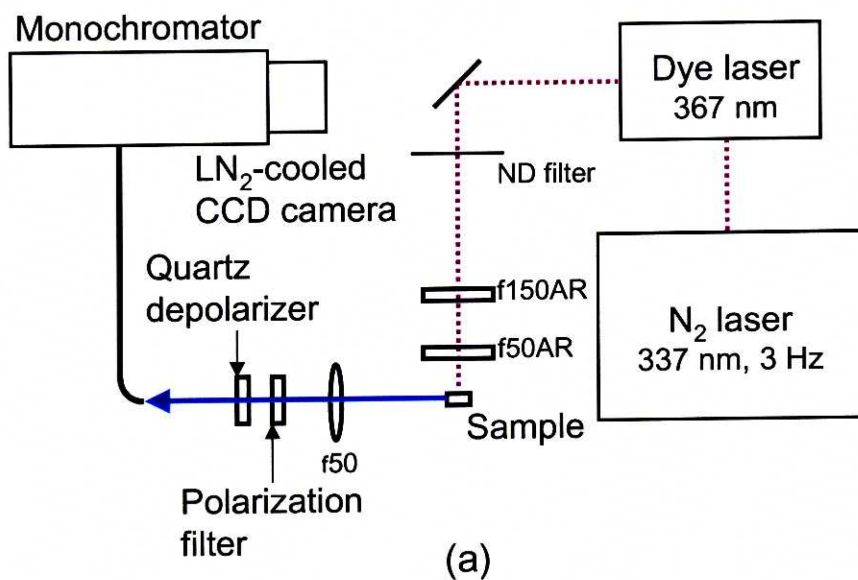

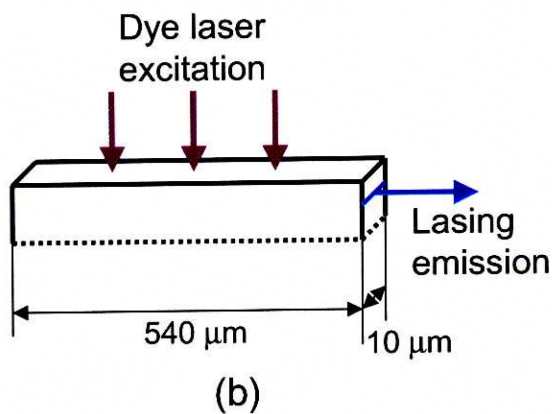

Figure 5.2: (a) Experimental setup of measuring laser characteristics under optical excitation. (b) The excitation laser is focused on the top of cavity with the beam shape of rectangular cross-section.

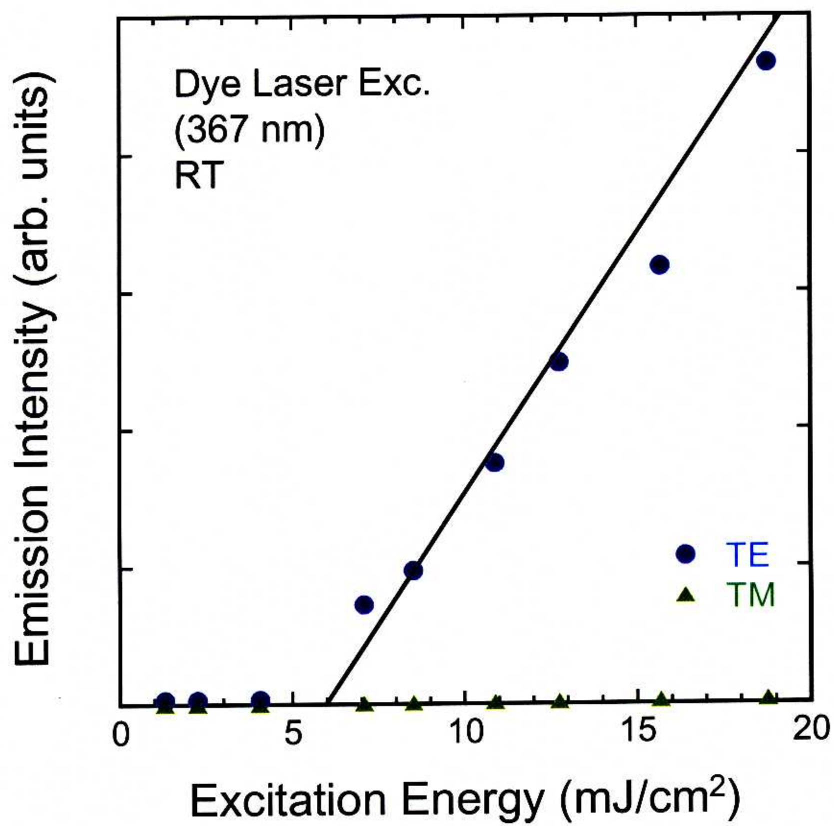

Figure 5.3: Dependence of the polarized emission intensity on the excitation energy per pulse at room temperature. The excitation source was a dye laser (367 nm).

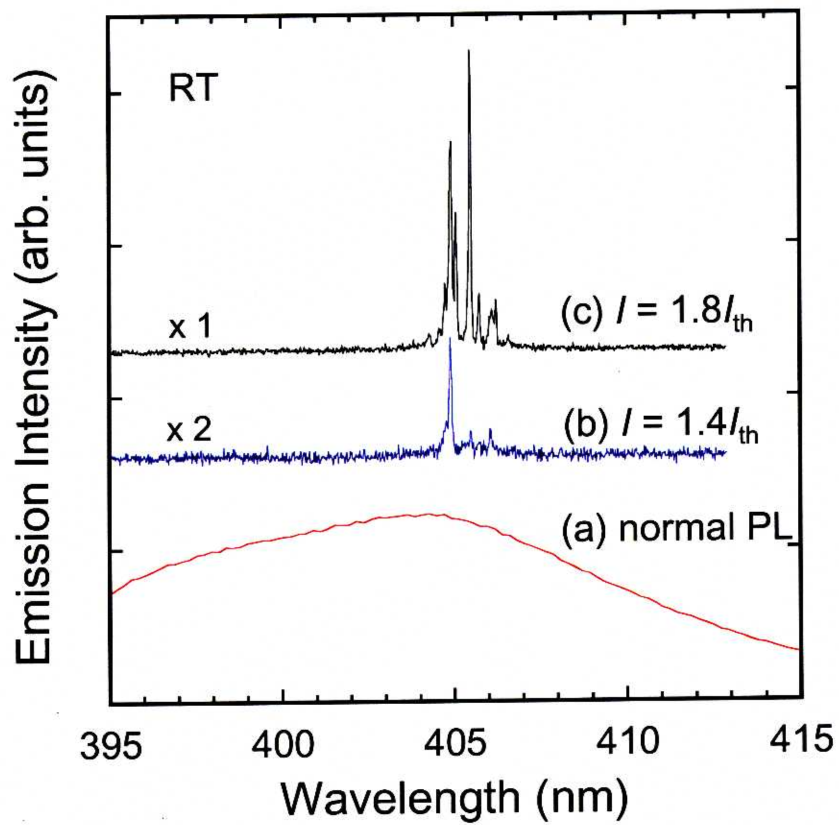

Figure 5.4: (a) Conventional PL spectrum, excited by a He–Cd laser (325 nm). The emission spectra above the threshold at (b) $I = 1.4I_{\mathrm{th}}$ and (c) $I = 1.8I_{\mathrm{th}}$, excited by a dye laser (367 nm).

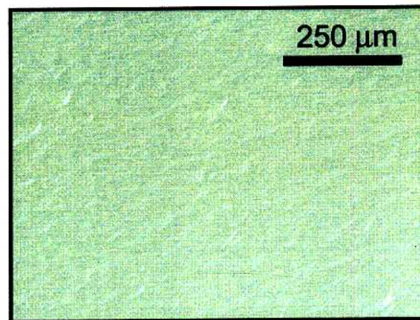

(a)

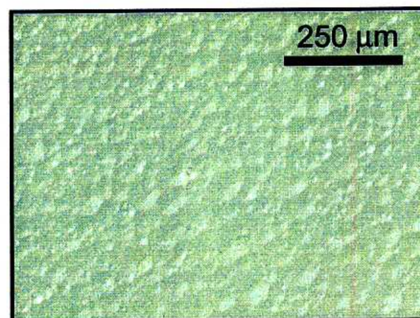

(b)

Figure 5.5: Nomarski microscope images of surface morphology of Mg-doped GaN grown at (a) 1045 and (b) 1071°C. The flow rates of TMG and Cp_2Mg were 44 and 0.053 μmol/min, respectively.

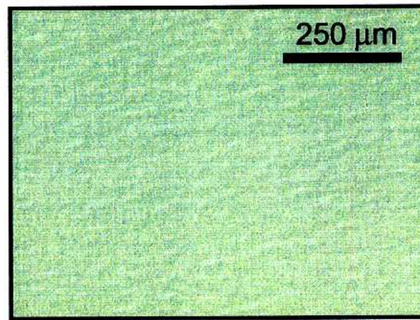

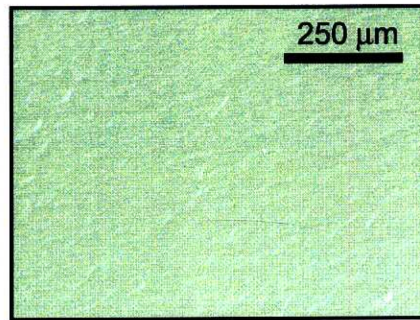

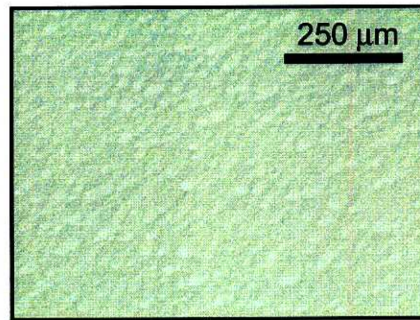

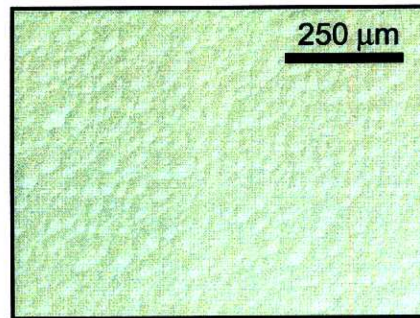

Figure 5.6: Nomarski microscope images of surface morphology of Mg-doped GaN under Cp_2Mg flow rate of (a) 0.044, (b) 0.053, (c) 0.062, and (d) 0.074 μmol/min. The flow rate of TMG was 44 μmol/min and the growth temperature was 1045 °C.

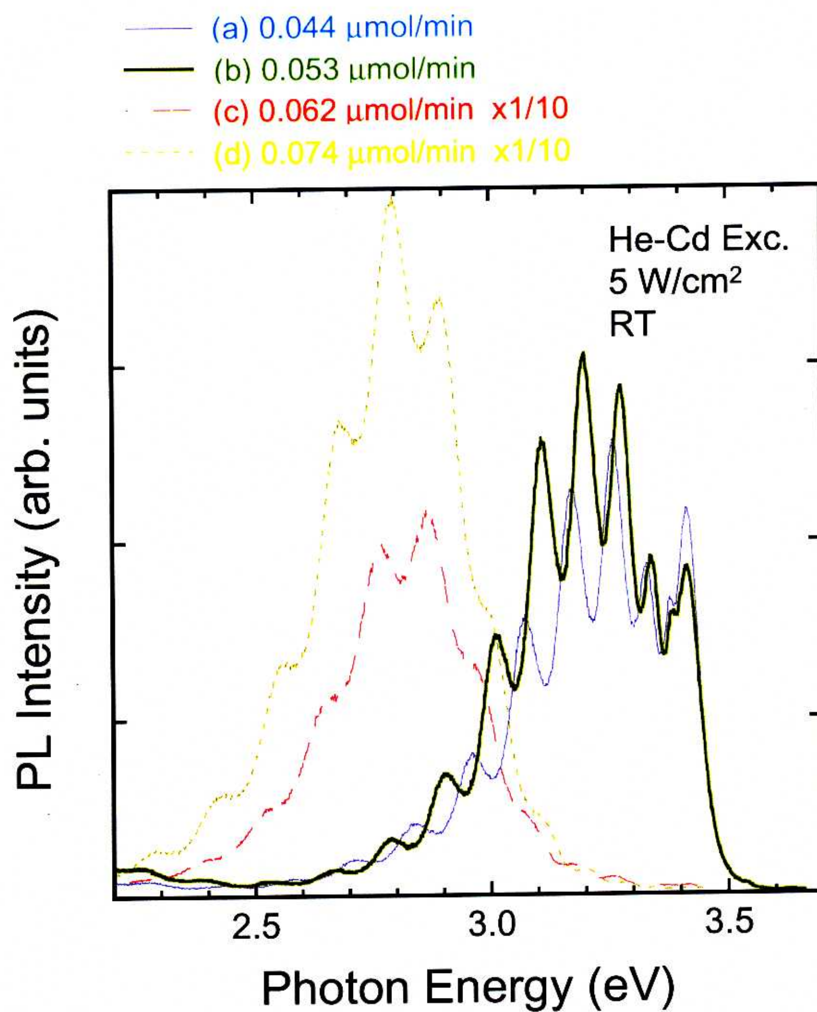

Figure 5.7: PL dependence on Cp_2Mg flow rate of (a) 0.044, (b) 0.053, (c) 0.062, and (d) 0.074 μmol/min. The flow rate of TMG was 44 μmol/min and the growth temperature was 1045 °C. The surface morphology is shown in Fig. 5.6.

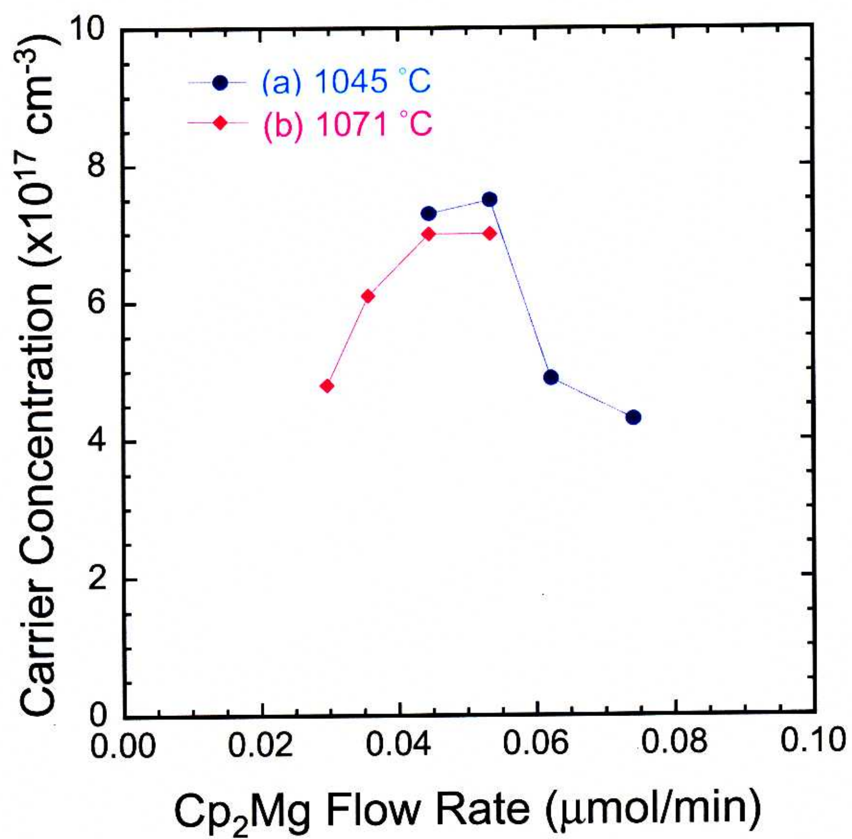

Figure 5.8: Dependence of *p*-type carrier concentration on the Cp_2Mg flow rate when the growth temperatures were (a) 1045 and (b) 1071 °C. The flow rate of TMG was 44 μmol/min.

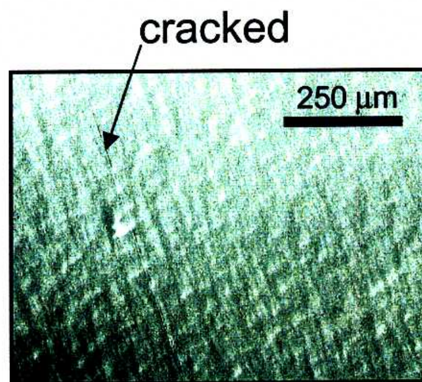

(a)

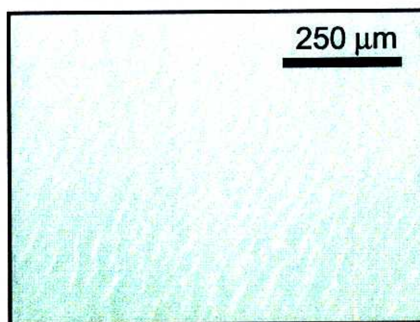

(b)

Figure 5.9: Nomarski microscope images of surface morphology of superlattices: (a) 200 pairs of 2.6-nm-thick GaN and 2.6-nm-thick $Al_{0.14}Ga_{0.86}N$ and (b) 180 pairs of 2.6-nm-thick GaN and 2.6-nm-thick $Al_{0.12}Ga_{0.88}N$.

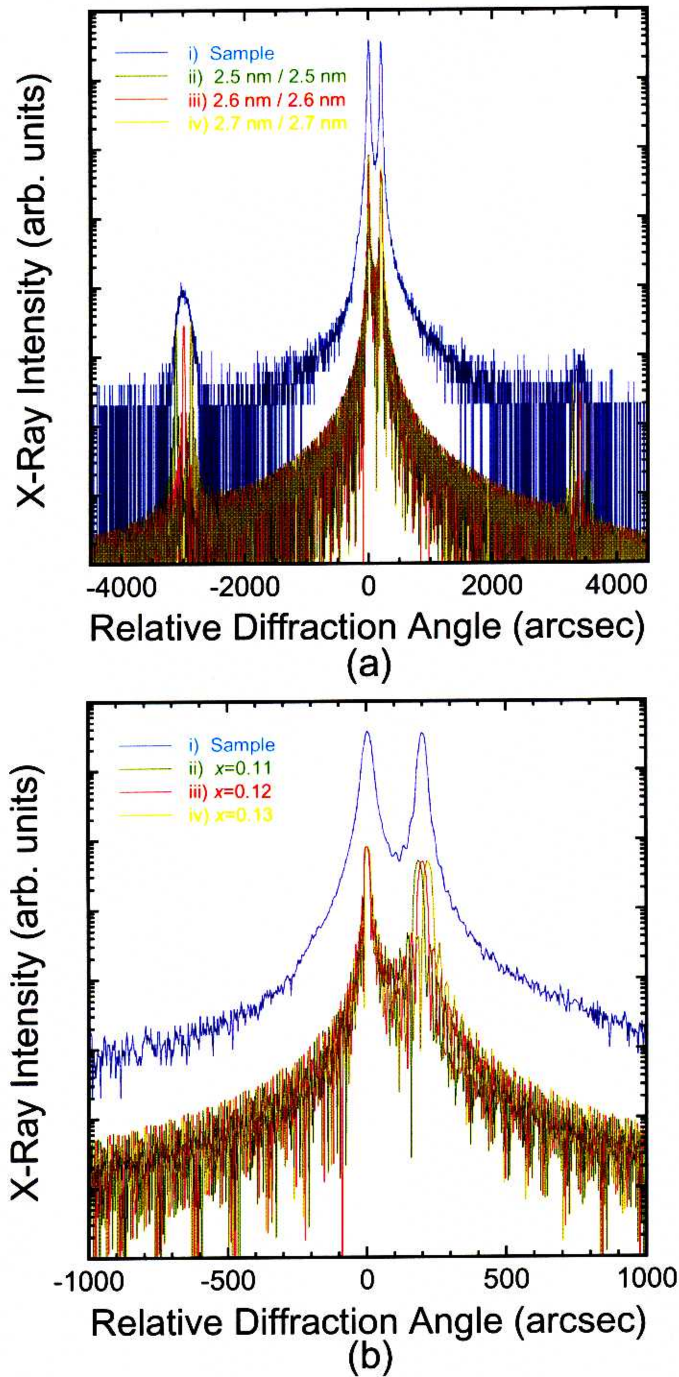

Figure 5.10: The $\omega/2\theta$ scan of (0002)-reflection XRD in 120 pairs of GaN/$Al_xGa_{1-x}N$ superlattices with the simulation of dependence on (a) layer thickness in GaN/$Al_{0.12}Ga_{0.88}N$ and (b) Al content x of $Al_xGa_{1-x}N$ layer in pairs of 2.6-nm-thick GaN and 2.6-nm-thick $Al_xGa_{1-x}N$.

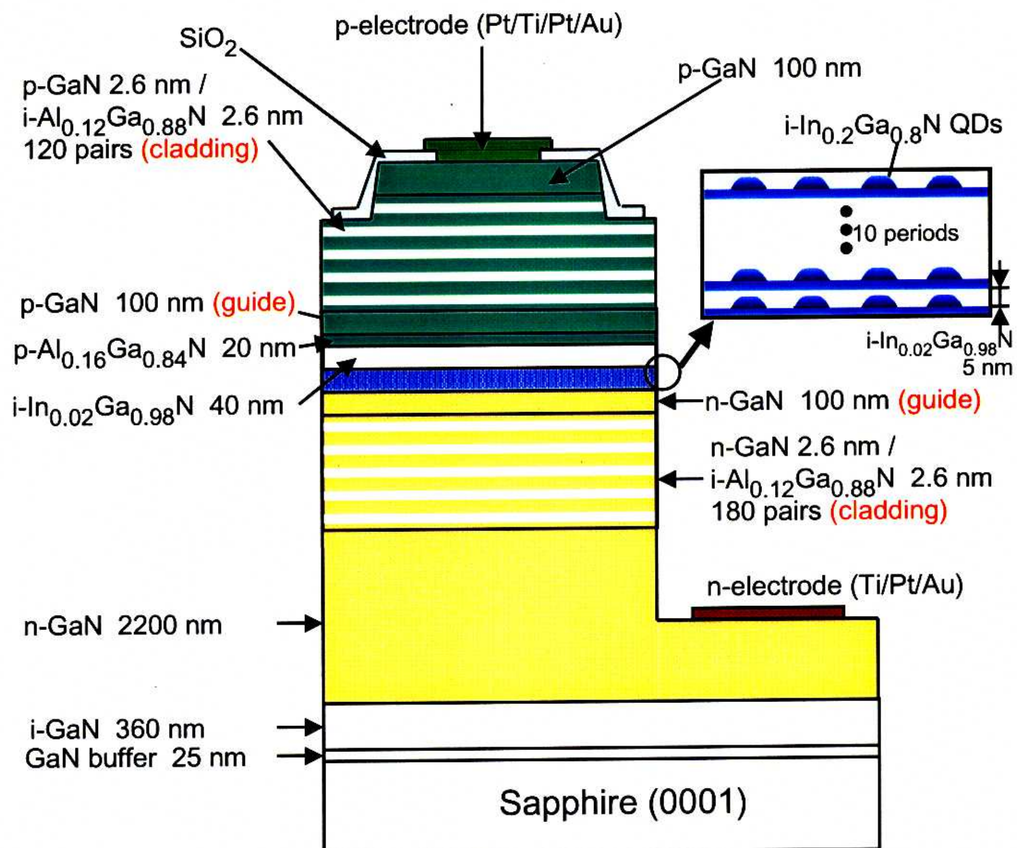

Figure 5.11: An illustration of $In_xGa_{1-x}N$ self-assembled QD lasers by current injection.

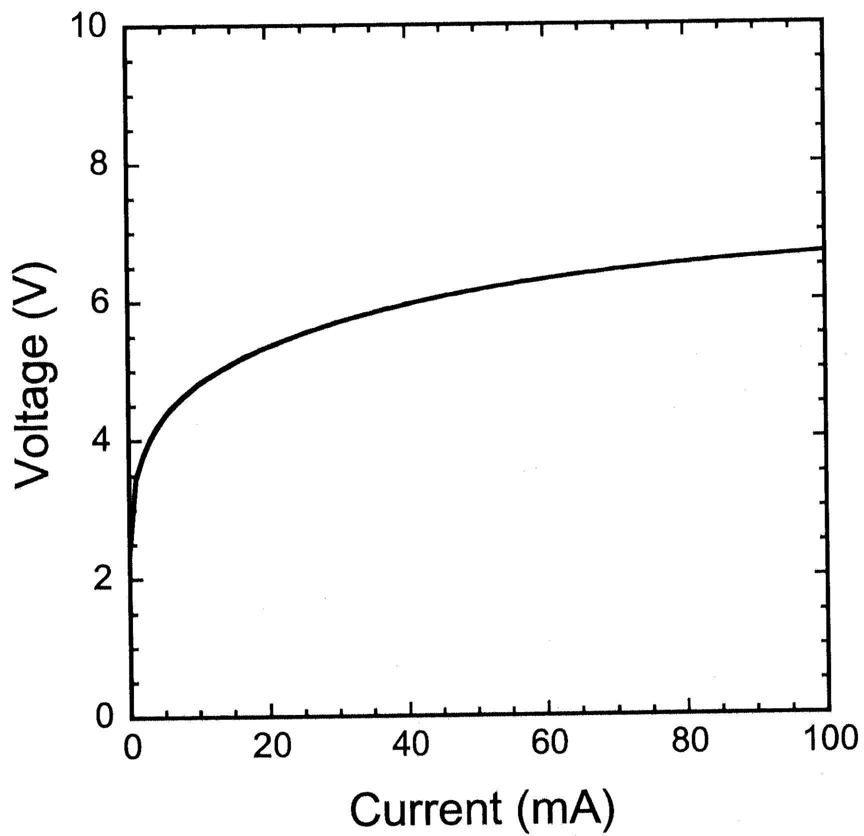

Figure 5.12: The I–V characteristic of $In_xGa_{1-x}N$ self-assembled QD lasers under dc operation at room temperature.

Chapter 6

Conclusions

6.1 Summary

In this thesis, the growth mechanism and optical properties of GaN-based QDs were investigated. Moreover, the lasers with $In_xGa_{1-x}N$ self-assembled QDs embedded in the active layer were demonstrated at room temperature.

In Chapter 2, the growth and optical properties of $In_xGa_{1-x}N$ self-assembled QDs were described. $In_xGa_{1-x}N$ self-assembled QDs were formed on a GaN layer without any surfactants using atmospheric-pressure MOCVD. The average diameter of the QDs was as small as 8.4 nm and average height was 2.1 nm. The QD density was 1.0×10^{10} cm^{-2}. The size and density of the QDs could be controlled by changing the growth conditions such as the InGaN coverage and growth temperature. The intense PL was observed from $In_xGa_{1-x}N$ self-assembled QDs at room temperature. The single dot spectroscopy was investigated by μ-PL, using the QD sample with 400-nm square apertures on the Al-masked surface. The linewidth of the PL was as narrow as 170 μeV, which was determined by a spectral resolution of the measurement system. This very sharp luminescence was a support of 0-D electronic states in the QDs. To increase the total QD density, vertically-stacked $In_xGa_{1-x}N$ QDs were also investigated. As the number of stacked layers increased, the total QD density and PL intensity increased.

In Chapter 3, selective growth of $In_xGa_{1-x}N$ QDs and their optical properties were investigated. The uniform array of hexagonal pyramids of GaN was realized with their radius of curvature 10-nm-scale. The $In_xGa_{1-x}N$ QDs were formed by performing the selective growth of $In_xGa_{1-x}N/In_{0.02}Ga_{0.98}N$ QWs on hexagonal pyramids of GaN. The intense PL from $In_xGa_{1-x}N$ was observed at the wavelength of 430 nm at room temperature. To identify the emitting areas of $In_xGa_{1-x}N$, the micro-PL intensity images were investigated with the spatial resolution of a few hundred nanometers. The PL at 430 nm was observed only from the tops of hexagonal pyramids, which indicated that $In_xGa_{1-x}N$ QDs were formed on the tops of hexagonal pyramids. To get higher-density $In_xGa_{1-x}N$ QDs, the selective growth was performed using a substrate prepared by EB lithography. The $In_xGa_{1-x}N$ QDs were formed even when such a fine pattern was fabricated.

In Chapter 4, the selectively-grown GaN QDs embedded in $Al_xGa_{1-x}N$ matrix were investigated. The uniform array of hexagonal pyramids was realized, including GaN QDs at the tops. The intense PL was observed from GaN QDs even at room temperature.

In Chapter 5, the application of GaN-based QDs to lasers was described. The lasers were fabricated with 10-layer stacked $In_xGa_{1-x}N$ self-assembled QDs embedded in the active layer. The lasers were characterized at room temperature under optical excitation. The clear threshold was observed in the emission intensity as a function of the excitation energy. Above the threshold, the emission linewidth was reduced to below 0.1 nm (resolution limit). These results support lasing action at room temperature. In addition, the growth conditions were investigated with respect to *p*-type GaN and $GaN/Al_{0.12}Ga_{0.88}N$ superlattices for cladding layer of laser structures. The *p-i-n* laser structure was fabricated and characterized with $In_xGa_{1-x}N$ self-assembled QDs embedded in the active layer.

6.2 Future prospect

In this thesis, the fabrication process and optical properties of GaN-based QDs were revealed. As the future prospect, the following items should be discussed.

Growth on GaN substrates In the epitaxial growth of GaN-based semiconductors, the Al_2O_3 or SiC substrates have been usually used. However, the dislocations due to mismatch of the lattice constant or thermal expansion coefficient affect the physical properties and the device performances. The research onto bulk GaN for the substrates have been intensively.[120–122] Indeed, the high output power of AlGaN QW LEDs is demonstrated using GaN substrates due to low dislocation density.[123] The homoepitaxy is also suitable to perform the fabrication of GaN-based QDs and investigate their physical properties.

Quantum dots combined with photonic crystals The photonic crystals[124] have attracted much attraction because of their possibility to realize the novel optical devices. For example, investigated were the microcavities with photonic crystals,[125–127] the ridge-type lasers with photonic crystal mirrors,[128] or the waveguides with photonic crystals[129] in the infrared region. As the emitting wavelength is shorter, the finer periodical structures are needed. From this reason, only a few studies have been conducted with respect to GaN-based photonic crystals.[130,131] It is possible to create the novel optical devices by combining the QDs where the electrons are confined with photonic crystals where the photons are confined.

Vertical cavity surface emitting lasers The blue vertical cavity surface emitting lasers (VCSELs) have attracted increasing attention,[132] since they should surpass conventional blue LDs in many applications, which can be formed in 2-D array of laser structures. The blue VCSELs with the active layer of $In_xGa_{1-x}N$ bulk or $In_xGa_{1-x}N$ QWs have been demonstrated.[133,134] The VCSELs with the active layer of GaN-based QDs are expected to have the superior characteristics and have much attraction of physical properties.

Intersubband transition in GaN-based quantum dots The intersubband transition have attracted much attention because of much flexibility of changing device characteristics such as emitting wavelength by designing band structures. The $GaN/Al_xGa_{1-x}N$

system has the large energy offset in conduction bands and is expected to be used as the ultrafast devices in optical communication systems, at the wavelength of 1.3 or 1.55 μm. The intersubband transition in GaN/$Al_xGa_{1-x}N$ MQWs has been demonstrated by the calculation[135] and experiments.[136–138] The intersubband transition in GaN-based QDs is also useful for ultrafast devices in optical communication systems.

Devices for quantum cryptography The quantum cryptography will be important in the future communication systems. One of the most important technologies in quantum cryptography is a device for realization of quantum key distribution. To realize quantum key distribution, the method using entangled photons is considered.[139] The single QDs have the possibility to generate the entangled photons, which was proposed theoretically[140] and discussed experimentally.[141] The short-wavelength light emitting QDs such as $In_xGa_{1-x}N$ QDs or GaN QDs are desirable to be used as the single photon sources for quantum key distribution.

The author hopes that the present study contributes to the further fundamental understanding of GaN-based QDs and applications to the novel devices.

Appendix A

Carrier Density at Transparent Condition

As briefly discussed in Chapter 1, the carrier density n_{tr} at transparent condition in the QWs increases when the effective mass of electrons m_c or the ratio of the effective mass of holes to that of electrons m_v/m_c is larger. In Appendix A, the calculation method of the carrier density at transparent condition is discussed.

The threshold current density I_{th} is represented using n_{tr} as eq. (1.2):

$$I_{\mathrm{th}} = \gamma e V n_{\mathrm{tr}}/\tau, \tag{A.1}$$

where e, V, and τ are the electron charge, the volume of active layer, and carrier lifetime, respectively. In Eq. (A.1), γ is a constant of which the value is in the range of 1.2–1.5.

Here, the electron density n of the conduction band in the QWs is given by

$$\begin{aligned} n &= \int_0^{\infty} \frac{m_c}{\pi\hbar^2} \frac{1}{l_z} \frac{1}{1 + e^{(\varepsilon - \varepsilon_c)/k_B T}} \, d\varepsilon \\ &= \frac{m_c}{\pi\hbar^2 l_z} k_B T \ln\left(1 + e^{\varepsilon_c/k_B T}\right), \end{aligned} \tag{A.2}$$

where l_z, ε_c, k_B, and T are the thickness of the QWs, chemical potential of electrons, Boltzmann constant, and temperature, respectively. The step function of $m_c/\pi\hbar^2$ is used as the density of states in the QWs. Also, the hole density p of the valence band in the

QWs is given by

$$p = \int_{-\infty}^{0} \frac{m_v}{\pi\hbar^2} \frac{1}{l_z} \left\{ 1 - \frac{1}{1 + e^{(\varepsilon - \varepsilon_v)/k_B T}} \right\} d\varepsilon$$
$$= \frac{m_v}{\pi\hbar^2 l_z} k_B T \ln\left(1 + e^{-\varepsilon_v/k_B T}\right), \tag{A.3}$$

where ε_v is the chemical potential of holes. The transparent condition is written as

$$\varepsilon_c - \varepsilon_v > E_g, \tag{A.4}$$

where E_g is the bandgap energy. To simply the calculation, the following assumption is used: $E_g \to 0$. Moreover, equation (A.4) can be re-written under the rough assumption:

$$\varepsilon_c - \varepsilon_v = 0. \tag{A.5}$$

Therefore, the electron density n and hole density p are under the function of ε_c. At transparent condition, the electron density n is equal to the hole density p, using eqs. (A.2) and (A.3):

$$\frac{m_c}{\pi\hbar^2 l_z} k_B T \ln\left(1 + e^{\varepsilon_c/k_B T}\right) = \frac{m_v}{\pi\hbar^2 l_z} k_B T \ln\left(1 + e^{-\varepsilon_c/k_B T}\right). \tag{A.6}$$

From Eq. (A.6), the function $A(x)$ is considered:

$$A(x) = \Gamma \ln\left(1 + \frac{1}{x}\right) - \ln(1 + x), \tag{A.7}$$

where x and Γ are defined as:

$$x = e^{\varepsilon_c/k_B T} \tag{A.8}$$

and

$$\Gamma = m_v/m_c. \tag{A.9}$$

If x at $A(x) = 0$ is calculated under various Γ, n_{tr} can be obtained from Eq. (A.2) or (A.3).

Bibliography

1) S. Nakamura and G. Fasol, *The Blue Laser Diode*, (Springer, Heidelberg, 1997).

2) I. Akasaki and H. Amano, "Crystal growth and conductivity control of group III nitride semiconductors and their applications to short wavelength light emitters," Jpn. J. Appl. Phys. **36**, 5393 (1997).

3) S. Nakamura, "The roles of structural imperfections in InGaN-based blue light-emitting diodes and laser diodes," Science **281**, 956 (1998).

4) H. Amano, N. Sawaki, I. Akasaki, and Y. Toyoda, "Metalorganic vapor phase epitaxial growth of a high quality GaN film using an AlN buffer layer," Appl. Phys. Lett. **48**, 353 (1986).

5) H. Amano, M. Kito, K. Hiramatsu, and I. Akasaki, "*p*-type conduction in Mg-doped GaN treated with low-energy electron beam irradiation (LEEBI)," Jpn. J. Appl. Phys. **28**, L2112 (1989).

6) S. Nakamura, "GaN growth using GaN buffer layer," Jpn. J. Appl. Phys. **30**, L1705 (1991).

7) S. Nakamura and T. Mukai, "High-quality InGaN films grown on GaN films," Jpn. J. Appl. Phys. **31**, L1457 (1992).

8) S. Nakamura, M. Senoh, N. Iwasa, and S. Nagahama, "High-brightness InGaN blue, green and yellow light-emitting diodes with quantum well structures," Jpn. J. Appl. Phys. **34**, L797 (1995); T. Mukai, M. Yamada, and S. Nakamura, "Characteristics of InGaN-based UV/blue/green/amber/red light-emitting diodes," *ibid.* **38**, 3976 (1999).

9) S. Nakamura, M. Senoh, S. Nagahama, N. Iwasa, T. Yamada, T. Matsushita, H. Kiyoku, and Y. Sugimoto, "InGaN-based multi-quantum-well-structure laser diodes," Jpn. J. Appl. Phys. **35**, L74 (1996); S. Nagahama, N. Iwasa, M. Senoh, T. Matsushita, Y. Sugimoto, H. Kiyoku, T. Kozaki, M. Sano, H. Matsumura, H. Umemoto, K. Chocho, and T. Mukai, "High-power

and long-lifetime InGaN multi-quantum-well laser diodes grown on low-dislocation-density GaN substrates," *ibid.* **39**, L647 (2000).

10) I. Akasaki, S. Sota, H. Sakai, T. Tanaka, M. Koike, and H. Amano, "Shortest wavelength semiconductor laser diode," Electron. Lett. **32**, 1105 (1996); T. Takeuchi, T. Detchprohm, M. Iwaya, N. Hayashi, K. Isomura, K. Kimura, M. Yamaguchi, H. Amano, I. Akasaki, Yw. Kaneko, R. Shioda, S. Watanabe, T. Hidaka, Y. Yamaoka, Ys. Kaneko, and N. Yamada, "Improvement of far-field pattern in nitride laser diodes," Appl. Phys. Lett. **75**, 2960 (1999).

11) K. Itaya, M. Onomura, J. Nishio, L. Sugiura, S. Saito, M. Suzuki, J. Rennie, S. Nunoue, M. Yamamoto, H. Fujimoto, Y. Kokubun, Y. Ohba, G. Hatakoshi, and M. Ishikawa, "Room temperature pulsed operation of nitride based multi-quantum-well laser diodes with cleaved facets on conventional c-face sapphire substrates," Jpn. J. Appl. Phys. **35**, L1315 (1996); M. Onomura, S. Saito, K. Sasanuma, G. Hatakoshi, M. Nakasuji, J. Rennie, L. Sugiura, S. Nunoue, J. Nishio, and K. Itaya, "Analysis of transverse modes of nitride-based laser diodes," IEEE J. Sel. Top. Quantum Electron. **5**, 765 (1999).

12) G. E. Bulman, K. Doverspike, S. T. Sheppard, T. W. Weeks, H. S. Kong, H. M. Dieringer, J. A. Edmond, J. D. Brown, J. T. Swindell, and J. F. Schetzina, "Pulsed operation lasing in a cleaved-facet InGaN/GaN MQW SCH laser grown on 6H-SiC," Electron. Lett. **33**, 1556 (1997); Y.-K. Song, M. Kuball, A. V. Nurmikko, G. E. Bulman, K. Doverspike, S. T. Sheppard, T. W. Weeks, M. Leonard, H. S. Kong, H. Dieringer, and J. Edmond, "Gain characteristics of InGaN/GaN quantum well diode lasers," Appl. Phys. Lett. **72**, 1418 (1998).

13) A. Kuramata, K. Domen, R. Soejima, K. Horino, S. Kubota, and T. Tanahashi, "InGaN laser diode grown on 6H-SiC substrate using low-pressure metal organic vapor phase epitaxy," Jpn. J. Appl. Phys. **36**, L1130 (1997); A. Kuramata, S. Kubota, R. Soejima, K. Domen, K. Horino, P. Hacke, and T. Tanahashi, "Continuous wave operation of InGaN laser diodes fabricated on SiC substrates," IEICE Trans. Electron. **E83-C**, 546 (2000).

14) M. P. Mack, A. Abare, M. Aizcorbe, P. Kozodoy, S. Keller, U. K. Mishra, L. Coldren, and S. DenBaars, "Characteristics of indium-gallium-nitride multiple-quantum-well blue laser diodes grown by MOCVD," MRS Internet J. Nitride Semicond. Res. **2**, 41 (1997); M. Hansen, P. Fini, L. Zhao, A. C. Abare, L. A. Coldren, J. S. Speck, and S. P. DenBaars, "Improved characteristics of InGaN multiple-quantum-well laser diodes grown on laterally epitaxially overgrown GaN on sapphire," Appl. Phys. Lett. **76**, 529 (2000).

15) F. Nakamura, T. Kobayashi, T. Tojyo, T. Asatsuma, K. Nagahama, H. Kawai, and M. Ikeda, "Room-temperature pulsed operation of a GaInN multiple-quantum-well laser diode," Elec-

tron. Lett. **34**, 1105 (1998); T. Tojyo, T. Asano, M. Takeya, T. Hino, S. Kijima, S. Goto, S. Uchida, and M. Ikeda, "GaN-based high power blue-violet laser diodes," Jpn. J. Appl. Phys. **40**, 3206 (2001).

16) M. Kneissl, D. P. Bour, N. M. Johnson, L. T. Romano, B. S. Krusor, R. Donaldson, J. Walker, and C. Dunnrowicz, "Characterization of AlGaInN diode lasers with mirrors from chemically assisted ion beam etching," Appl. Phys. Lett. **72**, 1539 (1998); W. S. Wong, M. Kneissl, P. Mei, D. W. Treat, M. Teepe, and N. M. Johnson, "Continuous-wave InGaN multiple-quantum-well laser diodes on copper substrates," *ibid.* **78**, 1198 (2001).

17) Y. Kimura, M. Miyachi, H. Takahashi, T. Tanaka, M. Nishitsuka, A. Watanabe, H. Ota, and K. Chikuma, "Room-temperature pulsed operation of GaN-based laser diodes on a-face sapphire substrate grown by low-pressure metalorganic chemical vapor deposition," Jpn. J. Appl. Phys. **37**, L1231 (1998); Y. Kimura, A. Ito, M. Miyachi, H. Takahashi, A. Watanabe, H. Ota, N. Ito, T. Tanabe, M. Sonobe, and K. Chikuma, "Optical gain and optical internal loss of GaN-based laser diodes measured by variable stripe length method with laser processing," *ibid.* **40**, L1103 (2001).

18) M. Kuramoto, C. Sasaoka, Y. Hisanaga, A. Kimura, A. A. Yamaguchi, H. Sunakawa, N. Kuroda, M. Nido, A. Usui, and M. Mizuta, "Room-temperature continuous-wave operation of InGaN multi-quantum-well laser diodes grown on an n-GaN substrate with a backside n-contact," Jpn. J. Appl. Phys. **38**, L184 (1999); M. Kuramoto, A. Kimura, C. Sasaoka, T. Arakida, M. Nido, and M. Mizuta, "Novel ridge-type InGaN multiple-quantum-well laser diodes fabricated by selective area re-growth on n-GaN substrates," *ibid.* **40**, L925 (2001).

19) M. Koike, S. Yamasaki, S. Nagai, Y. Tezen, S. Iwayama, A. Kojima, T. Hiramatsu, T. Umezaki, M. Itoh, H. Yamashita, M. Ohashi, A. Kimura, M. Sato, and K. Ohguchi, "RT-CW operation of GaN-based laser diodes improved by GaN/GaInN optical guiding layers," *Proc. Int. Workshop Nitride Semiconductors, Nagoya, 2000*, IPAP Conf. Series **1**, 886 (2000); M. Koike, S. Nagai, S. Yamasaki, Y. Tezen, A. Kojima, and S. Iwayama, "GaN-based MQW light emitting devices," Phys. Stat. Sol. (a) **188**, 9 (2001).

20) S. Ito, Y. Yamasaki, S. Omi, T. Ohno, K. Takatani, T. Okumura, Y. Ueta, Y. Tsuda, T. Yuasa, T. Kamikawa, D. Hanaoka, M. Ishida, and M. Taneya, "Analysis of lateral transverse modes of ridge-geometry AlGaInN laser diodes," *Proc. Int. Workshop Nitride Semiconductors, Nagoya, 2000*, IPAP Conf. Series **1**, 892 (2000).

21) S. Nakamura, M. Senoh, S. Nagahama, N. Iwasa, T. Matsushita, and T. Mukai, "Blue InGaN-based laser diodes with an emission wavelength of 450 nm," Appl. Phys. Lett. **76**,

22 (2000); S. Nagahama, T. Yanamoto, M. Sano, and T. Mukai, "Characteristics of InGaN laser diodes in the pure blue region," *ibid.* **79**, 1948 (2001).

22) Y. Arakawa and H. Sakaki, "Multidimensional quantum well laser and temperature dependence of its threshold current," Appl. Phys. Lett. **40**, 939 (1982).

23) M. Asada, Y. Miyamoto, and Y. Suematsu, "Gain and its threshold of three-dimensional quantum-box lasers," IEEE J. Quantum Electron. **QE-22**, 1915 (1986).

24) A. Yariv, "Scaling laws and minimum threshold currents for quantum-confined semiconductor lasers," Appl. Phys. Lett. **53**, 1033 (1988).

25) T. Takahashi and Y. Arakawa, "Theoretical analysis of gain and dynamic properties of quantum-well box lasers," Optoelectron. Devices Technol. **3**, 155 (1988).

26) Y. Arakawa, K. Vahala, and A. Yariv, "Quantum noise and dynamics in quantum well and quantum wire lasers," Appl. Phys. Lett. **45**, 950 (1984); Y. Arakawa and A. Yariv, "Quantum well lasers–gain, spectra, dynamics," IEEE J. Quantum Electron. **QE-22**, 1887 (1986).

27) D. Leonard, M. Krishnamurthy, C. M. Reaves, S. P. Denbaars, and P. M. Petroff, "Direct formation of quantum-sized dots from uniform coherent islands of InGaAs on GaAs surfaces," Appl. Phys. Lett. **63**, 3203 (1993).

28) N. Kirstaedter, N. N. Ledentsov, M. Grundmann, D. Bimberg, V. M. Ustinov, S. S. Ruvimov, M. V. Maximov, P. S. Kop'ev, Zh. I. Alferov, U. Richter, P. Werner, U. Gösele, and J. Heydenreich, "Low threshold, large T_0 injection laser emission from (InGa)As quantum dots," Electron. Lett. **30**, 1416 (1994).

29) D. L. Huffaker, G. Park, Z. Zou, O. B. Shchekin, and D. G. Deppe, "1.3 μm room-temperature GaAs-based quantum-dot laser," Appl. Phys. Lett. **73**, 2564 (1998).

30) K. Mukai, Y. Nakata, K. Otsubo, M. Sugawara, N. Yokoyama, and H. Ishikawa, "1.3-μm CW lasing of InGaAs–GaAs quantum dots at room temperature with a threshold current of 8 mA," IEEE Photon. Technol. Lett. **11**, 1205 (1999).

31) Y. Arakawa, M. Nishioka, H. Nakayama, and M. Kitamura, "Growth and optical properties of self-assembled quantum dots for semiconductor lasers with confined electrons and photons," IEICE Trans. Electron. **E79-C**, 1487 (1996).

32) Y. Narukawa, Y. Kawakami, M. Funato, Sz. Fujita, Sg. Fujita, and S. Nakamura, "Role of self-formed InGaN quantum dots for exciton localization in the purple laser diode emitting at 420 nm," Appl. Phys. Lett. **70**, 981 (1997).

33) S. Chichibu, T. Azuhata, T. Sota, and S. Nakamura, "Luminescences from localized states in InGaN epilayers", Appl. Phys. Lett. **70**, 2822 (1997).

34) M. Suzuki, T. Uenoyama, and A. Yanase, "First-principles calculations of effective-mass parameters of AlN and GaN," Phys. Rev. B **52**, 8132 (1995).

35) C. Kittel, *Introduction to Solid State Electronics 7th ed.*, (John Wiley & Sons, New York, 1996), p. 214.

36) T. Saito and Y. Arakawa, "Quantum confined electronic states in InGaN dots embedded in GaN: tight-binding calculation," *Proc. IEEE 27th Int. Symp. Compound Semiconductors*, (IEEE, Piscataway, 2000), p. 285.

37) S. Tanaka, S. Iwai, and Y. Aoyagi, "Self-assembling GaN quantum dots on $Al_xGa_{1-x}N$ surfaces using a surfactant," Appl. Phys. Lett. **69**, 4096 (1996).

38) X. Q. Shen, S. Tanaka, S. Iwai, and Y. Aoyagi, "The formation of GaN dots on $Al_xGa_{1-x}N$ surfaces using Si in gas-source molecular beam epitaxy," Appl. Phys. Lett. **72**, 344 (1998).

39) H. Hirayama, S. Tanaka, P. Ramvall, and Y. Aoyagi, "Intense photoluminescence from self-assembling InGaN quantum dots artificially fabricated on AlGaN surfaces," Appl. Phys. Lett. **72**, 1736 (1998).

40) P. Ramvall, P. Riblet, S. Nomura, Y. Aoyagi, and S. Tanaka, "Optical properties of GaN quantum dots," J. Appl. Phys. **87**, 3883 (2000).

41) A. Petersson, A. Gustafsson, L. Samuelson, S. Tanaka, and Y. Aoyagi, "Cathodoluminescence spectroscopy and imaging of individual GaN dots," Appl. Phys. Lett. **74**, 3513 (1999).

42) M. Kuball, J. Gleize, S. Tanaka, and Y. Aoyagi, "Resonant Raman scattering on self-assembled GaN quantum dots," Appl. Phys. Lett. **78**, 987 (2001).

43) S. Tanaka, H. Hirayama, Y. Aoyagi, Y. Narukawa, Y. Kawakami, Sz. Fujita, and Sg. Fujita, "Stimulated emission from optically pumped GaN quantum dots," Appl. Phys. Lett. **71**, 1299 (1997).

44) K. Kawasaki, D. Yamazaki, A. Kinoshita, H. Hirayama, K. Tsutsui, and Y. Aoyagi, "GaN quantum-dot formation by self-assembling droplet epitaxy and application to single-electron transistors," Appl. Phys. Lett. **79**, 2243 (2001).

45) N. Koguchi, S. Takahashi, and T. Chikyow, "New MBE growth method for InSb quantum well boxes," J. Cryst. Growth **111**, 688 (1991).

46) I. N. Stranski and L. Krastanow, "Zur theorie der orientierten ausscheidung von lonenkristallen aufeinander," Sitzungsberichte d. Akad. d. Wissenschaften in Wein, Abt. IIb, **146**, 797 (1937).

47) B. Daudin, F. Widmann, G. Feuillet, Y. Samson, M. Arlery, and J. L. Rouvière, "Stranski–Krastanov growth mode during the molecular beam epitaxy of highly strained GaN," Phys. Rev. B **56**, R7069 (1997).

48) B. Damilano, N. Grandjean, F. Semond, J. Massies, and M. Leroux, "From visible to white light emission by GaN quantum dots on Si(111) substrate," Appl. Phys. Lett. **75**, 962 (1999).

49) J. Brown, C. Elsass, C. Poblenz, P. M. Petroff, and J. S. Speck, "Temperature dependent photoluminescence of MBE grown gallium nitride quantum dots," Phys. Stat. Sol. (b) **228**, 199 (2001).

50) F. Widmann, B. Daudin, G. Feuillet, Y. Samson, J. L. Rouvière, and N. Pelekanos, "Growth kinetics and optical properties of self-organized GaN quantum dots," J. Appl. Phys. **83**, 7618 (1998).

51) B. Daudin, F. Widmann, J. Simon, G. Feuillet, J. L. Rouvière, N. T. Pelekanos, and G. Fishman, "Piezoelectric properties of GaN self-organized quantum dots," MRS Internet J. Nitride Semicond. Res. **4S1**, G9.2 (1999).

52) J. Gleize, J. Frandon, F. Demangeot, M. A. Renucci, C. Adelmann, B. Daudin, G. Feuillet, B. Damilano, N. Grandjean, and J. Massies, "Signature of GaN–AlN quantum dots by nonresonant Raman scattering," Appl. Phys. Lett. **77**, 2174 (2000).

53) J. Gleize, F. Demangeot, J. Frandon, M. A. Renucci, M. Kuball, B. Damilano, N. Grandjean, and J. Massies, "Direct signature of strained GaN quantum dots by Raman scattering," Appl. Phys. Lett. **79**, 686 (2001).

54) B. Damilano, N. Grandjean, S. Dalmasso, and J. Massies, "Room-temperature blue-green emission from InGaN/GaN quantum dots made by strain-induced islanding growth," Appl. Phys. Lett. **75**, 3751 (1999).

55) C. Adelmann, J. Simon, G. Feuillet, N. T. Pelekanos, B. Daudin, and G. Fishman, "Self-assembled InGaN quantum dots grown by molecular-beam epitaxy," Appl. Phys. Lett. **76**, 1570 (2000).

56) P. Lefebvre, T. Taliercio, A. Morel, J. Allègre, M. Gallart, B. Gil, H. Mathieu, B. Damilano, N. Grandjean, and J. Massies, "Effects of GaAlN barriers and of dimensionality on optical

recombination processes in InGaN quantum wells and quantum boxes," Appl. Phys. Lett. **78**, 1538 (2001).

57) M. Miyamura, K. Tachibana, T. Someya, and Y. Arakawa, "Stranski–Krastanow growth of GaN quantum dots by metalorganic chemical vapor deposition," J. Cryst. Growth (in print).

58) J. Wang, M. Nozaki, M. Lachab, Y. Ishikawa, R. S. Qhalid Fareed, T. Wang, M. Hao, and S. Sakai, "Metalorganic chemical vapor deposition selective growth and characterization of InGaN quantum dots," Appl. Phys. Lett. **75**, 950 (1999).

59) A. D. Andreev and E. P. O'Reilly, "Theory of the electronic structure of GaN/AlN hexagonal quantum dots," Phys. Rev. B **62**, 15851 (2000); A. D. Andreev and E. P. O'Reilly, "Optical transitions and radiative lifetime in GaN/AlN self-organized quantum dots," Appl. Phys. Lett. **79**, 521 (2001).

60) K. Tachibana, T. Someya, and Y. Arakawa, "Nanometer-scale InGaN self-assembled quantum dots grown by metalorganic chemical vapor deposition," Appl. Phys. Lett. **74**, 383 (1999).

61) D. Kapolnek, X. H. Wu, B. Heying, S. Keller, B. P. Keller, U. K. Mishra, S. P. DenBaars, and J. S. Speck, "Structural evolution in epitaxial metalorganic chemical vapor deposition grown GaN films on sapphire," Appl. Phys. Lett. **67**, 1541 (1995).

62) D. Leonard, K. Pond, and P. M. Petroff, "Critical layer thickness for self-assembled InAs islands on GaAs," Phys. Rev. B **50**, 11687 (1994).

63) P. Chen, Q. Xie, A. Madhukar, L. Chen, and A. Konkar, "Mechanisms of strained island formation in molecular-beam epitaxy of InAs on GaAs (100)," J. Vac. Sci. Technol. B **12**, 2568 (1994).

64) O. Moriwaki, T. Someya, K. Tachibana, S. Ishida, and Y. Arakawa, "Narrow photoluminescence peaks from localized states in InGaN quantum dot structures," Appl. Phys. Lett. **76**, 2361 (2000).

65) H. F. Hess, E. Betzig, T. D. Harris, L. N. Pfeiffer, and K. W. West, "Near-field spectroscopy of the quantum constituents of a luminescent system," Science **264**, 1740 (1994).

66) K. Ota, N. Usami, and Y. Shiraki, "Temperature dependence of microscopic photoluminescence spectra of quantum dots and quantum wells," Physica E **2**, 573 (1998).

67) K. Asaoka, Y. Ohno, S. Kishimoto, and T. Mizutani, "Microscopic photoluminescence study of InAs single quantum dots grown on (100) GaAs," Jpn. J. Appl. Phys. **38**, 546 (1999).

68) S. Chichibu, K. Wada, and S. Nakamura, "Spatially resolved cathodoluminescence spectra of InGaN quantum wells," Appl. Phys. Lett. **71**, 2346 (1997).

69) P. A. Crowell, D. K. Young, S. Keller, E. L. Hu, and D. D. Awschalom, "Near-field scanning optical spectroscopy of an InGaN quantum well," Appl. Phys. Lett. **72**, 927 (1998).

70) A. Vertikov, M. Kuball, A. V. Nurmikko, Y. Chen, and S.-Y. Wang "Near-field optical study of InGaN/GaN epitaxial layers and quantum wells," Appl. Phys. Lett. **72**, 2645 (1998).

71) Q. Xie, A. Madhukar, P. Chen, and N. P. Kobayashi, "Vertically self-organized InAs quantum box islands on GaAs (100)," Phys. Rev. Lett. **75**, 2542 (1995).

72) G. S. Solomon, J. A. Trezza, A. F. Marshall, and J. S. Harris, Jr., "Vertically aligned and electronically coupled growth induced InAs islands in GaAs," Phys. Rev. Lett. **76**, 952 (1996).

73) N. N. Ledentsov, V. A. Shchukin, M. Grundmann, N. Kirstaedter, J. Bohrer, O. Schmidt, D. Bimberg, V. M. Ustinov, A. Yu. Egorov, A. E. Zhukov, P. S. Kop'ev, S. V. Zaitsev, N. Yu. Gordeev, Zh. I. Alferov, A. I. Borovkov, A. O. Kosogov, S. S. Ruvimov, P. Werner, U. Gosele, and J. Heydenreich, "Direct formation of vertically coupled quantum dots in Stranski–Krastanow growth," Phys. Rev. B **54**, 8743 (1996).

74) Y. Sugiyama, Y. Nakata, K. Imamura, S. Muto, and N. Yokoyama, "Stacked InAs self-assembled quantum dots on (001) GaAs grown by molecular beam epitaxy," Jpn. J. Appl. Phys. **35**, 1320 (1996).

75) J. L. Rouvière, J. Simon, N. Pelekanos, B. Daudin, and G. Feuillet, "Preferential nucleation of GaN quantum dots at the edge of AlN threading dislocations," Appl. Phys. Lett. **75**, 2632 (1999).

76) E. Martinez-Guerrero, C. Adelmann, F. Chabuel, J. Simon, N. T. Pelekanos, G. Mula, B. Daudin, G. Feuillet, and H. Mariette, "Self-assembled zinc blende GaN quantum dots grown by molecular-beam epitaxy," Appl. Phys. Lett. **77**, 809 (2001).

77) F. Widmann, J. Simon, B. Daudin, G. Feuillet, J. L. Rouvière, N. T. Pelekanos, and G. Fishman, "Blue-light emission from GaN self-assembled quantum dots due to giant piezoelectric effect," Phys. Rev. B **58**, R15989 (1998).

78) V. Chamard, T. H. Metzger, E. Bellet-Amalric, B. Daudin, C. Adelmann, H. Mariette, and G. Mula, "Structure and ordering of GaN quantum dot multilayers," Appl. Phys. Lett. **79**, 1971 (2001).

79) Y. Kato, S. Kitamura, K. Hiramatsu, and N. Sawaki, "Selective growth of wurtzite GaN and $Al_xGa_{1-x}N$ on GaN/sapphire substrates by metalorganic vapor phase epitaxy," J. Cryst. Growth **144**, 133 (1994).

80) S. Kitamura, K. Hiramatsu, and N. Sawaki, "Fabrication of GaN hexagonal pyramids on dot-patterned GaN/sapphire substrates via selective metalorganic chemical vapor phase epitaxy," Jpn. J. Appl. Phys. **34**, L1184 (1995).

81) T. Tanaka, K. Uchida, A. Watanabe, and S. Minagawa, "Selective growth of gallium nitride layers with a rectangular cross-sectional shape and stimulated emission from the optical waveguides observed by photopumping," Appl. Phys. Lett. **68**, 976 (1996).

82) T. Akasaka, Y. Kobayashi, S. Ando, N. Kobayashi, and M. Kumagai, "Selective MOVPE of GaN and $Al_xGa_{1-x}N$ with smooth vertical facets," J. Cryst. Growth **189/190**, 72 (1998).

83) S. Bidnyk, B. D. Little, Y. H. Cho, J. Krasinski, J. J. Song, W. Yang, and S. A. McPherson, "Laser action in GaN pyramids grown on (111) silicon by selective lateral overgrowth," Appl. Phys. Lett. **73**, 2242 (1998).

84) T. Akasaka, S. Ando, and N. Kobayashi, "Electroluminescence from *p*-GaN/*n*-InGaN MQW hexagonal microprism fabricated by selective area metalorganic vapor phase epitaxy," *Proc. Int. Workshop Nitride Semiconductors, Nagoya, 2000*, IPAP Conf. Series **1**, 864 (2000).

85) A. Usui, H. Sunakawa, A. Sakai, and A. A. Yamaguchi, "Thick GaN epitaxial growth with low dislocation density by hydride vapor phase epitaxy," Jpn. J. Appl. Phys. **36**, L899 (1997).

86) T. S. Zheleva, O.-H. Nam, M. D. Bremser, and R. F. Davis, "Dislocation density reduction via lateral epitaxy in selectively grown GaN structures," Appl. Phys. Lett. **71**, 2472 (1997).

87) T. Nishinaga, T. Nakano, and S. Zhang, "Epitaxial lateral overgrowth of GaAs by LPE," Jpn. J. Appl. Phys. **27**, 1964 (1988).

88) O. Gfrörer, J. Off, A. Sohmer, F. Scholz, and A. Hangleiter, "Investigations of selectively grown GaN/InGaN epitaxial layers," Mater. Sci. Eng. B **50**, 268 (1997).

89) D. Kapolnek, S. Keller, R. D. Underwood, S. P. DenBaars, and U. K. Mishra, "Spatial control of InGaN luminescence by MOCVD selective epitaxy," J. Cryst. Growth **189/190**, 83 (1998).

90) K. Tachibana, T. Someya, S. Ishida, and Y. Arakawa, "Selective growth of InGaN quantum dot structures and their microphotoluminescence at room temperature," Appl. Phys. Lett. **76**, 3212 (2000).

91) K. Hiramatsu, S. Kitamura, and N. Sawaki, "Facets formation mechanism of GaN hexagonal pyramids on dot-patterns via selective MOVPE," *Proc. 1st Int. Symp. Gallium Nitride and Related Materials*, (MRS, Pittsburgh, 1996), p. 267.

92) K. Hiramatsu, K. Nishiyama, M. Onishi, H. Mizutani, M. Narukawa, A. Motogaito, H. Miyake, Y. Iyechika, and T. Maeda, "Fabrication and characterization of low defect density GaN using facet-controlled epitaxial lateral overgrowth (FACELO)," J. Cryst. Growth **221**, 316 (2000).

93) S. Tanaka, Y. Kawaguchi, N. Sawaki, M. Hibino, and K. Hiramatsu, "Defect structure in selective area growth GaN pyramid on (111)Si substrate," Appl. Phys. Lett. **76**, 2701 (2000).

94) Y. Nagamune, M. Nishioka, S. Tsukamoto, and Y. Arakawa, "GaAs quantum dots with lateral dimension of 25 nm fabricated by selective metalorganic chemical vapor deposition growth," Appl. Phys. Lett. **64**, 2495 (1994).

95) T. Someya and Y. Arakawa, "Microphotoluminescence intensity images of InGaN single quantum wells," Jpn. J. Appl. Phys. **38**, L1216 (1999).

96) H. Matsushima, M. Yamaguchi, K. Hiramatsu, and N. Sawaki, "Sub-micron fine structure of GaN by metalorganic vapor phase epitaxy (MOVPE) selective area growth (SAG) and buried structure by epitaxial lateral overgrowth (ELO)," J. Cryst. Growth **189/190**, 78 (1998).

97) J. Christen, M. Grundmann, and D. Bimberg, "Scanning cathodoluminescence microscopy: A unique approach to atomic-scale characterization of heterointerfaces and imaging of semiconductor inhomogeneities," J. Vac. Sci. Technol. B **9**, 2358 (1991); J. Christen and T. Riemann, "Optical micro-characterization of complex GaN structures," Phys. Stat. Sol. (b) **228**, 419 (2001).

98) For example, T. Nishida, H. Saito, and N. Kobayashi, "Milliwatt operation of AlGaN-based single-quantum-well light emitting diode in the ultraviolet region," Appl. Phys.

Lett. **78**, 3927 (2001); A. Kinoshita, H. Hirayama, M. Ainoya, Y. Aoyagi, and A. Hirata, "Room-temperature operation at 333 nm of $Al_{0.03}Ga_{0.97}N/Al_{0.25}Ga_{0.75}N$ quantum-well light-emitting diodes with Mg-doped superlattice layers," *ibid.* **77**, 175 (2000).

99) S. Nagahama, T. Yanamoto, M. Sano, and T. Mukai, "Ultraviolet GaN single quantum well laser diodes," Jpn. J. Appl. Phys. **40**, L785 (2001).

100) M. Iwaya, R. Nakamura, S. Terao, T. Ukai, S. Kamiyama, H. Amano, and I. Akasaki, "High-efficiency $GaN/Al_xGa_{1-x}N$ multi-quantum well light emitter grown on low-dislocation density $Al_xGa_{1-x}N$," *Proc. Int. Workshop Nitride Semiconductors, Nagoya, 2000*, IPAP Conf. Series **1**, 833 (2000).

101) S. Guha, A. Madhukar, and K. C. Rajkumar, "Onset of incoherency and defect introduction in the initial stages of molecular beam epitaxial growth of highly strained $In_xGa_{1-x}As$ on GaAs(100)," Appl. Phys. Lett. **57**, 2110 (1990).

102) F. Bertram, J. Christen, M. Schmidt, K. Hiramatsu, S. Kitamura, and N. Sawaki, "Direct imaging of local strain relaxation along the $\{1\bar{1}01\}$ side facets and the edges of hexagonal GaN pyramids by cathodoluminescence microscopy," Physica E **2**, 552 (1998).

103) T. Takeuchi, H. Takeuchi, S. Sota, H. Sakai, H. Amano, and I. Akasaki, "Optical properties of strained AlGaN and GaInN on GaN," Jpn. J. Appl. Phys. **36**, L177 (1997).

104) K. Tachibana, T. Someya, Y. Arakawa, R. Werner, and A. Forchel, "Room-temperature lasing oscillation in an InGaN self-assembled quantum dot laser," Appl. Phys. Lett. **75**, 2605 (1999).

105) O. Ambacher, D. Brunner, R. Dimitrov, M. Stutzmann, A. Sohmer, and F. Scholz, "Absorption of InGaN single quantum wells determined by photothermal deflection spectroscopy," Jpn. J. Appl. Phys. **37**, 745 (1998).

106) C.-K. Sun, T.-L. Chiu, S. Keller, G. Wang, M. S. Minsky, S. P. DenBaars, and J. E. Bowers, "Time-resolved photoluminescence studies of InGaN/GaN single-quantum-wells at room temperature," Appl. Phys. Lett. **71**, 425 (1997).

107) For example, O. G. Schmidt, N. Kirstaedter, N. N. Ledentsov, M.-H. Mao, D. Bimberg, V. M. Ustinov, A. Y. Egorov, A. E. Zhukov, M. V. Maximov, P. S. Kop'ev, and Z. I. Alferov, "Prevention of gain saturation by multi-layer quantum dot lasers," Electron. Lett. **32**, 1302 (1996); H. Shoji, Y. Nakata, K. Mukai, Y. Sugiyama, M. Sugawara, N. Yokoyama, and H.

Ishikawa, "Room temperature CW operation at the ground state of self-formed quantum dot lasers with multi-stacked dot layer," *ibid.* **32**, 2023 (1996).

108) S. Nakamura, T. Mukai, M. Senoh, and N. Iwasa, "Thermal annealing effects on *p*-type Mg-doped GaN films," Jpn. J. Appl. Phys. **31**, L139 (1992).

109) S. Nakamura, N. Iwasa, M. Senoh, and T. Mukai, "Hole compensation mechanism of *p*-type GaN films," Jpn. J. Appl. Phys. **31**, 1258 (1992).

110) H. Nakayama, P. Hacke, M. Rezaul, H. Khan, T. Detchprohm, K. Hiramatsu, and N. Sawaki, "Electrical transport properties of *p*-GaN," Jpn. J. Appl. Phys. **35**, L282 (1996).

111) R. Dingle, and M. Ilegems, "Donor–acceptor pair recombination in GaN," Solid State Commun. **9**, 175 (1971).

112) L. Eckey, U. von Gfug, J. Holst, A. Hoffmann, A. Kaschner, H. Siegle, C. Thomsen, B. Schineller, K. Heime, M. Heuken, O. Schön, and R. Beccard, "Photoluminescence and Raman study of compensation effects in Mg-doped GaN epilayers," J. Appl. Phys. **84**, 5828 (1998).

113) M. Smith, G. D. Chen, J. Y. Lin, H. X. Jiang, A. Salvador, B. N. Sverdlov, A. Botchkarev, H. Morkoc, and B. Goldenberg, "Mechanisms of band-edge emission in Mg-doped *p*-type GaN," Appl. Phys. Lett. **68**, 1883 (1996).

114) M. Arita, K. Tachibana, T. Someya, and Y. Arakawa, private communication.

115) S. Nakamura, M. Senoh, S. Nagahama, N. Iwasa, T. Yamada, T. Matsushita, H. Kiyoku, Y. Sugimoto, T. Kozaki, H. Umemoto, M. Sano, and K. Chocho, "InGaN/GaN/AlGaN-based laser diodes with modulation-doped strained-layer superlattices," Jpn. J. Appl. Phys. **36**, L1568 (1997).

116) A. Saxler, W. C. Mitchel, P. Kung, and M. Razeghi, "Aluminum gallium nitride short-period superlattices doped with magnesium," Appl. Phys. Lett. **74**, 2023 (1999).

117) P. Kozodoy, M. Hansen, S. P. DenBaars, and U. K. Mishra, "Enhanced Mg doping efficiency in $Al_{0.2}Ga_{0.8}N$/GaN superlattices," Appl. Phys. Lett. **74**, 3681 (1999).

118) K. Kumakura and N. Kobayashi, "Increased electrical activity of Mg-acceptors in $Al_xGa_{1-x}N$/GaN superlattices," Jpn. J. Appl. Phys. **38**, L1012 (1999).

119) I. D. Goepfert, E. F. Schubert, A. Osinsky, P. E. Norris, and N. N. Faleev, "Experimental and theoretical study of acceptor activation and transport properties in *p*-type $Al_xGa_{1-x}N$/GaN superlattices," J. Appl. Phys. **88**, 2030 (2000).

120) S. Porowski and I. Grzegory, "Thermodynamical properties of III–V nitrides and crystal growth of GaN at high N_2 pressure," J. Cryst. Growth **178**, 174 (1997).

121) M. K. Kelly, R. P. Vaudo, V. M. Phanse, L. Görgens, O. Ambacher, and M. Stutzmann, "Large free-standing GaN substrates by hydride vapor phase epitaxy and laser-induced liftoff," Jpn. J. Appl. Phys. **38**, L217 (1999).

122) K. Motoki, T. Okahisa, N. Matsumoto, M. Matsushima, H. Kimura, H. Kasai, K. Takemoto, K. Uematsu, T. Hirano, M. Nakayama, S. Nakahata, M. Ueno, D. Hara, Y. Kumagai, A. Koukitu, and H. Seki, "Preparation of large freestanding GaN substrates by hydride vapor phase epitaxy using GaAs as a starting substrate," Jpn. J. Appl. Phys. **40**, L140 (2001).

123) T. Nishida, H. Saito, and N. Kobayashi, "Efficient and high-power AlGaN-based ultraviolet light-emitting diode grown on bulk GaN," Appl. Phys. Lett. **79**, 711 (2001); T. Nishida and N. Kobayashi, "Ten-milliwatt operation of an AlGaN-based light emitting diode grown on GaN substrate," Phys. Stat. Sol. (a) **188**, 113 (2001).

124) E. Yablonobitch, "Inhibited spontaneous emission in solid-state physics and electronics," Phys. Rev. Lett. **58**, 2059 (1987).

125) C. J. M. Smith, H. Benisty, D. Labilloy, U. Oesterle, R. Houdre, T. F. Krauss, R. M. De La Rue, and C. Weisbuch, "Near-infrared microcavities confined by two-dimensional photonic bandgap crystals," Electron. Lett. **35**, 228 (1999).

126) O. Painter, R. K. Lee, A. Scherer, A. Yariv, J. D. O'Brien, P. D. Dapkus, and I. Kim, "Two-dimensional photonic band-gap defect mode laser," Science **284**, 1819 (1999); T. Yoshie, A. Scherer, H. Chen, D. Huffaker, and D. Deppe, "Optical characterization of two-dimensional photonic crystal cavities with indium arsenide quantum dot emitters," Appl. Phys. Lett. **79**, 114 (2001).

127) P. Pottier, C. Seassal, X. Letartre, J. L. Leclercq, P. Viktorovitch, D. Cassagne, and C. Jouanin, "Triangular and hexagonal high Q-factor 2-D photonic bandgap cavities on III–V suspended membranes," IEEE J. Lightwave Technol. **17**, 2058 (1999).

128) T. D. Happ, A. Markard, M. Kamp, A. Forchel, and S. Anand, "Single-mode operation of coupled-cavity lasers based on two-dimensional photonic crystals," Appl. Phys. Lett. **79**, 4091 (2001).

129) T. Baba, N. Fukaya, and J. Yonekura, "Observation of light propagation in photonic crystal optical waveguides with bends," Electron. Lett. **35**, 654 (1999).

130) T. Yoshie, C. C. Cheng, and A. Scherer, "Two-dimensional photonic crystals for GaN-based blue light emitters," *Ext. Abst. 16th Int. Semiconductor Laser Conf.*, (IEEE, New York, 1998), p. 189.

131) C. Marinelli, M. Bordovsky, L. J. Sargent, M. Gioannini, J. M. Rorison, R. V. Penty, I. H. White, P. J. Heard, M. Benyoucef, M. Kuball, G. Hasnain, T. Takeuchi, and R. P. Schneider, "Design and performance analysis of deep-etch air/nitride distributed Bragg reflector gratings for AlInGaN laser diodes," Appl. Phys. Lett. **79**, 4076 (2001).

132) K. Iga, "Possibility of green/blue/UV surface emitting lasers," *Proc. 1st Int. Symp. Blue Laser and Light Emitting Diodes*, (Ohmsha, Tokyo, 1996), p. 263.

133) T. Someya, K. Tachibana, J. Lee, T. Kamiya, and Y. Arakawa, "Lasing emission from an $In_{0.1}Ga_{0.9}N$ vertical cavity surface emitting laser," Jpn. J. Appl. Phys. **37**, L1424 (1998); T. Someya, R. Werner, A. Forchel, M. Catalano, R. Cingolani, and Y. Arakawa, "Room temperature lasing at blue wavelengths in gallium nitride microcavities," Science **285**, 1905 (1999).

134) Y.-K. Song, H. Zhou, M. Diagne, A. V. Nurmikko, R. P. Schneider, Jr., C. P. Kuo, M. R. Krames, R. S. Kern, C. Carter-Coman, and F. A. Kish, "A quasicontinuous wave, optically pumped violet vertical cavity surface emitting laser," Appl. Phys. Lett. **76**, 1662 (2000).

135) N. Suzuki and N. Iizuka, "Feasibility study on ultrafast nonlinear optical properties of 1.55-μm intersubband transition in AlGaN/GaN quantum wells," Jpn. J. Appl. Phys. **36**, L1006 (1997).

136) N. Suzuki and N. Iizuka, "Effect of polarization field on intersubband transition in AlGaN/GaN quantum wells," Jpn. J. Appl. Phys. **38**, L363 (1999); N. Iizuka, K. Kaneko, N. Suzuki, T. Asano, S. Noda, and O. Wada, "Ultrafast intersubband relaxation ($\leq$150 fs) in AlGaN/GaN multiple quantum wells," Appl. Phys. Lett. **77**, 648 (2000).

137) K. Hoshino, T. Someya, M. Helm, K. Hirakawa, and Y. Arakawa, "Sharp intersubband absorption spectra in AlGaN/GaN multiple quantum wells," in *Conf. Lasers and Electro-Optics*, OSA Technical Digest, (OSA, Washington DC, 2000), p. 243.

138) C. Gmachl, H. M. Ng, and A. Y. Cho, "Intersubband absorption in GaN/AlGaN multiple quantum wells in the wavelength range of λ~1.75–4.2 μm," Appl. Phys. Lett. **77**, 334

(2000); C. Gmachl, H. M. Ng, S.-N. George Chu, and A. Y. Cho, "Intersubband absorption at $\lambda \sim 1.55$ μm in well- and modulation-doped GaN/AlGaN multiple quantum wells with superlattice barriers," *ibid.* **77**, 3722 (2000); C. Gmachl, H. M. Ng, and A. Y. Cho, "Intersubband absorption in degenerately doped GaN/$Al_xGa_{1-x}N$ coupled double quantum wells," *ibid.* **79**, 1590 (2001).

139) E. Waks, A. Zeevi, and Y. Yamamoto, "Security of quantum key distribution with entangled photons against individual attacks," quant-ph/0012078 (2000).

140) O. Benson, C. Santori, M. Pelton, and Y. Yamamoto, "Regulated and entangled photons from a single quantum dot," Phys. Rev. Lett. **84**, 2513 (2000).

141) C. Santori, M. Pelton, G. Solomon, Y. Dale, and Y. Yamamoto, "Triggered single photons from a quantum dot," Phys. Rev. Lett. **86**, 1502 (2001); G. S. Solomon, M. Pelton, and Y. Yamamoto, "Single-mode spontaneous emission from a single quantum dot in a three-dimensional microcavity," *ibid.* **86**, 3903 (2001).

Publication List

Technical Journals Related to This Work

1. K. Tachibana, T. Someya, and Y. Arakawa, "Natural formation of InGaN self-assembled quantum dots on a GaN buffer," The Transactions of IEICE C-I **J81-C-I**, 474 (1998). (in Japanese)

2. K. Tachibana, T. Someya, and Y. Arakawa, "Nanometer-scale InGaN self-assembled quantum dots grown by metalorganic chemical vapor deposition," Applied Physics Letters **74**, 383 (1999).

3. K. Tachibana, T. Someya, and Y. Arakawa, "MOCVD growth of nanometer-scale InGaN self-assembling quantum dots," IOP Conference Series **162**, 735 (1999).

4. K. Tachibana, T. Someya, Y. Arakawa, R. Werner, and A. Forchel, "Room temperature lasing action in an InGaN quantum dot laser under optical excitation," OSA Technical Digest of Quantum Electronics and Laser Science Conference, QPD7/1 (1999).

5. Y. Arakawa, T, Someya, and K. Tachibana, "GaN-based blue light emitting VCSELs and quantum dot lasers," 1999 Digest of LEOS Summer Topical Meetings, III75 (1999).

6. K. Tachibana, T. Someya, Y. Arakawa, R. Werner, and A. Forchel, "Room-temperature lasing oscillation in an InGaN self-assembled quantum dot laser," Applied Physics Letters **75**, 2605 (1999).

7. K. Tachibana, T. Someya, and Y. Arakawa, "MOCVD growth and optical characterization of stacked InGaN quantum dots for laser applications," Physica Status Solidi (a) **176**, 629 (1999).

8. O. Moriwaki, T. Someya, K. Tachibana, S. Ishida, and Y. Arakawa, "Narrow photoluminescence peaks from localized states in InGaN quantum dot structures," Applied Physics Letters **76**, 2361 (2000).

9. Y. Arakawa, T. Someya, and K. Tachibana, "Progress in GaN-based nanostructures for blue light emitting quantum dot lasers and vertical cavity surface emitting lasers *(Invited)*," IEICE Transaction on Electronics **E83-C**, 564 (2000).

10. K. Tachibana, T. Someya, R. Werner, A. Forchel, and Y. Arakawa, "MOCVD growth of a stacked InGaN quantum dot structure and its lasing oscillation at room temperature," Physica E **7**, 944 (2000).

11. K. Tachibana, T. Someya, S. Ishida, and Y. Arakawa, "Light emission from a single InGaN quantum dot formed by selective area growth," OSA Technical Digest of Conference on Lasers and Electro-Optics, 247 (2000).

12. O. Moriwaki, T. Someya, K. Tachibana, S. Ishida, and Y. Arakawa, "Observation of sharp photoluminescence lines from self-assembled InGaN quantum dots," OSA Technical Digest of Quantum Electronics and Laser Science Conference, 75 (2000).

13. K. Tachibana, T. Someya, S. Ishida, and Y. Arakawa, "Selective growth of InGaN quantum dot structures and their microphotoluminescence at room temperature," Applied Physics Letters **76**, 3212 (2000).

14. K. Tachibana, T. Someya, and Y. Arakawa, "Growth of InGaN self-assembled quantum dots and their application to lasers," IEEE Journal of Selected Topics in Quantum Electronics **6**, 475 (2000).

15. K. Tachibana, T. Someya, S. Ishida, and Y. Arakawa, "Formation of uniform 10-nm-scale InGaN quantum dots by selective MOCVD growth and their micro-photoluminescence intensity images," Journal of Crystal Growth **221**, 576 (2000).

16. Y. Arakawa, T. Someya, and K. Tachibana, "Growth and physics of nitride-based quantum dots for optoelectronics applications," IPAP Conference Series **1**, 403 (2000).

17. K. Tachibana, T. Someya, S. Ishida, and Y. Arakawa, "High-density InGaN quantum dots fabricated by selective MOCVD growth," IPAP Conference Series **1**, 417 (2000).

18. Y. Arakawa, T. Someya, and K. Tachibana, "Progress in growth and physics of nitride-based quantum dots," Physica Status Solidi (b) **224**, 1 (2001).

19. K. Tachibana, M. Miyamura, T. Someya, S. Ishida, and Y. Arakawa, "Strong emission from selectively-grown GaN quantum dots," OSA Technical Digest of Conference on Lasers and Electro-Optics, 240 (2001).

20. K. Tachibana, T. Someya, S. Ishida, and Y. Arakawa, "Uniform array of GaN quantum dots in AlGaN matrix by selective MOCVD growth," Physica Status Solidi (b) **228**, 187 (2001).

21. K. Tachibana, T. Someya, S. Ishida, and Y. Arakawa, "Fabrication of GaN quantum dots by metalorganic chemical vapor selective deposition," Journal of Crystal Growth (in print).

International Conferences Related to This Work

1. K. Tachibana, T. Someya, and Y. Arakawa, "MOCVD growth of nanometer-scale InGaN self-assembling quantum dots," 25th International Symposium on Compound Semiconductors, Fr3A-4, Nara, Japan (1998).

2. K. Tachibana, T. Someya, and Y. Arakawa, "Growth of InGaN/GaN quantum dots for laser applications," Third Symposium on Atomic-Scale Surface and Interface Dynamics, Fukuoka, Japan (1999).

3. K. Tachibana, T. Someya, Y. Arakawa, R. Werner, and A. Forchel, "Room temperature lasing action in an InGaN quantum dot laser under optical excitation," Quantum Electronics and Laser Science Conference, Postdeadline, QPD7, Baltimore, MD, USA (1999).

4. K. Tachibana, T. Someya, and Y. Arakawa, "MOCVD growth and optical characterization of stacked InGaN quantum dots for laser applications," Third International Conference on Nitride Semiconductors, Tu_08, Montpellier, France (1999).

5. K. Tachibana, T. Someya, R. Werner, A. Forchel, and Y. Arakawa, "MOCVD growth of a stacked InGaN quantum dot structure and its lasing oscillation at room temperature," The 9th International Conference on Modulated Semiconductor Structures, J05, Fukuoka, Japan (1999).

6. Y. Arakawa, T. Someya, and K. Tachibana, "GaN-based blue light emitting VCSELs and quantum dot lasers *(Invited)*," 1999 IEEE/LEOS Summer Topical Meetings: Nanostructures and Quantum Dots, FB1.1, San Diego, CA, USA (1999).

7. Y. Arakawa, T. Someya, and K. Tachibana, "Growth of nitride quantum dots for optoelectronic applications *(Invited)*," SPIE Photonics West 2000, Physics and Simulation of Optoelectronic Devices VIII, 3944-09, San Jose, CA, USA (2000).

8. T. Someya, K. Tachibana, S. Ishida, and Y. Arakawa, "Selective growth of InGaN quantum dots by MOCVD," The Fourth Symposium on Atomic-Scale Surface and Interface Dynamics, Tsukuba, Japan (2000).

9. O. Moriwaki, T. Someya, K. Tachibana, and Y. Arakawa, "Micro-photoluminescence study of a single InGaN quantum dot," The Fourth Symposium on Atomic-Scale Surface and Interface Dynamics, Tsukuba, Japan (2000).

10. T. Saito, T. Someya, K. Tachibana, S. Ishida, O. Moriwaki, and Y. Arakawa, "Formation of InGaN quantum dots: MOCVD growth and electronic structures," The Third SANKEN International Symposium on Advanced Nanoelectronics: Devices, Materials and Computing, P1-35, Osaka, Japan (2000).

11. K. Tachibana, T. Someya, S. Ishida, and Y. Arakawa, "Light emission from a single InGaN quantum dot formed by selective area growth," Conference on Lasers and Electro-Optics, CWB6, San Francisco, CA, USA (2000).

12. O. Moriwaki, T. Someya, K. Tachibana, S. Ishida, and Y. Arakawa, "Observation of sharp photoluminescence lines from self-assembled InGaN quantum dots," Quantum Electronics and Laser Science Conference, QTuD2, San Francisco, CA, USA (2000).

13. Y. Arakawa, T. Someya, Y. Toda, and K. Tachibana, "Growth and optical properties of III–V quantum dots for optoelectronics applications *(Invited)*," The Tenth International Conference on Metalorganic Vapor Phase Epitaxy, We-I2, Sapporo, Japan (2000).

14. K. Tachibana, T. Someya, S. Ishida, and Y. Arakawa, "Formation of uniform 10-nm-scale InGaN quantum dots by selective MOCVD growth and their micro-photoluminescence intensity images," The Tenth International Conference on Metalorganic Vapor Phase Epitaxy, We-P41, Sapporo, Japan (2000).

15. Y. Arakawa, T. Someya, K. Tachibana, and K. Hoshino, "Growth and physics of nitride-based quantum dots and heterostructures *(Invited)*," The Fourth European GaN Workshop, Nottingham, UK (2000).

16. Y. Arakawa, K. Tachibana, T. Someya, O. Moriwaki, and S. Ishida, "Growth and optical properties of GaN-based quantum dots *(Invited)*," International Conference on Semiconductor Quantum Dots, Munich, Germany (2000).

17. Y. Arakawa, T. Someya, and K. Tachibana, "Growth and physics of nitride-based quantum dots for optoelectronics applications *(Invited)*," International Workshop on Nitride Semiconductors, MM2-2, Nagoya, Japan (2000).

18. K. Tachibana, T. Someya, S. Ishida, and Y. Arakawa, "High-density InGaN quantum dots fabricated by selective MOCVD growth," International Workshop on Nitride Semiconductors, PMD-46, Nagoya, Japan (2000).

19. Y. Arakawa, T. Someya, K. Tachibana, and K. Hoshino, "Growth and optical properties of nitride-based quantum dots and heterostructures *(Invited)*," The 10th Seoul International Symposium on the Physics of Semiconductors and Applications-2000, A38, Cheju, Korea (2000).

20. K. Tachibana, T. Someya, S. Ishida, and Y. Arakawa, "Selective growth of GaN quantum dots by MOCVD," The Fifth Symposium on Atomic-Scale Surface and Interface Dynamics, Tokyo, Japan (2001).

21. K. Tachibana, T. Someya, and Y. Arakawa, "Formation of GaN-based quantum dots for laser applications *(Invited)*," 6th International Symposium on Advanced Physical Fields "Growth of Well-defined Nanostructures," P-47, Tsukuba, Japan (2001).

22. K. Tachibana, M. Miyamura, T. Someya, S. Ishida, and Y. Arakawa, "Strong emission from selectively-grown GaN quantum dots," Conference on Lasers and Electro-Optics, CTuW3, Baltimore, MD, USA (2001).

23. K. Tachibana, T. Someya, S. Ishida, and Y. Arakawa, "Uniform array of GaN quantum dots in AlGaN matrix by selective MOCVD growth," The Fourth International Conference on Nitride Semiconductors, B10.2, Denver, CO, USA (2001).

24. K. Tachibana, T. Someya, S. Ishida, and Y. Arakawa, "Fabrication of GaN quantum dots by metalorganic chemical vapor selective deposition," The Thirteenth International Conference on Crystal Growth, 01a-S11-02, Kyoto, Japan (2001).

Domestic Conferences Related to This Work

1. K. Tachibana, T. Someya, and Y. Arakawa, "Natural formation of InGaN self-assembled quantum dots grown by MOCVD," The 59th Autumn Meeting 1998, The Japan Society of Applied Physics, 17p-YG-14, Higashi-Hiroshima (1998).

2. K. Tachibana, T. Someya, A. Forchel, and Y. Arakawa, "Lasing operation of InGaN quantum dot lasers at room temperature," The 46th Spring Meeting 1999, The Japan Society of Applied Physics and Related Societies, 31p-N-2, Noda (1999).

3. K. Tachibana, T. Someya, S. Ishida, and Y. Arakawa, "Formation of InGaN nanostructures by selective MOCVD growth," The 60th Autumn Meeting 1999, The Japan Society of Applied Physics, 2p-W-16, Kobe (1999).

4. K. Tachibana, T. Someya, and Y. Arakawa, "Growth and optical properties of stacked InGaN quantum dot structure," The 60th Autumn Meeting 1999, The Japan Society of Applied Physics, 2p-W-18, Kobe (1999).

5. O. Moriwaki, K. Tachibana, S. Ishida, Y. Toda, T. Someya, and Y. Arakawa, "Microphotoluminescence from InGaN quantum dot structure," The 60th Autumn Meeting 1999, The Japan Society of Applied Physics, 2p-W-18, Kobe (1999).

6. K. Tachibana, T. Someya, S. Ishida, and Y. Arakawa, "Formation of InGaN quantum dots by selective MOCVD growth and their micro-photoluminescence," The 47th Spring Meeting 2000, The Japan Society of Applied Physics and Related Societies, 29p-YQ-14, Tokyo (2000).

7. O. Moriwaki, K. Tachibana, S. Ishida, T. Someya, and Y. Arakawa, "Microphotoluminescence from InGaN quantum dot structures (2)," The 47th Spring Meeting 2000, The Japan Society of Applied Physics and Related Societies, 29p-YQ-16, Tokyo (2000).

8. K. Tachibana, T. Someya, S. Ishida, and Y. Arakawa, "Fabrication of InGaN quantum dot structures by selective growth," 19th Electronic Materials Symposium, H9, Izu-Nagaoka (2000).

9. K. Tachibana, T. Someya, S. Ishida, and Y. Arakawa, "Fabrication of GaN quantum dots by selective MOCVD growth," The 61st Autumn Meeting 2000, The Japan Society of Applied Physics, 6a-L-9, Sapporo (2000).

10. K. Tachibana, T. Someya, and Y. Arakawa, "MOCVD growth and optical properties of GaN-based quantum dots," 22nd Shimoda Workshop on Advanced Semiconductor Materials and Devices, Karuizawa (2000).

11. K. Tachibana, T. Someya, S. Ishida, and Y. Arakawa, "Temperature dependence of photoluminescence from selectively-grown GaN quantum dots," The 48th Spring Meeting 2001, The Japan Society of Applied Physics and Related Societies, 29p-L-8, Tokyo (2001).

12. K. Tachibana, T. Someya, and Y. Arakawa, "Fabrication of GaN-based quantum dots and their application to lasers," IEICE Lasers and Quantum Electronics, LQE2001-25, Tokyo (2001).

13. K. Tachibana, T. Someya, S. Ishida, and Y. Arakawa, "Fabrication of GaN quantum dot structures by selective growth and their optical properties," 20th Electronic Materials Symposium, C9, Nara (2001).

Technical Journals Related to Other Works

1. S. Naritsuka, Y. S. Chang, K. Tachibana, and T. Nishinaga, "Vertical cavity surface emitting laser fabricated on GaAs laterally grown on Si substrate," Proceedings of 27th State-of-the-Art Program on Compound Semiconductors, 86 (1997).

2. K. Suzuki, R. A. Hogg, K. Tachibana, and Y. Arakawa, "Density control of GaSb/GaAs self-assembled quantum dots (~ 25 nm) grown by molecular beam epitaxy," Japanese Journal of Applied Physics **37**, L203 (1998).

3. R. A. Hogg, K. Suzuki, K. Tachibana, L. Finger, K. Hirakawa, and Y. Arakawa, "Optical spectroscopy of self-assembled type II GaSb/GaAs quantum dot structures grown by molecular beam epitaxy," Applied Physics Letters **72**, 2856 (1998).

4. K. Suzuki, R. A. Hogg, K. Tachibana, and Y. Arakawa, "Growth and optical properties of self-assembled type II GaSb/GaAs quantum dots," Proceedings of 10th International Conference on Indium Phosphide and Related Materials, 155 (1998).

5. T. Someya, K. Tachibana, J. Lee, T. Kamiya, and Y. Arakawa, "Lasing emission from an $In_{0.1}Ga_{0.9}N$ vertical cavity surface emitting laser," Japanese Journal of Applied Physics **37**, L1424 (1998).

6. T. Someya, K. Hoshino, J. C. Harris, K. Tachibana, and Y. Arakawa, "Photoluminescence from sub-nanometer-thick $GaN/Al_{0.8}Ga_{0.2}N$ quantum wells," Applied Physics Letters **77**, 1336 (2000).

7. T. Someya, K. Hoshino, J. Harris, K. Tachibana, S. Kako, and Y. Arakawa, "Emission at 247 nm from GaN quantum wells grown by MOCVD," MRS Internet Journal of Nitride Semiconductor Research **5S1**, W12.8 (2000). http://nsr.mij.mrs.org/5S1/W12.8/

8. M. Miyamura, K. Tachibana, T. Someya, and Y. Arakawa, "Self-assembled growth of GaN quantum dots using low-pressure MOCVD," Physica Status Solidi (b) **228**, 191 (2001).

9. M. Miyamura, K. Tachibana, T. Someya, and Y. Arakawa, "Stranski–Krastanow growth of GaN quantum dots by metalorganic chemical vapor deposition," Journal of Crystal Growth (in print).

10. M. Miyamura, K. Tachibana, and Y. Arakawa, "UV photoluminescence spectrum of GaN self-assembled quantum dots grown by MOCVD," *to be published in* IOP Conference Series.

11. M. Miyamura, K. Tachibana, and Y. Arakawa, "High density and size-controlled GaN self-assembled quantum dots grown by metalorganic chemical vapor deposition," *submitted to* Applied Physics Letters.

International Conferences Related to Other Works

1. S. Naritsuka, Y. S. Chang, K. Tachibana, and T. Nishinaga, "Vertical cavity surface emitting laser fabricated on GaAs laterally grown on Si substrate," 192nd Electrochemical Society Meeting, 1761, Paris, France (1997).

2. K. Suzuki, R. A. Hogg, K. Tachibana, and Y. Arakawa, "Growth and optical properties of self-assembled type II GaSb/GaAs quantum dots," 10th International Conference on Indium Phosphide and Related Materials, TuP-21, Tsukuba, Japan (1998).

3. T. Someya, K. Tachibana, Y. Arakawa, J. Lee, and T. Kamiya, "Lasing oscillation in InGaN vertical cavity surface emitting lasers," 16th International Semiconductor Laser Conference, Postdeadline, PD-1, Nara, Japan (1998).

4. T. Someya, K. Hoshino, J. Harris, K. Tachibana, S. Kako, and Y. Arakawa, "Emission at 290 nm from GaN quantum wells grown by MOCVD," 1999 MRS Fall Meeting, W12.8, Boston, MA, USA (1999).

5. M. Miyamura, K. Tachibana, T. Someya, and Y. Arakawa, "Self-assembled growth of GaN quantum dots," The Fifth Symposium on Atomic-Scale Surface and Interface Dynamics, Tokyo, Japan (2001).

6. M. Miyamura, K. Tachibana, T. Someya, and Y. Arakawa, "Self-assembled growth of GaN quantum dots using low-pressure MOCVD," The Fourth International Conference on Nitride Semiconductors, B10.3, Denver, CO, USA (2001).

7. M. Miyamura, K. Tachibana, T. Someya, and Y. Arakawa, "Stranski–Krastanow growth of GaN quantum dots by metalorganic chemical vapor deposition," The Thirteenth International Conference on Crystal Growth, 01a-S11-03, Kyoto, Japan (2001).

8. M. Miyamura, K. Tachibana, and Y. Arakawa, "UV photoluminescence spectrum of GaN self-assembled quantum dots grown by MOCVD," 28th International Symposium on Compound Semiconductors, Late News, WeP-33, Tokyo, Japan (2001).

9. M. Miyamura, K. Tachibana, and Y. Arakawa, "UV photoluminescence from size-controlled GaN quantum dots grown by MOCVD," Fourth International Symposium on Blue Laser and Light Emitting Diodes, ThA5, Córdoba, Spain (2002).

Domestic Conferences Related to Other Works

1. K. Suzuki, R. A. Hogg, K. Tachibana, and Y. Arakawa, "MBE growth of GaSb quantum dots on GaAs," The 58th Autumn Meeting 1997, The Japan Society of Applied Physics, 5a-S-4, Akita (1997).

2. R. A. Hogg, K. Suzuki, K. Tachibana, K. Hirakawa, and Y. Arakawa, "Optical properties of GaSb quantum dots on GaAs," The 58th Autumn Meeting 1997, The Japan Society of Applied Physics, 5a-S-5, Akita (1997).

3. K. Suzuki, K. Tachibana, R. A. Hogg, and Y. Arakawa, "Growth and optical properties of self-assembling GaSb/GaAs quantum dots by molecular beam epitaxy," Second Symposium on Atomic-Scale Surface and Interface Dynamics, Tokyo (1998).

4. K. Suzuki, R. A. Hogg, K. Tachibana, and Y. Arakawa, "Formation of type-II GaSb/GaAs self-assembled quantum dots," The 45th Spring Meeting 1998, The Japan Society of Applied Physics and Related Societies, 30p-PB-20, Tokyo (1998).

5. K. Tachibana, K. Suzuki, and Y. Arakawa, "Fabrication of self-assembled AlSb/GaAs V-grooves," The 45th Spring Meeting 1998, The Japan Society of Applied Physics and Related Societies, 30p-ZM-16, Tokyo (1998).

6. T. Someya, K. Tachibana, M. Nishioka, and Y. Arakawa, "InGaN quantum wells grown on highly-reflective GaN/AlGaN quarter-wave reflectors by MOCVD," 17th Electronic Materials Symposium, SB12, Izu-Nagaoka (1998).

7. T. Someya, K. Tachibana, M. Nishioka, and Y. Arakawa, "Atmospheric-pressure MOCVD growth of highly-reflective GaN/$Al_{0.3}Ga_{0.7}N$ DBRs," The 59th Autumn Meeting 1998, The Japan Society of Applied Physics, 18p-YC-3, Higashi-Hiroshima (1998).

8. T. Someya, K. Tachibana, J. C. Harris, and Y. Arakawa, "Atmospheric-pressure MOCVD growth of GaN/$Al_{0.5}Ga_{0.5}N$ quantum wells and their photoluminescence at 302 nm," The 60th Autumn Meeting 1999, The Japan Society of Applied Physics, 4a-V-5, Kobe (1999).

9. M. Miyamura, K. Tachibana, T. Someya, and Y. Arakawa, "GaN self-assembled quantum dots grown by MOCVD," The 48th Spring Meeting 2001, The Japan Society of Applied Physics and Related Societies, 29p-L-7, Tokyo (2001).

10. M. Miyamura, K. Tachibana, T. Someya, and Y. Arakawa, "Self-assembled growth of GaN quantum dots," 20th Electronic Materials Symposium, K6, Nara (2001).

11. M. Miyamura, K. Tachibana, and Y. Arakawa, "S–K growth of high quality GaN quantum dots by MOCVD," The 49th Spring Meeting 2002, The Japan Society of Applied Physics and Related Societies, 29p-ZM-22, Hiratsuka (2002).

12. M. Miyamura, K. Tachibana, and Y. Arakawa, "Optical properties of GaN quantum dots grown by S–K mode," The 49th Spring Meeting 2002, The Japan Society of Applied Physics and Related Societies, 29p-ZM-23, Hiratsuka (2002).

13. S. Kako, M. Miyamura, K. Tachibana, and Y. Arakawa, "Time-resolved photoluminescence spectroscopy of self-assembled GaN quantum dots," The 49th Spring Meeting 2002, The Japan Society of Applied Physics and Related Societies, 28a-YH-5, Hiratsuka (2002).